THE UNIVERSITY OF MICHIGAN

COLLEGE OF ENGINEERING
Department of Electrical Engineering
Space Physics Research Laboratory

Final Report

DIURNAL SURVEY OF THE THERMOSPHERE

D. R. Taeusch
G. R. Carignan
A. F. Nagy
H. B. Niemann

ORA Project 07446

under contract with:

NATIONAL AERONAUTICS AND SPACE ADMINISTRATION

GEORGE C. MARSHALL SPACE FLIGHT CENTER

CONTRACT NO. NAS8-20232

HUNTSVILLE, ALABAMA

administered through:

OFFICE OF RESEARCH ADMINISTRATION   ANN ARBOR

October 1967

ACKNOWLEDGMENTS

TABLE OF CONTENTS

LIST OF TABLES

LIST OF TABLES (Concluded)

LIST OF FIGURES

LIST OF FIGURES (Concluded)

1. INTRODUCTION

The results of the launchings of eight Marshall-University of Michigan Probes (MUMP), Nike-Tomahawk sounding rocket payloads are summarized in this report. The MUMP is similar to the Thermosphere Probe (TP), described by Spencer, Brace, Carignan, Taeusch and Niemann (1965), which was developed by the Space Physics Research Laboratory of The University of Michigan jointly with the Goddard Space Flight Center, Laboratory for Atmospheric and Biological Science. The MUMPS were developed by the Space Physics Research Laboratory for the Marshall Space Flight Center, Aero-Astrodynamics Laboratory.

The purpose of the payloads was to study the variability of the earth's atmospheric parameters in the altitude region between 120 and 350 km. The payloads described herein each included an omegatron mass analyzer (Niemann and Kennedy, 1966), an electron temperature probe (Spencer, Brace and Carignan, 1962), and an aspect determination system consisting principally of a lunar or a solar sensor. This complement of instruments permitted the determination of the molecular nitrogen density and temperature, the electron density and temperature, and the ion density in the altitude range of approximately 140 to 320 km over Cape Kennedy, Florida.

Six of the MUMP payloads described herein were launched on January 24, 1967, for the purpose of establishing the diurnal variation of the thermosphere under relatively quiet solar activity levels. The additional two payloads were launched on April 25, 1967, as a follow-on day-night pair to reestablish the maximum-minimum density and temperature values for this day.

A general description of the payload kinematics, the orientation analysis, and the technique for the reduction of the data is given by Taeusch, Carignan, Niemann and Nagy (1965). The reduction of the data was performed at the Space Physics Research Laboratory and the results are included in the present report.

1

2. BACKGROUND FOR THE EXPERIMENT

2.1 NEUTRAL PARTICLES

It has been established that the atmospheric parameters above 100 kilometers altitude vary temporarily because of the variable nature of the solar energy input. The primary variations are periodic following the eleven-year sunspot cycle of our sun, the twenty-four hour diurnal cycle of our rotating earth, and the yearly seasonal cycle due to the latitude change of the sub-solar point on earth. Also, two secondary variations have been observed. A twenty-seven day variation has been observed by Jacchia (1963) and has been correlated with the solar decimeter flux and the twenty-seven day rotational period of the sun. A semi-annual variation, observed by Paetzold and Zschorner (1960) and by Jacchia (1964), is believed to be due to changes in atmospheric circulation when the sub-solar point is near the equator (soltices) (Johnson, 1964).

In terms of the magnitudes of the periodic variations, the eleven-year solar cycle dominates the general atmospheric behavior. Jacchia (1964) reports that the maximum daytime exospheric temperature varies from about 2100°K to about 800°K during the five-and-one-half year interval from maximum to minimum solar activity. The effect of this temperature variation on the atmospheric density is large and variable with altitude, since the scale heights of the constituents change by about a factor of 2.6 during this time.

The diurnal variation in temperature depends upon the latitude and the time of year; however, Jacchia (1964) has stated that the maximum variation has been observed to be approximately 30 per cent from sub-solar to anti-solar locations on earth and that this diurnal percentage variation is relatively constant for all levels of solar activity.

The observed semi-annual temperature variations are on the order of 15 to 20 per cent with the July minimum deeper than the January minimum and the October maximum higher than the April maximum because of a superimposed "annual" effect (Jacchia, 1964). The twenty-seven day variation is on the order of 10 per cent at low latitudes which makes it difficult to observe during periods of variable solar activity.

An attempt to describe the above mentioned variations usually results in "model" atmosphere, which, for the thermosphere, predicts the diurnal variation of atmospheric parameters for various solar activity levels. Most of the models to date are based on satellite drag data, because of the limited number of measurements by other means. Therefore, the models reflect variations as deduced from these data (Jacchia, 1960; Jacchia, 1961; Harris and Priester, 1964; McElroy, 1964; CIRA, 1965). The major problem to date is that the data, on which the models are based, yield total density and temperature as the derived quantities. Therefore, model composition values are deduced from

2

assumed diffusion levels and assumed total densities well below the lowest altitude where drag data are available. The required assumptions are usually in the form of establishing a constant pressure, temperature, density, and composition at 120 km for all times of day and all levels of solar activity. These assumptions cause relatively small predicted variation in densities, during all variable conditions, up to about 200 km. Undoubtedly these predictions do not give a good physical picture of the real atmospheric behavior at altitudes between 120 and 200 km, as is borne out by recent direct measurements utilizing the Thermosphere Probe (Spencer, et al., 1965a,b). Therefore, it is apparent that the description of atmospheric behavior in the thermosphere must consider variability of the parameters at 120 km and lower.

With these facts in mind, more measurements of atmospheric parameters in the 120 to 300 km region are required, if the variability in this region is to be understood. To date, aeronomy satellites have not been used to measure parameters in the lower region because of the resulting shortened lifetime. Also, satellite measurements do not provide good altitude-density profiles. Instrumented sounding rockets provide the desired data essentially only for one time of day at one geographical location. Separating the various effects previously discussed from data obtained at different times of year, day, latitude, etc., is an almost impossible task; and, therefore, a problem exists of how best to utilize a given payload to provide data of maximum usefulness.

Measurements to be made in the next year or so will not be capable in themselves of yielding information on the eleven-year solar cycle effect. Therefore, it is reasonable to attempt to make all measurements when solar activity is at the same level for each; thus, only the diurnal, the semi-annual, and the seasonal variations remain to be investigated. Of these, the diurnal variation is the most significant. Measurements of atmospheric parameters over the time period of one earth rotation would yield much information bearing on the atmospheric time constant and response to the energy input which, in turn, bears on currently assumed rate coefficients for the various physical processes.

Measurements of the density profiles of neutral nitrogen yield neutral particle temperature with an estimated error of ± 5 per cent (Spencer, et al., 1965a,b), if one assumes that hydrostatic equilibrium exists. Since a discrepancy exists between model diurnal variations of temperature as deduced from satellite drag data, (Jacchia, 1965a,b; Harris and Priester, 1964), the sounding rocket techniques should be able to add significantly to the value of the extensive drag results by yielding better diurnal temperature variation information for input to future models.

2.2 CHARGED PARTICLES

Studies of the diurnal behavior of the electron densities in the E and bottomside F-region began with the introduction of the ionosonde

many years ago. The advent of direct probings by rockets and satellites provided the opportunity of making detailed density measurements in the D, E, and lower F-region and provided the first opportunity for measurements in the topside ionosphere. Rocket and satellite-borne Langmuir probes were also the first to make measurements of the electron and ion temperatures in the ionosphere (Krassovsky, 1959; Boggess, et al., 1959; Bourdeau, et al., 1962; Nagy, et al., 1963). It is difficult to establish a true diurnal pattern by using data from satellite-borne experiments, because of the intricacies involved in separating latitude, longitude, altitude, and seasonal effects in the results obtained. It is also difficult to obtain a complete diurnal pattern by using data from rockets flown to date, because it is necessary to combine the results from numerous flights, carried out on different days sometimes under widely varying conditions. The incoherent backscatter technique (e.g., Evans, 1965a) is very well suited for diurnal measurements of electron density and electron and ion temperature. These measurements are, however, usually restricted to altitudes above about 200 km and have a height resolution of about 50 km. The usual time taken for the measurements of one complete profile by this technique is in the order of one hour, although consecutive measurements have been made during an eclipse (Evans, 1965b) in 15-minute time intervals.

The purpose of the rocket program, which is described in this report, was to obtain information on the diurnal variation of the electron temperature and density as well as neutral particle temperature and density in an altitude range where good diurnal measurements are lacking. By the appropriate selection of the launch times, it was also possible to investigate a number of specific problems, which will be discussed briefly in Section 9.

3. GENERAL FLIGHT INFORMATION

The general flight information for the MUMP payloads are tabulated below. The Table of Events for each flight, which follow on the next pages, gives flight times and altitudes of significant events occurring during the flight. Some of these have been estimated and are so marked. The others have been obtained from the telemetry records and radar trajectories, where applicable.

Launch Date: January 24, 1967

Location: Cape Kennedy, Florida

                      Longitude: 28° 27.5'N

                      Latitude: 80° 31.5'W

MUMP NO.	Test Number	(EST) Local Time	G.M. Time	Local Solar Time	Solar Zenith χ Angle
8	ETR-1474	0400	0900	0326	132.4°
6	ETR-1828	0651	1151	0618	95.6°
3	ETR-1165	1009	1509	0935	60.0°
1	ETR-0381	1434	1934	1400	55.5°
2	ETR-0611	1750	2250	1712	90.0°
7	ETR-0851	2200	0300	2126	143.7°

Launch Date: April 25, 1967

MUMP NO.	Test Number	(EST) Local Time	G.M. Time	Local Solar Time	Solar Zenith χ Angle
4	ETR-1942	0130	0630	0055	135.3°
5	ETR-4803	1400	1900	1325	27.8°

TABLE I

TABLE OF EVENTS

ETR 0381

Mump 1

Event	Flight Time (sec)	Altitude (km)	Remarks
Lift Off	0	0	
1st Stage Burn Out	3.587	1.4 (est.)	
2nd Stage Ignition	12.137	7.0 (est.)	
2nd Stage Burn Out	21.158	20.7 (est.)	
Despin	43.083	71.3	
TP Ejection	44.878	75.2	
Omegatron Breakoff	79.904	144.2	
Omegatron Filaments On. M28	80.440	146.7	
Peak Altitude	287.74	336.12	
Omegatron to Mass 16	Not Applicable		
Omegatron to Mass 32	Not Applicable		
Omegatron to Mass 28	Not Applicable		
L.O.S.	547.0	39.0	

Launch Date:	January 24, 1967
Launch Time:	19:33:59.940 GMT
Location:	Cape Kennedy, Florida
Apogee Parameters:	
Altitude:	336.12 km
Horizontal Velocity:	471.10 m/sec
Flight Time:	287.74 sec
TP Motion:	
Tumble Period:	1.514 sec
Roll Rate	-50 deg/sec

TABLE II

TABLE OF EVENTS

ETR 0611

MUMP 2

Event	Flight Time (sec)		Altitude (km)		Remarks
Lift Off	0		0		
1st Stage Burn Out	4.0	(est.)	1.6	(est.)	
2nd Stage Ignition	13.0	(est.)	7.2	(est.)	
2nd Stage Burn Out	21.5	(est.)	20.5	(est.)	
Despin	41.0	(est.)	66.	(est.)	
TP Ejection	42.862		69.7		
Omegatron Breakoff	78.320		139.5		
Omegatron Filaments On. M28	78.704		140.2		
Peak Altitude	279.96		319.58		
Omegatron to Mass 16	Not Applicable				
Omegatron to Mass 32	Not Applicable				
Omegatron to Mass 28	Not Applicable				
L.O.S.	541.0		24.0		

Launch Date:	January 24, 1967
Launch Time:	22:50:00.428 GMT
Location:	Cape Kennedy, Florida
Apogee Parameters:	
Altitude:	319.58 km
Horizontal Velocity:	457.24 m/sec
Flight Time:	279.96 sec
TP Motion:	
Tumble Period:	3.32 sec
Roll Rate:	0 deg/sec

7

TABLE III

TABLE OF EVENTS

ETR 1165

MUMP 3

Event	Flight Time (sec)	Altitude (km)	Remarks
Lift Off	0	0	
1st Stage Burn Out	3.45 (est.)	1.7 (est.)	
2nd Stage Ignition	12.002	7.2 (est.)	
2nd Stage Burn Out	20.434	20.6 (est.)	
Despin	43.352	72.0 (est.)	
TP Ejection	44.822	76.0 (est.)	
Omegatron Breakoff	77.532	138.8	
Omegatron Filaments On. M28	78.335	140.1	
Peak Altitude	382.61	324.22	
Omegatron to Mass 16	Not Applicable		
Omegatron to Mass 32	Not Applicable		
Omegatron to Mass 28	Not Applicable		
L.O.S.	543.0	30.0	

Launch Date:	January 24, 1967
Launch Time:	15:08:54.448 GMT
Location:	Cape Kennedy, Florida
Apogee Parameters:	
Altitude:	324.22 km
Horizontal Velocity:	551.69 m/sec
Flight Time:	282.61 sec
TP Motion:	
Tumble Period:	1.086 sec
Roll Rate:	-125 deg/sec

TABLE IV

TABLE OF EVENTS

ETR 1942

MUMP 4

Event	Flight Time (sec)	Altitude (km)	Remarks
Lift Off	0	0	
1st Stage Burn Out	3.524	1.4 (est.)	
2nd Stage Ignition	12.0 (est.)	7.0 (est.)	
2nd Stage Burn Out	21.926	21.0 (est.)	
Despin	43.734	71.9	
TP Ejection	46.557	78.2	
Omegatron Breakoff	78.121	142.0	
Omegatron Filaments On. M28	78.719	143.1	
Peak Altitude	287.971	337.511	
Omegatron to Mass 16	Not Applicable		
Omegatron to Mass 32	Not Applicable		
Omegatron to Mass 28	Not Applicable		
L.O.S.	546.0	43.0	

Launch Date:	April 25, 1967
Launch Time:	06:30:00.499 GMT
Location:	Cape Kennedy, Florida
Apogee Parameters:	
Altitude:	337.511 km
Horizontal Velocity:	384.41 m/sec
Flight Time:	287.971 sec
TP Motion:	
Tumble Period:	1.160 sec
Roll Rate:	0 deg/sec

9

TABLE V

TABLE OF EVENTS

ETR 4803

MUMP 5

Event	Flight Time (sec)	Altitude (km)	Remarks
Lift Off	0	0	
1st Stage Burn Out	3.574	1.4 (est.)	
2nd Stage Ignition	12.480	7.0 (est.)	
2nd Stage Burn Out	21.398	21.0 (est.)	
Despin	44.5 (est.)	74.7 (est.)	
TP Ejection	47.2 (est.)	80.6 (est.)	
Omegatron Breakoff	76.704	139.9	
Omegatron Filaments On. M28	77.373	141.1	
Peak Altitude	286.68	334.73	
Omegatron to Mass 16	Not Applicable		
Omegatron to Mass 32	Not Applicable		
Omegatron to Mass 28	Not Applicable		
L.O.S.	548.0	34.0	

Launch Date:	April 25, 1967
Launch Time:	19:00:00.110 GMT
Location:	Cape Kennedy, Florida
Apogee Parameters:	
Altitude:	334.733 km
Horizontal Velocity:	419.65 m/sec
Flight Time:	286.680 sec
TP Motion:	
Tumble Period:	1.497 sec
Roll Rate:	-46 deg/sec

TABLE VI

TABLE OF EVENTS
ETR 1828
MUMP 6

Event	Flight Time (sec)	Altitude (km)	Remarks
Lift Off	0	0	
1st Stage Burn Out	3.830	2.0	(est.)
2nd Stage Ignition	12.160	7.2	(est.)
2nd Stage Burn Out	20.878	20.8	(est.)
Despin	43.292	71.5	(est.)
TP Ejection	45.286	76.0	(est.)
Omegatron Breakoff	75.697	135.0	
Omegatron Filaments On. M28	76.435	136.6	
Peak Altitude	283.190	324.8	
Omegatron to Mass 16	Not Applicable		
Omegatron to Mass 32	Not Applicable		
Omegatron to Mass 28	Not Applicable		
L.O.S.	548.0	24.0	

Launch Date: January 24, 1967

Launch Time: 11:51:26.420 GMT

Location: Cape Kennedy, Florida

Apogee Parameters:
    Altitude: 324.82 km
    Horizontal Velocity: 574.79 m/sec
    Flight Time: 283.190 sec

TP Motion:
    Tumble Period: 1.137 sec
    Roll Rate: -50 deg/sec

TABLE VII

TABLE OF EVENTS

ETR 0851

MUMP 7

Event	Flight Time (sec)	Altitude (km)	Remarks
Lift Off	0	0	
1st Stage Burn Out	3.4 (est.)	1.4 (est.)	
2nd Stage Ignition	12.000	7.0 (est.)	
2nd Stage Burn Out	21.0 (est.)	20.7 (est.)	
Despin	43.0 (est.)	70.2	
TP Ejection	45.751	76.2	
Omegatron Breakoff	66.994	119.3	
Omegatron Filaments On. M28	67.681	121.9 (est.)	
Peak Altitude	283.97	327.3	
Omegatron to Mass 16	Not Applicable		
Omegatron to Mass 32	Not Applicable		
Omegatron to Mass 28	Not Applicable		
L.O.S.	539.0	39.0	

Launch Date: January 25, 1967

Launch Time: 3:00:00.059 GMT

Location: Cape Kennedy, Florida

Apogee Parameters:
    Altitude: 327.3 km
    Horizontal Velocity: 525.75 m/sec
    Flight Time: 283.97 sec

TP Motion:
    Tumble Period: 1.511 sec
    Roll Rate: -200 deg/sec

TABLE VIII

TABLE OF EVENTS

ETR 1474

MUMP 8

Event	Flight Time (sec)	Altitude (km)	Remarks
Lift Off	0	0	
1st Stage Burn Out	3.122	1.4 (est.)	
2nd Stage Ignition	12.265	7.2 (est.)	
2nd Stage Burn Out	21.240	20.8 (est.)	
Despin	42.898	71.2 (est.)	
TP Ejection	45.301	75.8 (est.)	
Omegatron Breakoff	78.271	140.3	
Omegatron Filaments On. M28	78.968	141.6	
Peak Altitude	282.928	325.36	
Omegatron to Mass 16	Not Applicable		
Omegatron to Mass 32	Not Applicable		
Omegatron to Mass 28	Not Applicable		
L.O.S.	539.0	36.0	

Launch Date:	January 24, 1967
Launch Time:	9:00:00.252 GMT
Location:	Cape Kennedy, Florida
Apogee Parameters:	
Altitude:	325.36 km
Horizontal Velocity:	506.44 m/sec
Flight Time:	282.928 sec
TP Motion:	
Tumble Period:	1.546 sec
Roll Rate:	-25 deg/sec

4. LAUNCH VEHICLE

The launch vehicles used for each flight were a two-stage Nike-Tomahawk combination. The first stage, the solid propellant Nike booster, has an average thrust of 49,000 lb and burns for approximately 3.5 sec. The Nike is 135 in. long, 16.5 in. in diameter, and weighs 1338 lb unburned. The center of gravity (CG) was 75.7 in. from the nozzle exit plant (NEP). The second stage was Thiokol's Tomahawk solid propellant motor. The average thrust is approximately 11,000 lb and it burns for about 9 sec. The Tomahawk, 142 in. long and 9 in. in diameter, weighs 530 lb unburned. The CG was 72.125 in. from the NEP. The payloads were 78.4 in. long and weighed 132 lb. The total vehicle was 355 in. long and weighed 2000 lb. Drawings and photographs of the vehicle are given in Figures 1, 2, and 3.

The predicted performance for the vehicle was 322 km peak altitude at 281 sec flight time. The actual performances were discussed in the previous section.
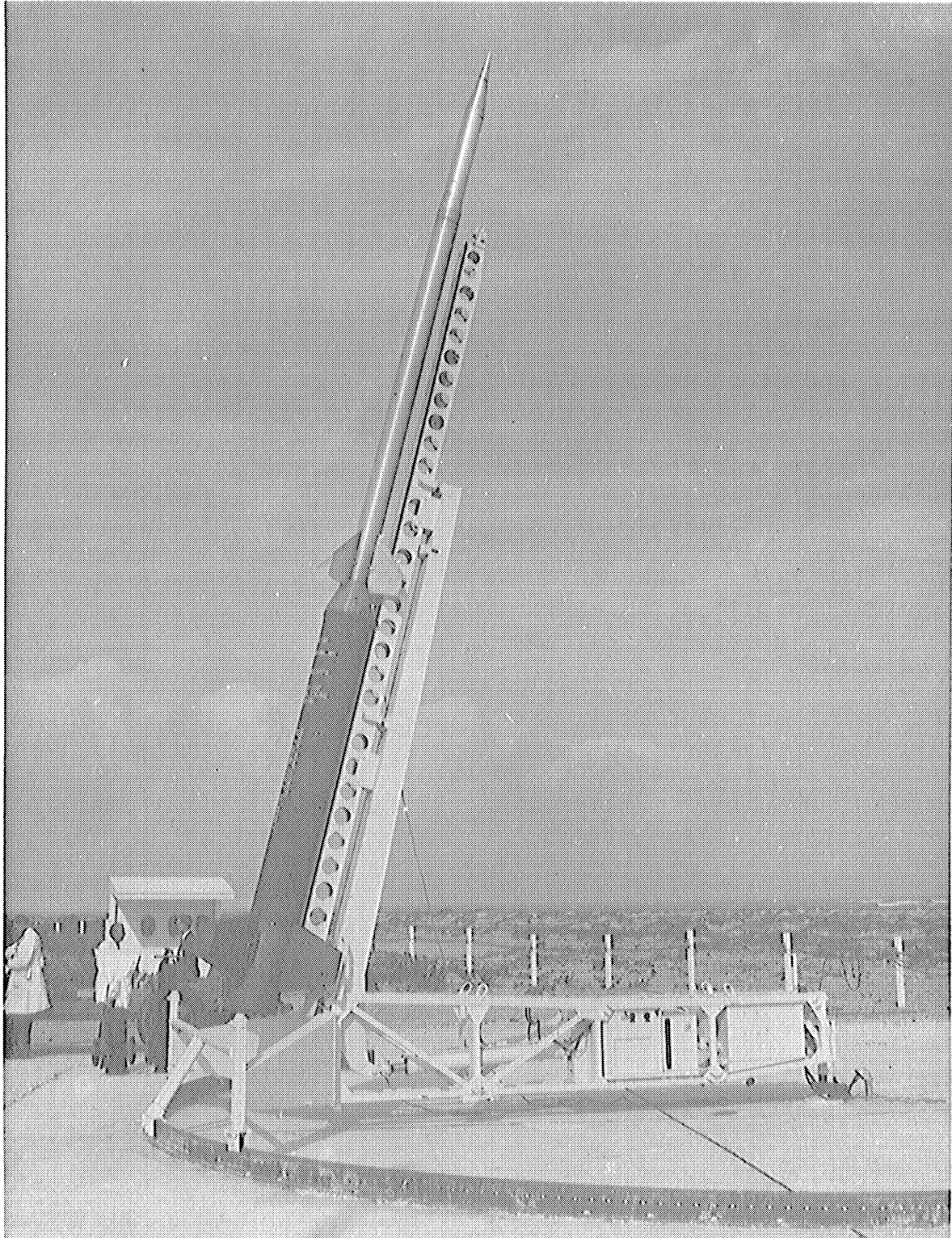
Figure 1. Nike-Tomahawk with MUMP payload.

15

Figure 2. Nike-Tomahawk with MUMP payload.
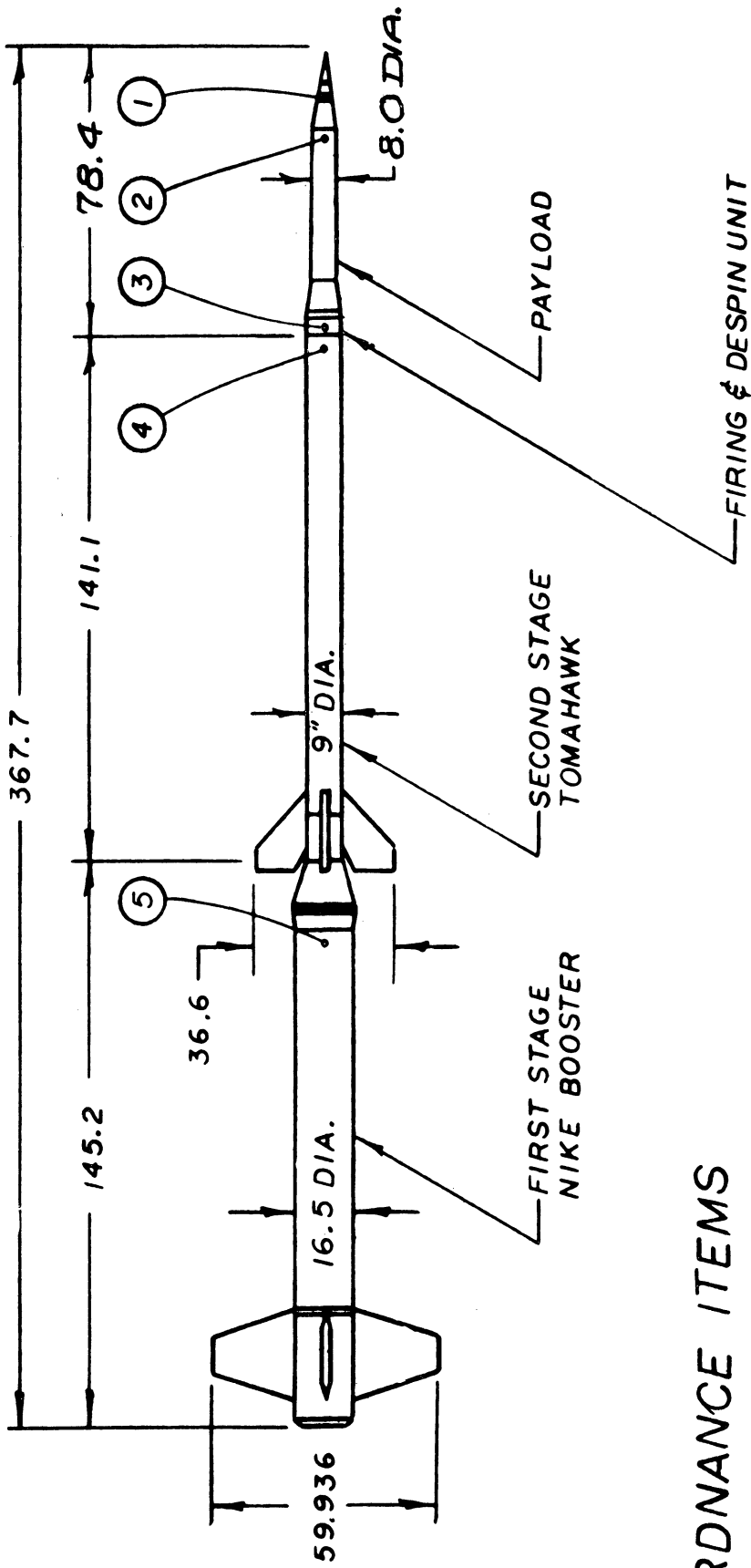
ORDNANCE ITEMS

1. NOSE CONE OPENING PRIMERS.
2. BREAKOFF LINEAR ACTUATORS
3. DESPIN INITIATION PRIMERS
4. SECOND STAGE IGNITER
5. NIKE BOOSTER IGNITER

Figure 3. Nike-Tomahawk dimensions.

17

5. NOSE CONE

A diagram of a day shot of a typical payload including nose cone, despin mechanisms, and adapter sections is shown in Figure 4. Figure 5 shows a typical payload of a night shot. The weights, dimensions, and instrumentation placement are also given on the figures. Figure 6 is a photograph of the TP in the nose cone. An assembly drawing of the 8" nose cone is given in Figure 7.

The payload is programmed to despin at about 70 km altitude, and the MUMP is ejected and tumbled at about 75 km. The breakoff device is removed at about 110 km, and the omegatron filaments are turned on a few seconds later. The timing for each particular payload has been described previously.

A determination of the total payload moments of inertia, performed at The Bendix Systems Division in Ann Arbor, is included in their report in the appendix. Figures 76 through 78 show the test setup and the instrument package test setup.

NASA	
T. P. NO.	MUMP - (DAY SHOT)
TYPE OF ROCKET	NIKE - TOMAHAWK
DATE OF SHOT	JANUARY 24,1967
LOCATION	CAPE KENNEDY
TIME	
ALTITUDE	

RESULTS - DATA OK

MISC. NOTES -1. DAY SHOT
OMEG
E.S.P.
-2. O & O OSCILLATORS
REMOVED FROM OSC DECKS
-3. DESPIN FLOWN

9.00 DIA
8.00 DIA

SECTION 1

1. OMEG ASS'Y & BO
2. OMEG ADAPTER
3. OMEG AMP
4. REG DECK
5. OM X 5 DECK·
6. OSC DECK 1
7. OSC DECK 2
8. AUX DECK

CG.=43.63
28.56

SECTION 2

1. 3 ADCOLE ASPECT SENSOR
2. ELECTRONICS FOR SENSOR
3. SINGLE PROBE

14.06
12.88
30.44
36.09
78.39

SECTION 3

1. TRANSMITTER & BATT. DECK
2. ESP DECK
3. SCO DECK
4. COMM DECK
5. CONTROL DECK
6.

WEIGHT 50.13 LB

2.00
5.12
6.62

WEIGHT 82.75 LB

TOTAL WEIGHT OF PROBE AND NOSE CONE 132.88 LB

Figure 4. Payload diagram for a day shot.

NASA	
T. P. NO.	MUMP- (NIGHT SHOT)
TYPE OF ROCKET	NIKE - TOMAHAWK
DATE OF SHOT	JANUARY 24, 1967
LOCATION	CAPE KENNEDY
TIME	
ALTITUDE	

RESULTS - DATA OK

MISC. NOTES -1. NIGHT SHOT
      OMEG
      E.S.P.
   -2. O & O^2 OSCILLATORS
     REMOVED FROM OSC DECKS
   -3. DESPIN FLOWN

SECTION 1

 1. OMEG ASS'Y & BO
 2. OMEG ADAPTER
 3. OMEG AMP
 4. REG DECK
 5. OM X 5 DECK
 6. OSC DECK 1
 7. OSC DECK 2
 8. AUX DECK

SECTION 2

 1. SINGLE PROBE

SECTION 3

 1. TRANSMITTER & BATT. DECK
 2. ESP DECK
 3. SCO DECK
 4. COMM DECK
 5. CONTROL DECK
 6. LUNAR ASPECT SENSOR
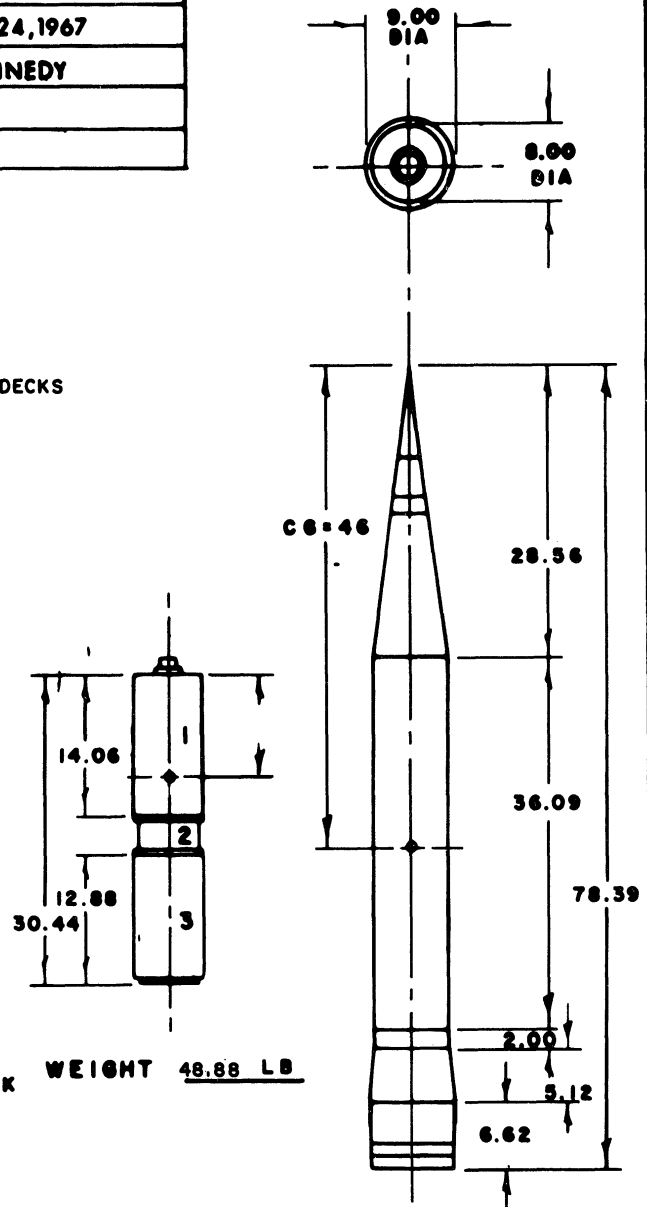
WEIGHT 48.88 LB

WEIGHT 82.75 LB

TOTAL WEIGHT OF PROBE AND NOSE CONE   131.63   LB

Figure 5. Payload diagram for a night shot.

20
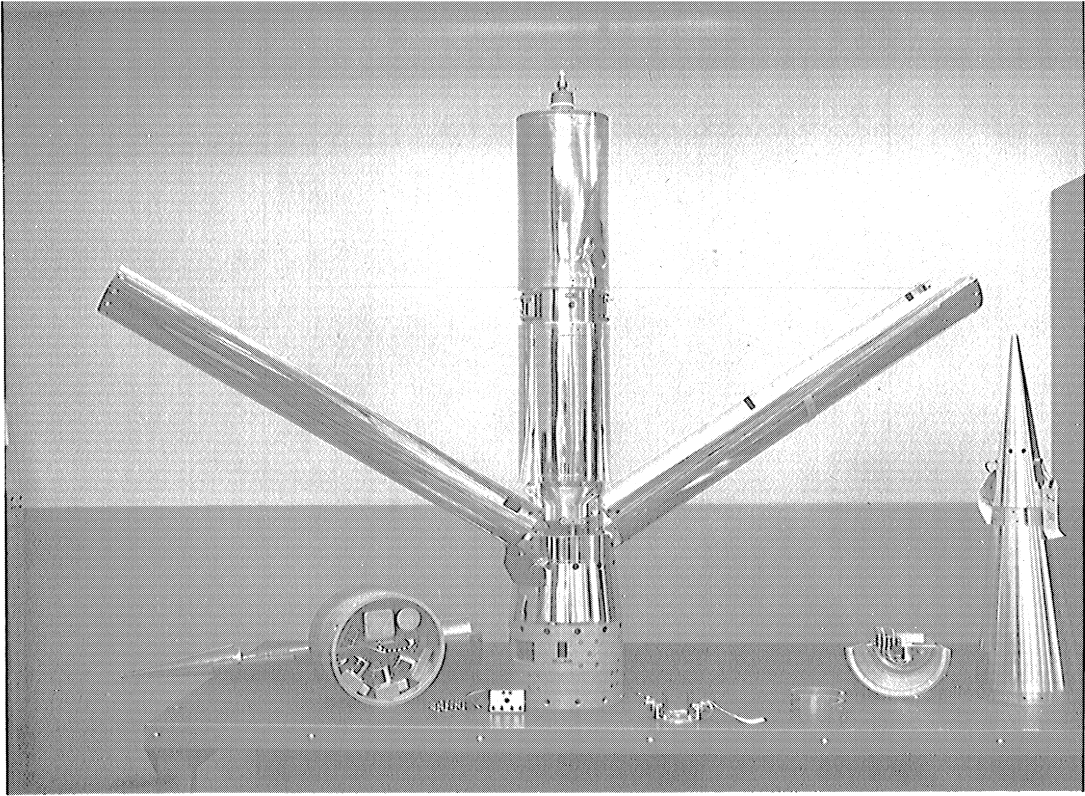
Figure 6. Thermosphere probe in nose cone.
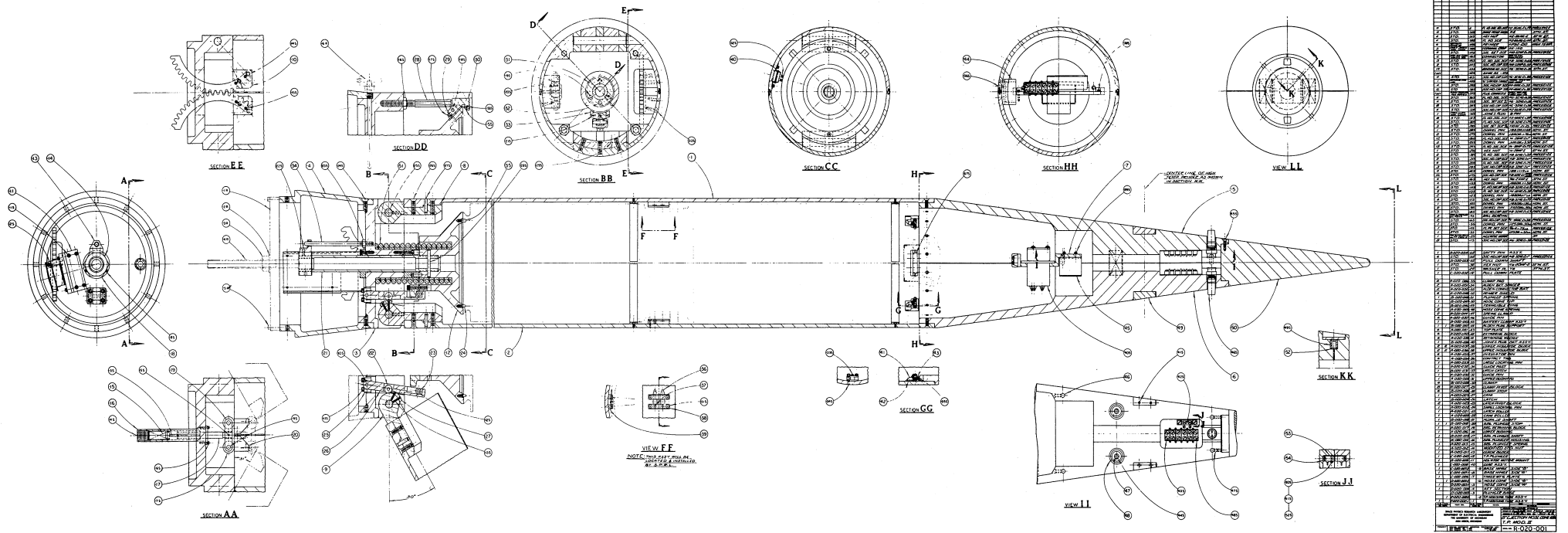
Figure 7. Assembly drawing, 8-in. nose cone.

6. MARSHALL-UNIVERSITY OF MICHIGAN PROBE (MUMP)

The MUMP, a cylinder 30.44 in. long and 7.25 in. in diameter, weighs 50 lb. The prime instruments for this payload are an omegatron mass analyzer and an electron temperature probe unit. Supporting instrumentation includes a lunar or solar aspect sensor for the determination of the TP aspect. The diagram in Figure 8 shows the instrumentation and supporting electronics location, and Figure 9 shows the block diagram. Figure 10 is a picture of the completely assembled TP.

6.1 OMEGATRON

The omegatron used in these payloads was of the type described by Niemann and Kennedy (1966). An expanded view of the system is shown in Figure 11. Tables 9 through 16 list the operating parameters of the gauge and associated electronics. The characteristics of the linear electrometer amplifier current detector, used to monitor the omegatron output current, are also listed.

These omegatrons are essentially identical to those flown previously on NASA's 18.02 and 18.03 (Taeusch and Carignan, 1966a,b). The breakoff unit, omegatron envelope, and omegatron magnet assembly are shown in Figures 12, 13, and 14.

The calibrations of all omegatrons were performed in December and January preceding the launch. The vacuum system used could accommodate four of the flight gauges at one time plus reference Bayard-Alpert ionization gauges used as secondary standards.

A two-stage oil diffusion pump vacuum system was used as a pressure calibration system. To obtain extremely low oil backstreaming, the second stage oil diffusion pump was equipped with a cold cap and two six-inch Granville-Phillips liquid N_2 cold traps. A typical background pressure, after the system has been baked at 360°C for 48 hours, was about 2×10^{-10} torr. Dry nitrogen was leaked into the system as a calibration gas. Calibration data were taken from background pressures to 3×10^{-5} torr. Above this pressure the omegatron becomes highly nonlinear.

Figure 15 is a photograph of an actual calibration set-up. Four omegatrons were calibrated at a time against four Bayard-Alpert ionization gauges (B-A gauges). The B-A gauges were used as secondary references. Two B-A gauges were previously calibrated by the Ball Brothers Corporation against a McLeod gauge. In order to provide continuity, one other gauge was used as reference from previous calibrations of earlier omegatron experiments. Since only four omegatrons could be calibrated at one time, to obtain an accurate

relative calibration of the omegatrons, combinations in pairs were used where each group was calibrated twice.

Gauge outputs and all critical supply voltages were printed by a datum system employing a 50 channel time multiplexer, an NLS integrating digital voltmeter, and a Hewlett-Packard printer. Also, all gauge outputs were analog-recorded on an eight-channel Sanborn recorder. After calibration, the omegatrons were prepared for pinch-off in pairs, and their output currents were compared at two different pressures. Thus it was determined that no damage had been done to the instrument during reassembly. Calibration curves of the omegatrons are shown in Figures 16-23. The omegatron currents were plotted against particle number densities which were calculated from the reference pressure values.

TABLE IX

OMEGATRON DATA

ETR 0381

MUMP 1

Omegatron Gauge Parameters:

Beam Current:	2.02	μamps
Electron Collector Bias:	77.65	volts
Filament Bias:	-91.50	volts
Cage Bias:	-0.194	volts
Top Bias:	-0.609	volts
RF Amplitude:		
M28	3.70	V_{p-p}
RF Frequency:		
M28	144.93	kHz

Monitor

Filament		
OFF:	0.114	V
ON:	3.183	V (steady)
Beam		
OFF:	0.266	V
ON:	3.114	V
Thermistor Pressure	Filament OFF:	4.368V
(zero pressure)	Filament ON:	4.013V
Bias:	4.024	V
RF:		
M28	3.740	V

Calibration

Sensitivity:	2.00×10^{-5} amps/torr
Maximum Linear Pressure (5%):	1.3×10^{-5} torr

TABLE IX (CONCLUDED)

Electrometer Amplifier

Range	Range Indicator	Range Resistor	M28ZPV
1	0.0 v	8.645×10^{9}	5.066
2	0.7 v	2.350×10^{10}	5.066
3	1.4 v	6.388×10^{10}	5.066
4	2.1 v	1.832×10^{11}	5.067
5	2.8 v	5.128×10^{11}	5.068
6	3.5 v	1.434×10^{12}	5.0714
7	4.2 v	4.047×10^{12}	5.0807
8	4.9 v	9.700×10^{12}	5.106

calibration voltage 0.571 v

Miscellaneous

+28 power current all on: 300ma
Preflight gauge pressure (N_2): 3.45×10^{-5} torr
Magnetic field strength: 2700 gauss

TABLE X

OMEGATRON DATA

ETR 0611

MUMP 2

Omegatron Gauge Parameters

Beam Current:	2.005	μamps
Electron Collector Bias:	77.22	volts
Filament Bias:	-92.87	volts
Cage Bias:	-0.209	volts
Top Bias:	-0.609	volts
RF Amplitude:		
M28	4.00	V_{p-p}
RF Frequency:		
M28	143.59	kHz

Monitor

Filament			
OFF:	0.106	V	
ON:	3.091	V	
Beam			
OFF:	0.678	V	
ON:	2.916	V	
Thermistor Pressure	Filament OFF:	2.140V	
(zero pressure)	Filament ON:	2.000V	
Bias:	4.082	V	
RF:			
M28	3.694	V	

Calibration

Sensitivity:	1.82×10^{-5}	amps/torr
Maximum Linear Pressure (5%):	9×10^{-6}	torr

TABLE X (CONCLUDED)

Electrometer Amplifier

Range	Range Indicator	Range Resistor	M28ZPV
1	0.0 v	9.119×10^9	4.884
2	0.7 v	2.479×10^{10}	4.884
3	1.4 v	6.738×10^{10}	4.884
4	2.1 v	1.832×10^{11}	4.884
5	2.8 v	4.979×10^{11}	4.885
6	3.5 v	1.353×10^{12}	4.887
7	4.2 v	4.047×10^{12}	4.897
8	4.9 v	1.00×10^{13}	4.902

calibration voltage 0.524 v

Miscellaneous

```
+28 power current all on:        370 ma
Preflight gauge pressure (N2):   5.9 x 10^-5 torr
Magnetic field strength:         2680 gauss
```

+28 power current all on: 370 ma

Preflight gauge pressure (N_2): 5.9×10^{-5} torr

Magnetic field strength: 2680 gauss

TABLE XI

OMEGATRON DATA

ETR 1165

MUMP 3

Omegatron Gauge Parameters

Beam Current:	1.99	µamps
Electron Collector Bias:	78.24	volts
Filament Bias:	-92.10	volts
Cage Bias:	-0.204	volts
Top Bias:	-0.602	volts
RF Amplitude:		
M28	4.00	V_{p-p}
RF Frequency:		
M28	140.06	kHz

Monitor

Filament		
OFF:	0.108	V
ON:	3.199	V
Beam		
OFF:	0.350	V
ON:	3.700	V
Thermistor Pressure:	Filament OFF:	2.333V
(zero pressure)	Filament ON:	2.110V
Bias:	4.129	V
RF:		
M28	3.548	V

Calibration

Sensitivity:	1.96×10^{-5}	amps/torr
Maximum Linear Pressure (5%):	1.2×10^{-5}	torr

29

TABLE XI (CONCLUDED)

Electrometer Amplifier

Range	Range Indicator	Range Resistor	M28ZPV
1	0.0 v	8.483×10^9	4.980
2	0.7 v	2.306×10^{10}	4.980
3	1.4 v	6.268×10^{10}	4.980
4	2.1 v	1.832×10^{11}	4.981
5	2.8 v	5.049×10^{11}	4.981
6	3.5 v	1.361×10^{12}	4.987
7	4.2 v	3.746×10^{12}	5.000
8	4.9 v	9.538×10^{12}	5.029

calibration voltage 0.577 volts

Miscellaneous

+28 power current all on: 375 ma

Preflight gauge pressure (N_2): 5.6×10^{-6} torr

Magnetic field strength: 2620 gauss

TABLE XII

OMEGATRON DATA

ETR 1494

MUMP 4

Omegatron Gauge Parameters

Beam Current:	2.00	µamps
Electron Collector Bias:	77.58	volts
Filament Bias:	-89.45	volts
Cage Bias:	-.2010	volts
Top Bias:	-.599	volts
RF Amplitude:		
M28	3.90	V_{p-p}
RF Frequency:		
M28	136.68	kHz

Monitor

Filament		
OFF:	.1104	V
ON:	3.165	V
Beam		
OFF:	0.270	V
ON:	3.454	V
Thermistor Pressure:	Filament OFF:	2.086V
(zero pressure)	Filament ON:	1.917V
Bias:	4.093	V
RF:		
M28	3.698	V

Calibration

Sensitivity:	2.03×10^{-5} amps/torr
Maximum Linear Pressure (5%):	7×10^{-6} torr

TABLE XII (CONCLUDED)

Electrometer Amplifier

Range	Range Indicator	Range Resistor	M28 ZPV
1	0.0 v	9.119×10^{9}	5.003
2	0.7 v	2.479×10^{10}	5.003
3	1.4 v	6.738×10^{10}	5.003
4	2.1 v	1.832×10^{11}	5.0015
5	2.8 v	4.979×10^{11}	4.999
6	3.5 v	1.353×10^{12}	4.987
7	4.2 v	3.679×10^{12}	4.973
8	4.9 v	1.000×10^{13}	4.918

calibration voltage 0.663 v

Miscellaneous

+29 power current all on:	320 ma
Preflight gauge pressure (N_2):	14×10^{-5} torr
Magnetic field strength:	2540 gauss

TABLE XIII

OMEGATRON DATA

ETR 4803

MUMP 5

Omegatron Gauge Parameters

Beam Current:	2.005	μamps
Electron Collector Bias:	77.45	volts
Filament Bias:	-89.27	volts
Cage Bias:	-0.204	volts
Top Bias:	-0.604	volts
RF Amplitude:		
M28	3.98	V_{p-p}
RF Frequency:		
M28	143.43	kHz

Monitor

Filament
OFF:	0.115 V
ON:	3.036 V

Beam
OFF:	0.525 V
ON:	3.471 V

Thermistor Pressure:	Filament OFF:	3.027V
(zero pressure)	Filament ON:	2.860V
Bias:	4.115 V	
RF:		
M28	3.376 V	

Calibration

Sensitivity:	1.90×10^{-5} amps/torr
Maximum Linear Pressure (5%):	6×10^{-6} torr

TABLE XIII (CONCLUDED)

Electrometer Amplifier

Range	Range Indicator	Range Resistor	M28ZPV
1	0.0 v	9.119×10^{9}	4.964
2	0.7 v	2.479×10^{10}	4.964
3	1.4 v	6.738×10^{10}	4.964
4	2.1 v	1.832×10^{11}	4.963
5	2.8 v	4.979×10^{11}	4.962
6	3.5 v	1.258×10^{12}	4.96
7	4.2 v	3.863×10^{12}	4.950
8	4.9 v	1.130×10^{13}	4.926

calibration voltage 0.586 volts

Miscellaneous

+28 power current all on: 390 ma
Preflight gauge pressure (N_2): 3.33×10^{-5} torr
Magnetic field strength: 2660 gauss

TABLE XIV

OMEGATRON DATA

ETR 1828

MUMP 6

Omegatron Gauge Parameters

Beam Current:	2.02	μamps
Electron Collector Bias:	76.5	volts
Filament Bias:	-89.95	volts
Cage Bias:	-0.206	volts
Top Bias:	-0.613	volts
RF Amplitude:		
M28	4.00	V_{p-p}
RF Frequency:		
M28	139.12	kHz

Monitor

Filament		
OFF:	0.113	V
ON:	2.900	V
Beam		
OFF:	0.600	V
ON:	3.880	V
Thermistor Pressure:	Filament OFF:	2.283V
(zero pressure)	Filament ON:	2.136V
Bias:	3.833	V
RF:		
M28	3.797	V

Calibration

Sensitivity:	2.23×10^{-5}	amps/torr
Maximum Linear Pressure (5%):	8×10^{-6}	torr

TABLE XIV (CONCLUDED)

Electrometer Amplifier

Range	Range Indicator	Range Resistor	M28ZPV
1	0.0 v	9.119×10^9	5.028
2	0.7 v	2.479×10^{10}	5.028
3	1.4 v	6.738×10^{10}	5.028
4	2.1 v	1.832×10^{11}	5.029
5	2.8 v	5.037×10^{11}	5.030
6	3.5 v	1.435×10^{12}	5.034
7	4.2 v	4.016×10^{12}	5.046
8	4.9 v	1.077×10^{13}	5.073

calibration voltage 0.648 v

Miscellaneous

+28 power current all on: 320 ma
Preflight gauge pressure (N_2): 3.45×10^{-5} torr
Magnetic field strength: 2600 gauss

TABLE XV

OMEGATRON DATA

ETR 0851

MUMP 7

Omegatron Gauge Parameters

Beam Current:	1.99	μ amps
Electron Collector Bias:	78.24	volts
Filament Bias:	-92.02	volts
Cage Bias:	-0.205	volts
Top Bias:	-0.601	volts
RF Amplitude:		
M28	4.00	V_{p-p}
RF Frequency:		
M28	143.23	kHz

Monitor

Filament		
OFF:	0.112	V
ON:	3.436	V
Beam:		
OFF:	0.642	V
ON:	3.886	V
Thermistor Pressure:	Filament OFF:	1.842V
(zero pressure)	Filament ON:	1.696V
Bias:	4.099	V
RF:		
M28	3.392	V

Calibration

Sensitivity:	2.03×10^{-5} amps/torr
Maximum Linear Pressure (5%):	7×10^{-6} torr

TABLE XV (CONCLUDED)

Electrometer Amplifier

Range	Range Indicator	Range Resistor	M28ZPV
1	0.0 v	9.119×10^9	5.062
2	0.7 v	2.479×10^{10}	5.062
3	1.4 v	6.738×10^{10}	5.062
4	2.1 v	1.832×10^{11}	5.062
5	2.8 v	4.979×10^{11}	5.062
6	3.5 v	1.353×10^{12}	5.061
7	4.2 v	4.075×10^{12}	5.061
8	4.9 v	1.123×10^{13}	5.057

calibration voltage 0.622 v

Miscellaneous

+28 power current all on: 400 ma
Preflight gauge pressure (N_2): 2.5×10^{-5} torr
Magnetic field strength: 2660 gauss

TABLE XVI

OMEGATRON DATA

ETR 1474

MUMP 8

Omegatron Gauge Parameters

Beam Current:	2.00	μamps
Electron Collector Bias:	78.70	volts
Filament Bias:	-89.80	volts
Cage Bias:	-.197	volts
Top Bias:	-.596	volts
RF Amplitude:		
M28	4.00	V_{p-p}
RF Frequency:		
M28	143.42	kHz

Monitor

Filament				
OFF:	.1025	V		
ON:	3.324	V		
Beam				
OFF:	.8460	V		
ON:	4.129	V		
Thermistor Pressure:	Filament OFF:	2.119V		
(zero pressure)	Filament ON:	1.874V		
Bias:	4.188	V		
RF:				
M28	3.625	V		

Calibration

Sensitivity:	2.12×10^{-5} amps/torr
Maximum Linear Pressure (5%):	9×10^{-6} torr

TABLE XVI (CONCLUDED)

Electrometer Amplifier

Range	Range Indicator	Range Resistor	M28ZPV
1	0.0 v	9.119×10^9	4.978
2	0.7 v	2.479×10^{10}	4.978
3	1.4 v	6.738×10^{10}	4.978
4	2.1 v	1.832×10^{11}	4.9771
5	2.8 v	4.953×10^{11}	4.9715
6	3.5 v	1.330×10^{12}	4.9712
7	4.2 v	3.374×10^{12}	4.9613
8	4.9 v	9.087×10^{12}	4.954

calibration voltage 0.459 v

Miscellaneous

+28 power current all on: 338 ma
Preflight gauge pressure (N_2): 3.8×10^{-5} torr
Magnetic field strength: 2680 gauss
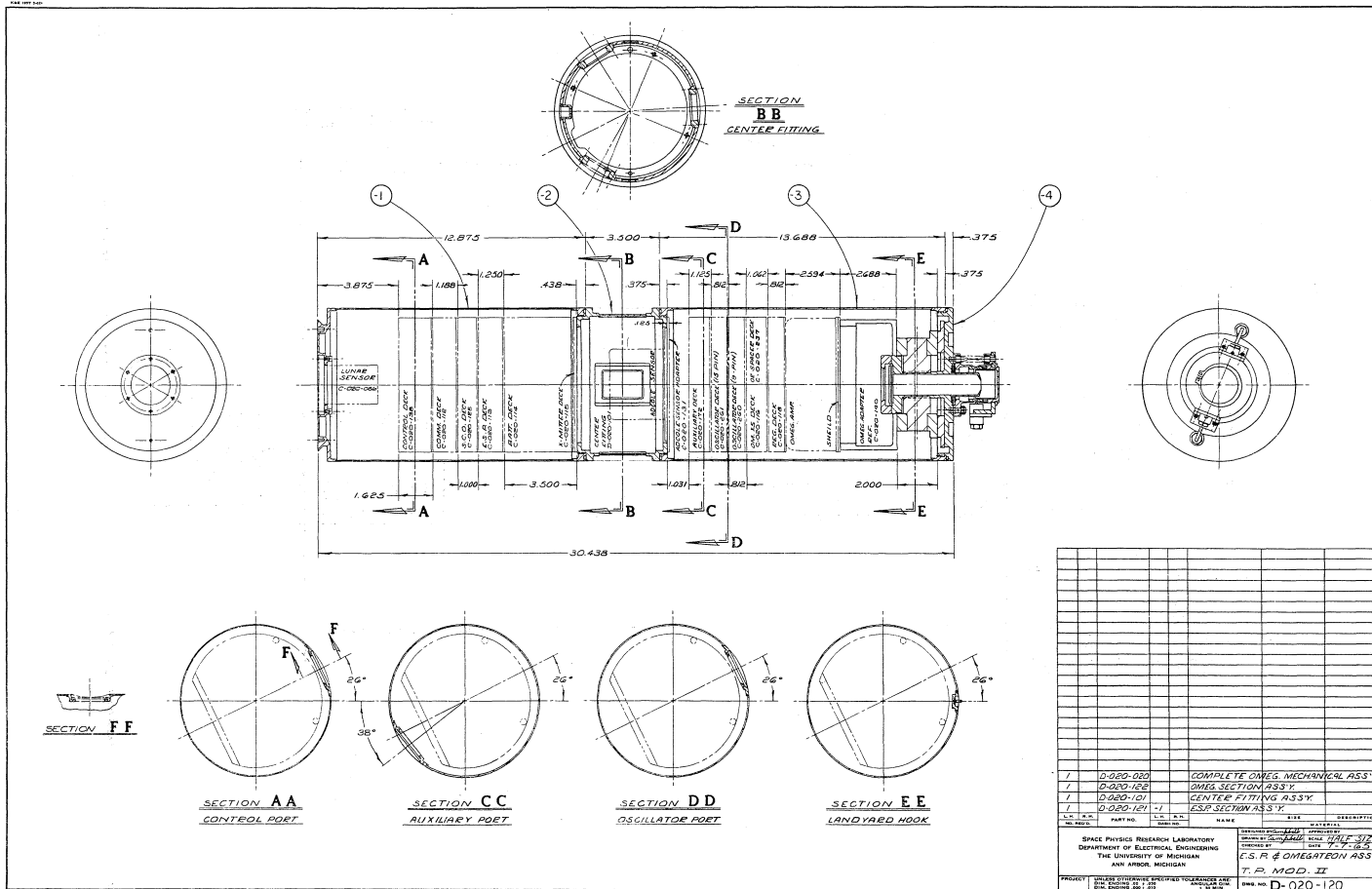
Figure 8. Thermosphere probe assembly.

PULL OFFS

po2 po3 po4   po1

ledex
control

OMEGATRON SYSTEM
amplifier
oscillator
filament regulator
gage
mass timer

OM SCO
CALIBRATOR

VECTOR SCO's

70KC   OM

monitor

CONTROL LEDEX

voltage monitors

amp control

filament control

RAYMOND
TIMER

OM
BREAKOFF

REFERENCE
VOLTAGES

OM POWER

control

POWER CONTROL

ELECTROSTATIC

PROBE SYSTEM

COMMUTATOR

7.35KC   COMM

VECTOR
2 WATT
TRANSMITTER
231.4 m c

ext. power

40KC   ESP-D

22KC   ESP-F

INTERNAL
POWER

19-HR-1's

ADCOLE   SPRL
SOLAR   LUNAR
            OR
ASPECT   ASPECT
SYSTEM   SYSTEM

10.5 kc ASPECT

XTMR POWER

ESP/COMM/ASPECT POWER

Figure 9. Block diagram (lunar and solar).
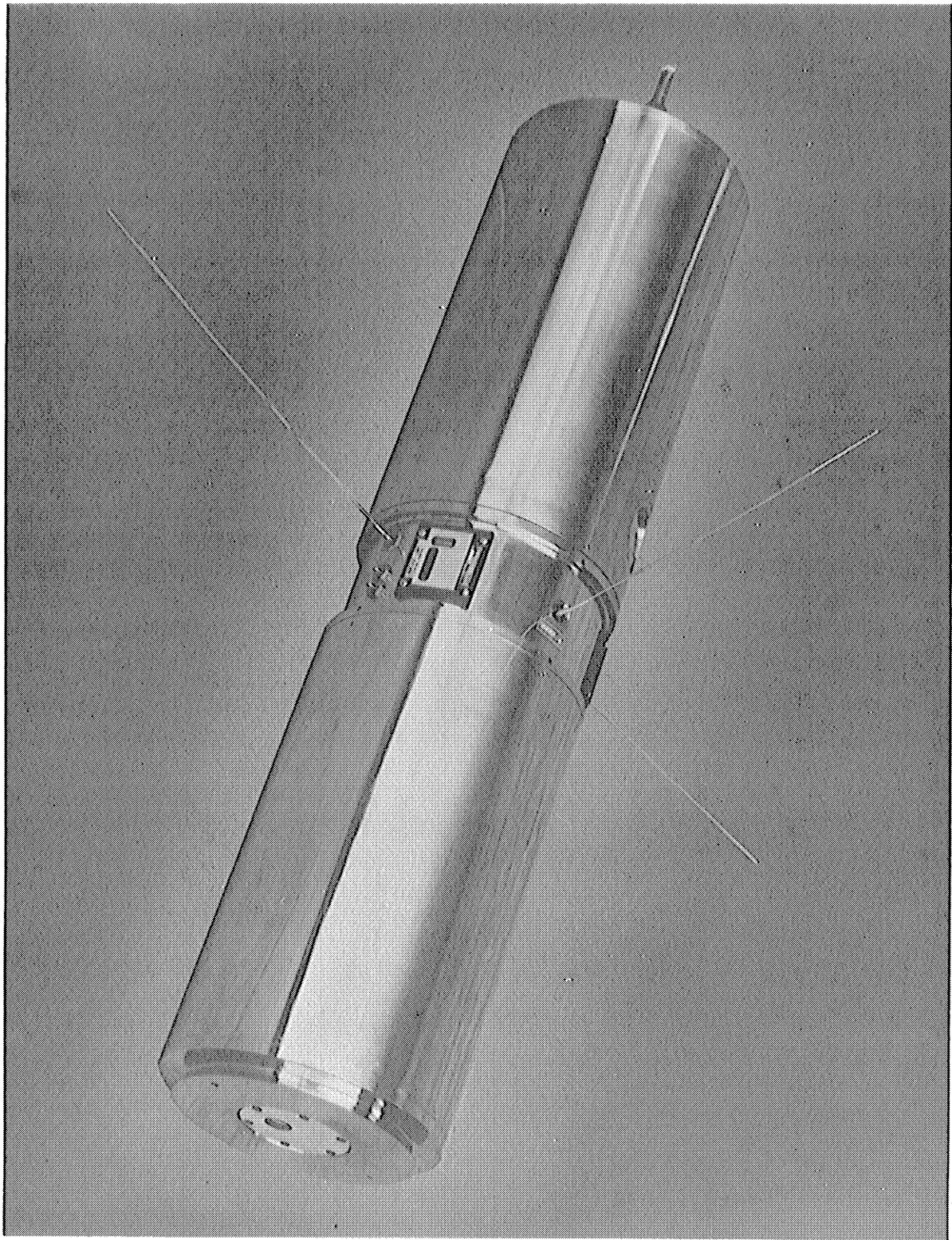
Figure 10. Assembled thermosphere probe.

28 &WO FREQUENCY

28 AMPLITUDE

BIAS ADJUST

BEAM ADJUST

MU-METAL

OSCILLATOR DECK

SPACER

REGULATOR DECK

OMEGATRON AMPLIFIER

AUXILIARY DECK

OMEGATRON ADAPTER

OM ENVELOPE

BREAK-OFF CONFLAT FLANGE

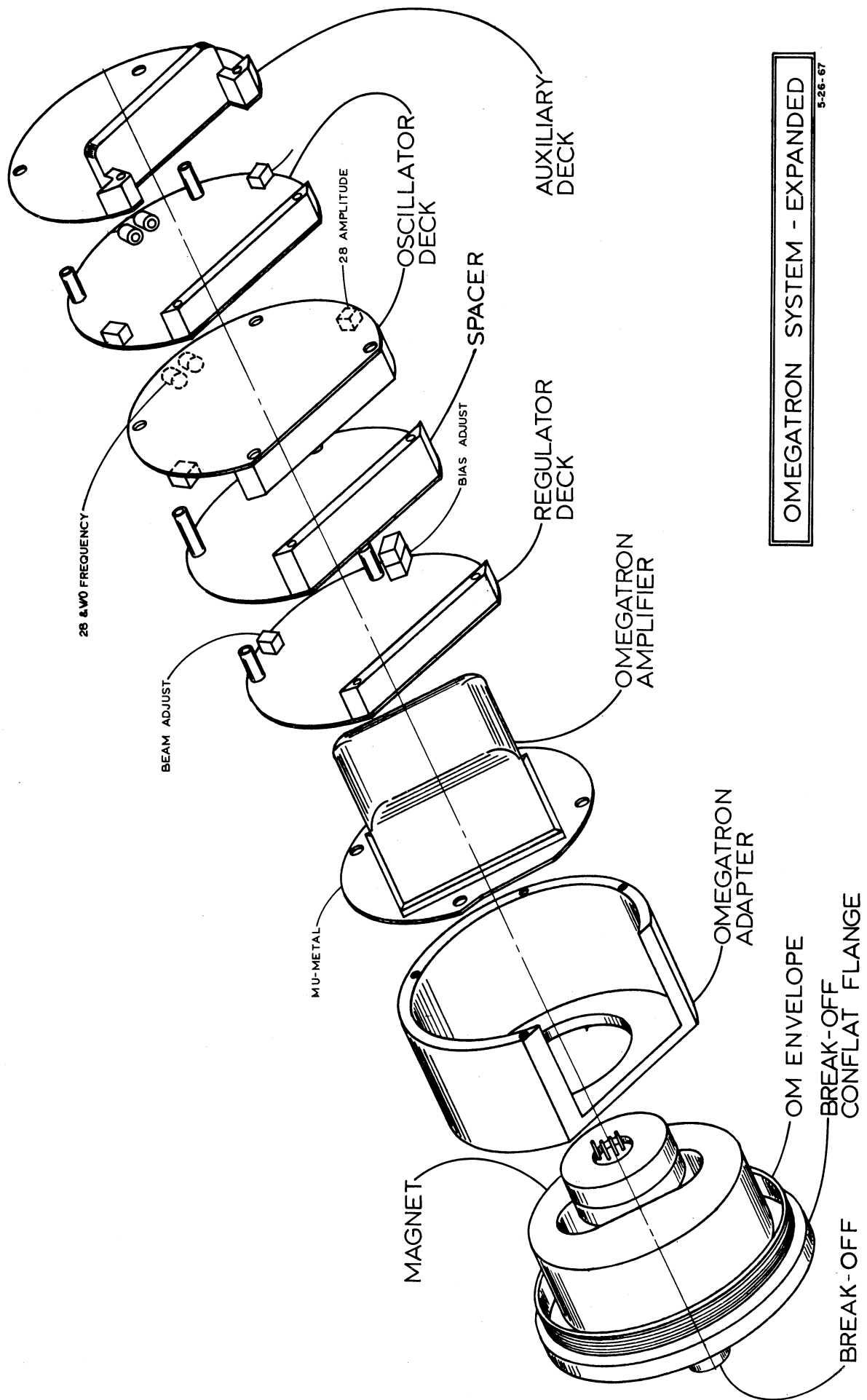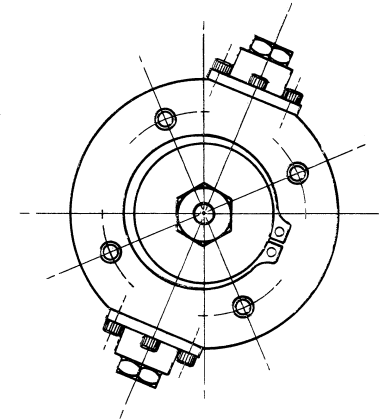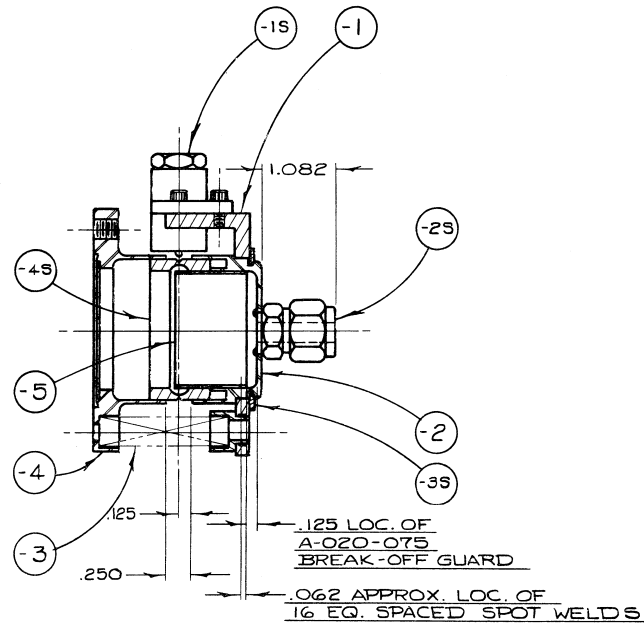BREAK-OFF

MAGNET

OMEGATRON SYSTEM - EXPANDED

5-26-67

Figure 11. Omegatron expanded view.

44

OPERATION PROCEDURE

1. MACHINE C-020-074-BREAK-OFF BASE WITHOUT
   CONFLAT GROOVE.
2. MACHINE C-020-077-BREAK-OFF HAT & HELI-ARC WELD
   MODIFIED CRAWFORD SWAGELOK #600-1-4W-316 TO HAT.
   LEAK CHECK HELI-ARC WELD - MUST BE VACUUM TIGHT.
3. SEND DETAILS C-020-074 & C-020-077 TO COORS PORCELIN
   CO. TO BRAZE COORS' BREAK-OFF CERAMIC SEAL RING TO
   DETAILS C-020-074 & C-020-077.
4. SPOT WELD A-020-075-BREAK-OFF GUARD TO C-020-077-
   BREAK-OFF HAT AT U. OF M. AFTER BRAZING OF CERAMIC SEAL.
5. LEAK CHECK COMPLETE UNIT.
6. FINAL MACHINING OF CONFLAT GROOVE ON C-020-074-
   BREAK-OFF BASE.

1.082

.125 LOC. OF
A-020-075
BREAK-OFF GUARD

.062 APPROX. LOC. OF
16 EQ. SPACED SPOT WELDS

.125
.250

L.H.	R.H.	PART NO.		NAME	MATERIAL
1			-4S	BREAK-OFF CERAMIC	COORS PORCELIN CO.
1		WALDES KOHINOOR #5102-168	-3S	RETAINING RING	TRUARC
1		#600-1-4W-316	-2S	CRAWFORD FITTING CO.	SWAGELOK (MOD.)
2		CONAX CORP. #1617-031-01	-1S	LINEAR ACTUATOR	
1		A-020-075	-5	BREAK-OFF GUARD	
1		C-020-074	-4	BREAK-OFF BASE	
4		A-020-079	-3	OMEGATRON BREAK-OFF	SPRING
1		C-020-077	-2	BREAK-OFF HAT	
1		C-020-078	-1	BREAK-OFF ACTUATOR ASS'Y.	

| L.H. | R.H. | PART NO. | L.H. | R.H. | NAME | SIZE | DESCRIPTION |
| NO. REQ'D. | | | DASH NO. | | | MATERIAL | |

SPACE PHYSICS RESEARCH LABORATORY
DEPARTMENT OF ELECTRICAL ENGINEERING
THE UNIVERSITY OF MICHIGAN
ANN ARBOR, MICHIGAN

DESIGNED BY		APPROVED BY	
DRAWN BY BILL MEYER	SCALE FULL
CHECKED BY	DATE 8-18-65

BREAK-OFF PROCEDURE
ASS'Y.
OMEGATRON T.P. MOD. II

PROJECT | UNLESS OTHERWISE SPECIFIED TOLERANCES ARE:
DIM. ENDING .00 ± .030   ANGULAR DIM.
DIM. ENDING .000 ± .010   ± 30 MIN.

DWG. NO. C-020-073

Figure 12. Omegatron breakoff unit.

45

Figure 13. Omegatron envelope.

.343-O.D. AND .260 I.D. TUBE
TO BE SNUG S.F. IN BOTH
SIDES OF MAGNETS
AS SHOWN 2 PLACES

±.004
4.750 CENT.

1.500
FOR TUBING
ONLY

15° TYP.

.062 TYP.

±.005
1.000 CENT.

.188 DIA. S.F. FOR DOWEL
NOTE: THESE HOLES TO
MATCH PINS ON DWG.
C-020-103

.210 DIA. THRU
2 HOLES TYP.

NOTE:
WORK TO BE DONE ON
G.E. MAGNETS WHICH WILL
BE FURNISHED BY U OF M.
1. MAGNETS ARE IN (2) PARTS
   SPLIT ON VERTICAL ₵
2. E.D.M. (2) HOLES IN EACH
   MAGNET FOR -2 (TO BE IN
   LINE)
3. E.D.M. (2) .188 DIA. HOLES
4. E.D.M. (4) .210 DIA. HOLES
5. MATERIAL ON MAGNET
   WHERE -1 IS SHOWN
   TO BE REMOVED BY
   GRINDING (IT IS THE
   SAME AREA TAKEN UP
   BY -1)
6. BOTTOM, TOP & SURFACES
   WHERE MAGNET FITS
   TOGETHER TO BE
   GROUND FLAT &
   SQUARE.

-3S   -2   -2S   -1   -1S

.030
.040 RAD. TOP & BOTTOM

1.188 DIA. P.F.   1.312 DIA.

.250

.375

±.001
.562

±.002
1.125

±.005
5.125 CENT.

.375 REF.

1.000

2.000 REF.

MODIFIED G.E. MAGNET
DWG. 5E159B, AS SHOWN

NO. REQ'D.		PART NO.	DASH NO.	NAME	SIZE	DESCRIPTION
2	STD.		-3S	HEX. NUT	1/4-28NF-2	PARKERIZE
4	STD.		-2S	LOCK WASHER	1/4"	PARKERIZE
2	STD.		-1S	SOC. HD. CAP SCR.	1/4-28NF-2×2.00	PARKERIZE
2			-2	SLEEVE	.260 I.D. .343 O.D. ×1.500	C.R.S.
2			-1	POLE CAP	.375×1.312 DIA.	C.R.S.

SPACE PHYSICS RESEARCH LABORATORY
DEPARTMENT OF ELECTRICAL ENGINEERING
THE UNIVERSITY OF MICHIGAN
ANN ARBOR, MICHIGAN

DESIGNED BY
DRAWN BY BIHLMEYER   SCALE FULL SIZE
CHECKED BY   DATE 9-27-65
APPROVED BY

"E" MAGNET MODIFICATIONS
OMEGATRON MAGNET
OMEGATRON, T.P. MOD. II

PROJECT

UNLESS OTHERWISE SPECIFIED TOLERANCES ARE:
DIM. ENDING .00 ± .030   ANGULAR DIM.
DIM. ENDING .000 ± .010   ± 30 MIN.

DWG. NO. C-020-178

Figure 14. Omegatron magnet assembly

47
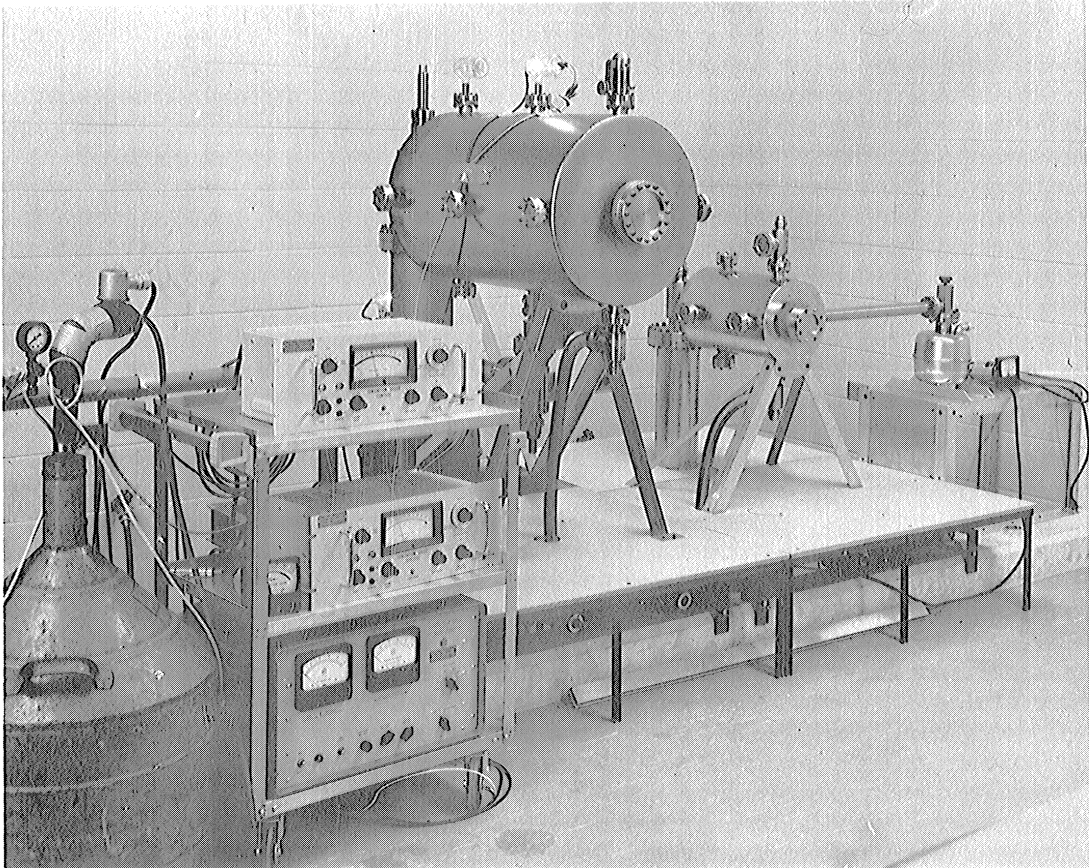
Figure 15. Calibration system.
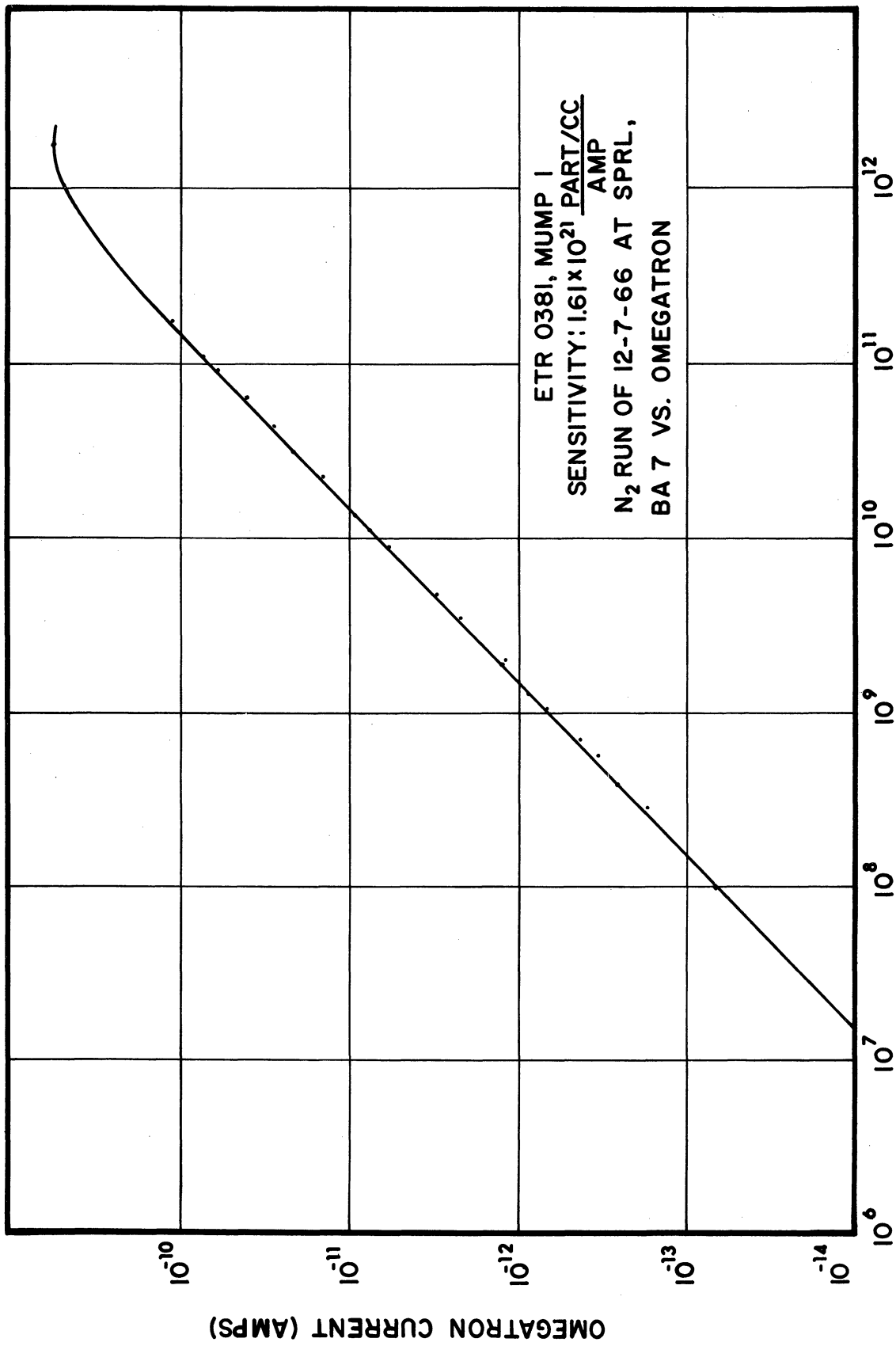
NUMBER DENSITY (PART/CC)
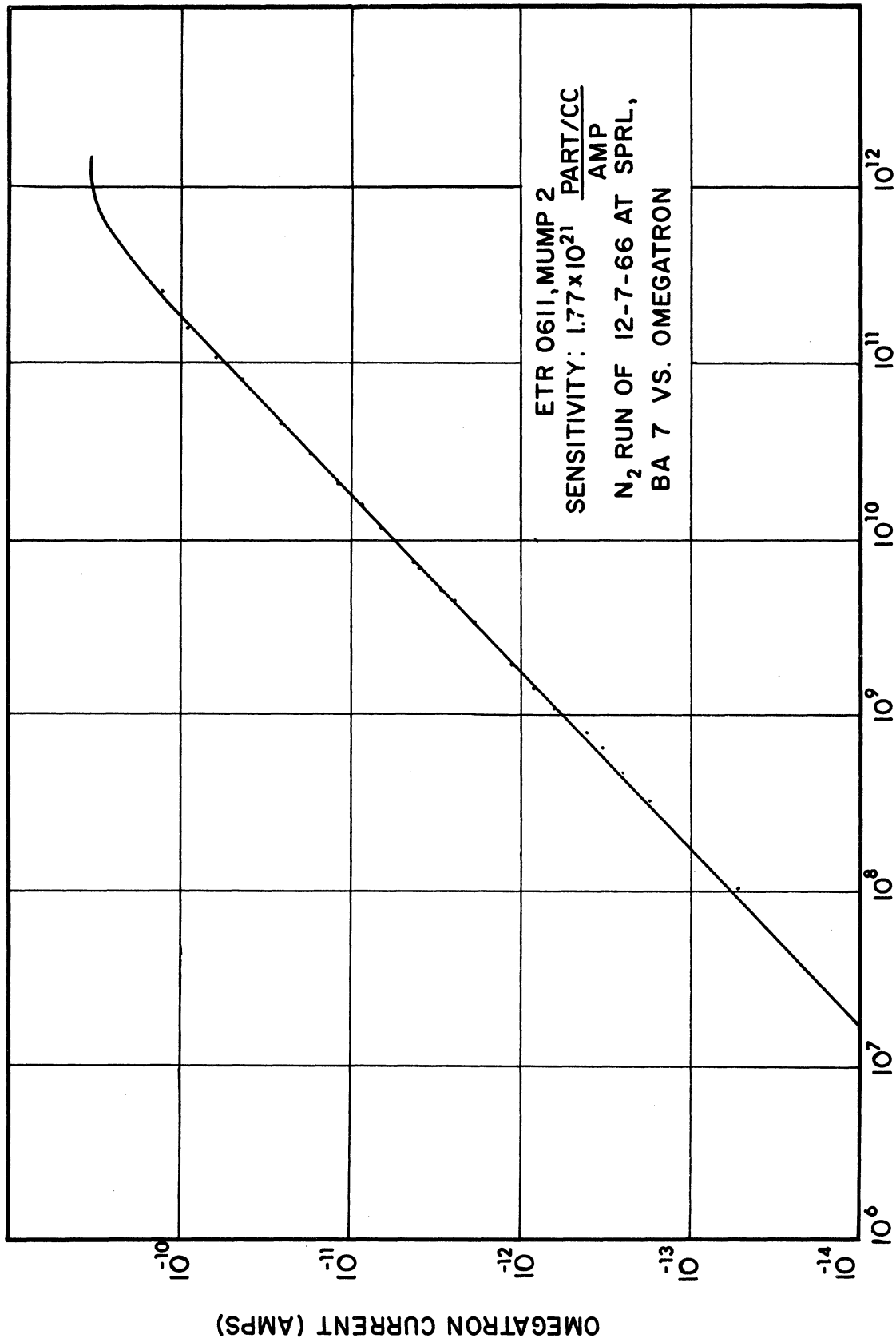
ETR 0381, MUMP I

SENSITIVITY: $1.61 \times 10^{21} \dfrac{\text{PART/CC}}{\text{AMP}}$

N_2 RUN OF 12-7-66 AT SPRL,
BA 7 VS. OMEGATRON

OMEGATRON CURRENT (AMPS)

3-30-67

Figure 16. Omegatron calibration of MUMP 1.

49

NUMBER DENSITY (PART/CC)

ETR 0611, MUMP 2

SENSITIVITY: 1.77×10^{21} $\dfrac{\text{PART/CC}}{\text{AMP}}$

N_2 RUN OF 12-7-66 AT SPRL,
BA 7 VS. OMEGATRON

OMEGATRON CURRENT (AMPS)

6-12-67

Figure 17. Omegatron calibration of MUMP 2.

50

Figure 18. Omegatron calibration of MUMP 3.

51

ETR 1942, MUMP 4
SENSITIVTY: 1.61×10^{21} PART/CC/AMP
2ND N_2 RUN OF 3-29-67, AT SPRL
OMEGATRON VS BA7

NUMBER DENSITY (PART/CC)

OMEGATRON CURRENT (AMPS)

6-2-67

Figure 19. Omegatron calibration of MUMP 4.

52

ETR 4803, MUMP 5
SENSITIVITY: 1.69×10^{21} PART/CC/AMP
2ND N_2 RUN OF 3-29-67, AT SPRL
OMEGATRON VS BA7

NUMBER DENSITY (PART/CC)

OMEGATRON CURRENT (AMPS)

6-2-67
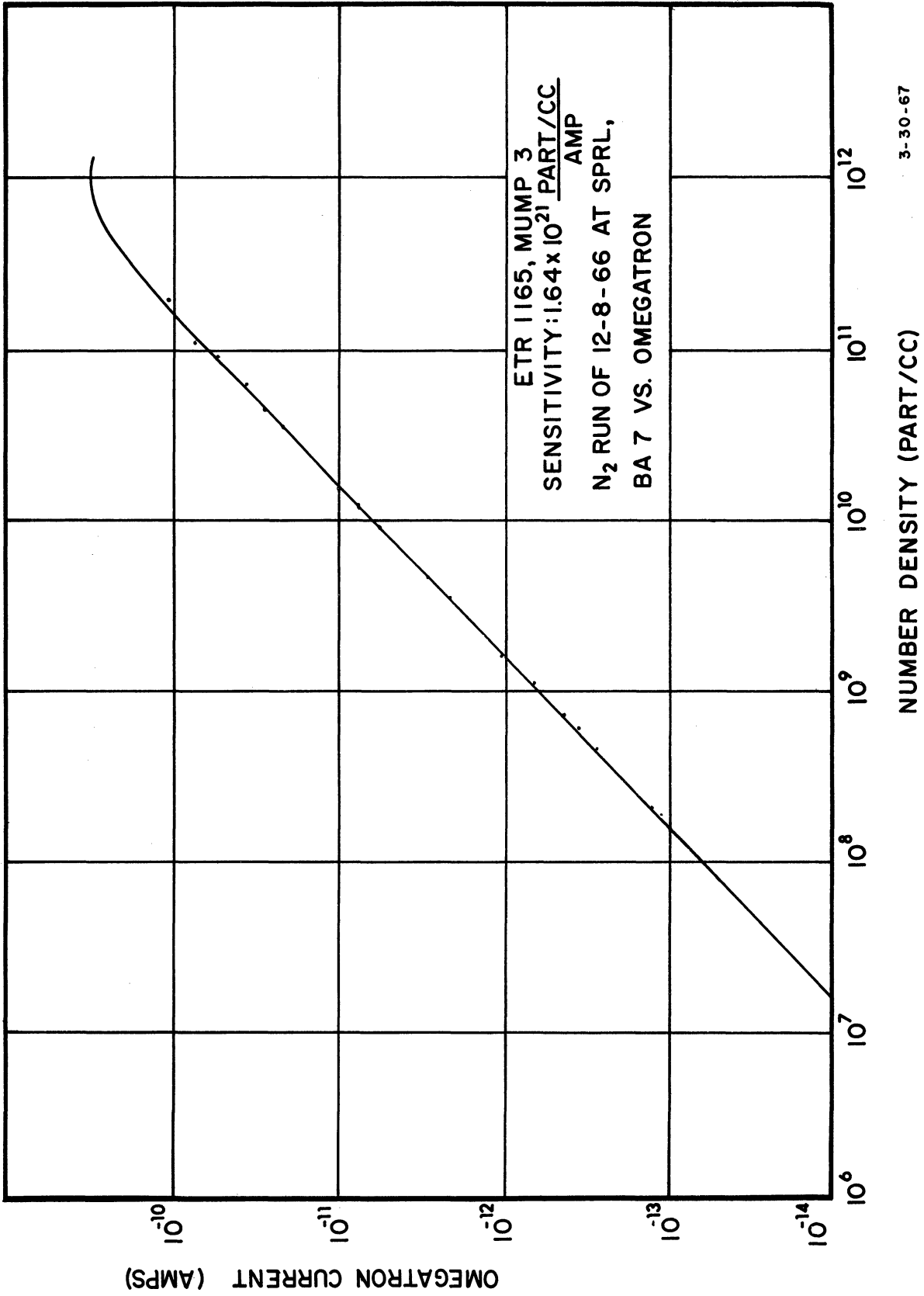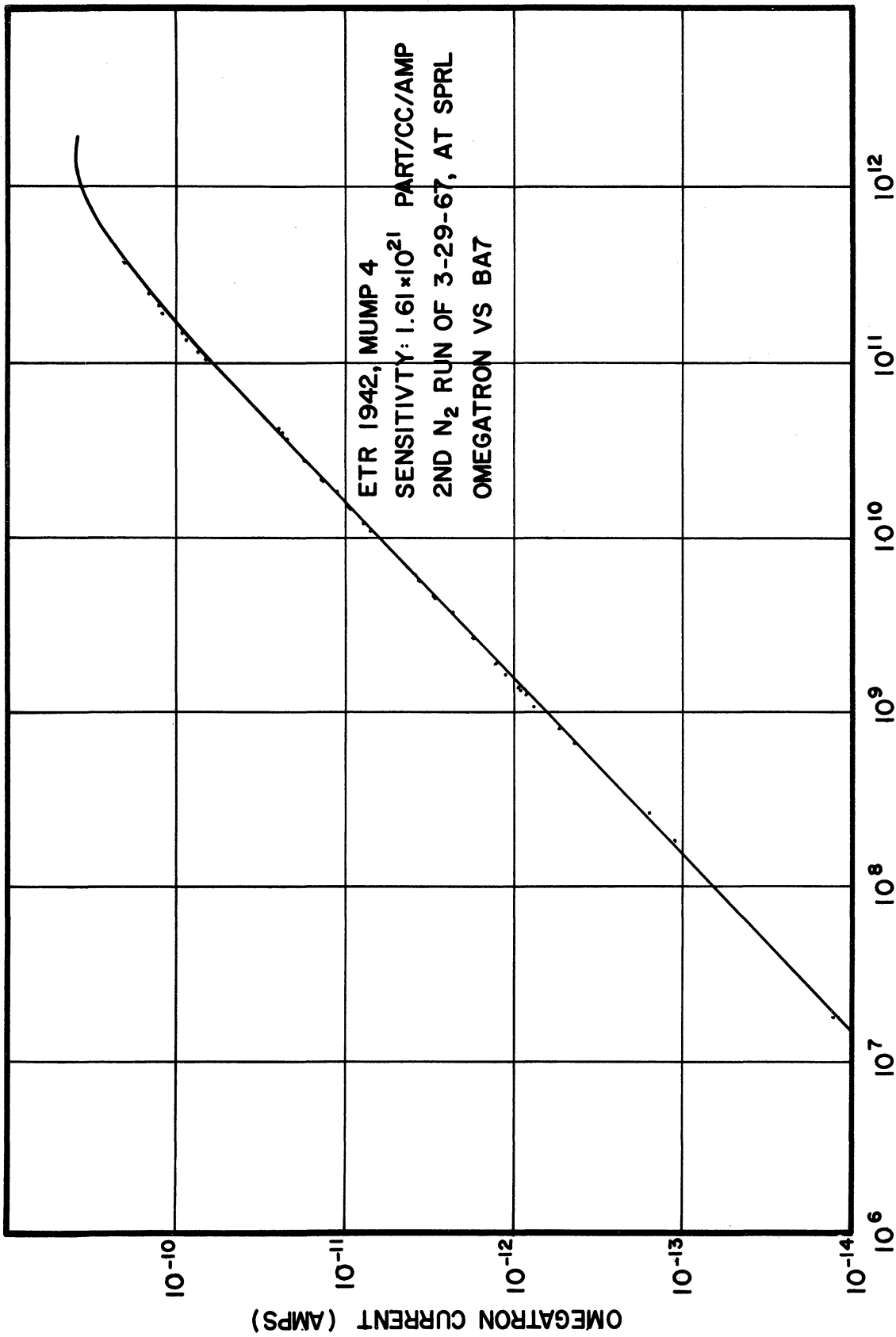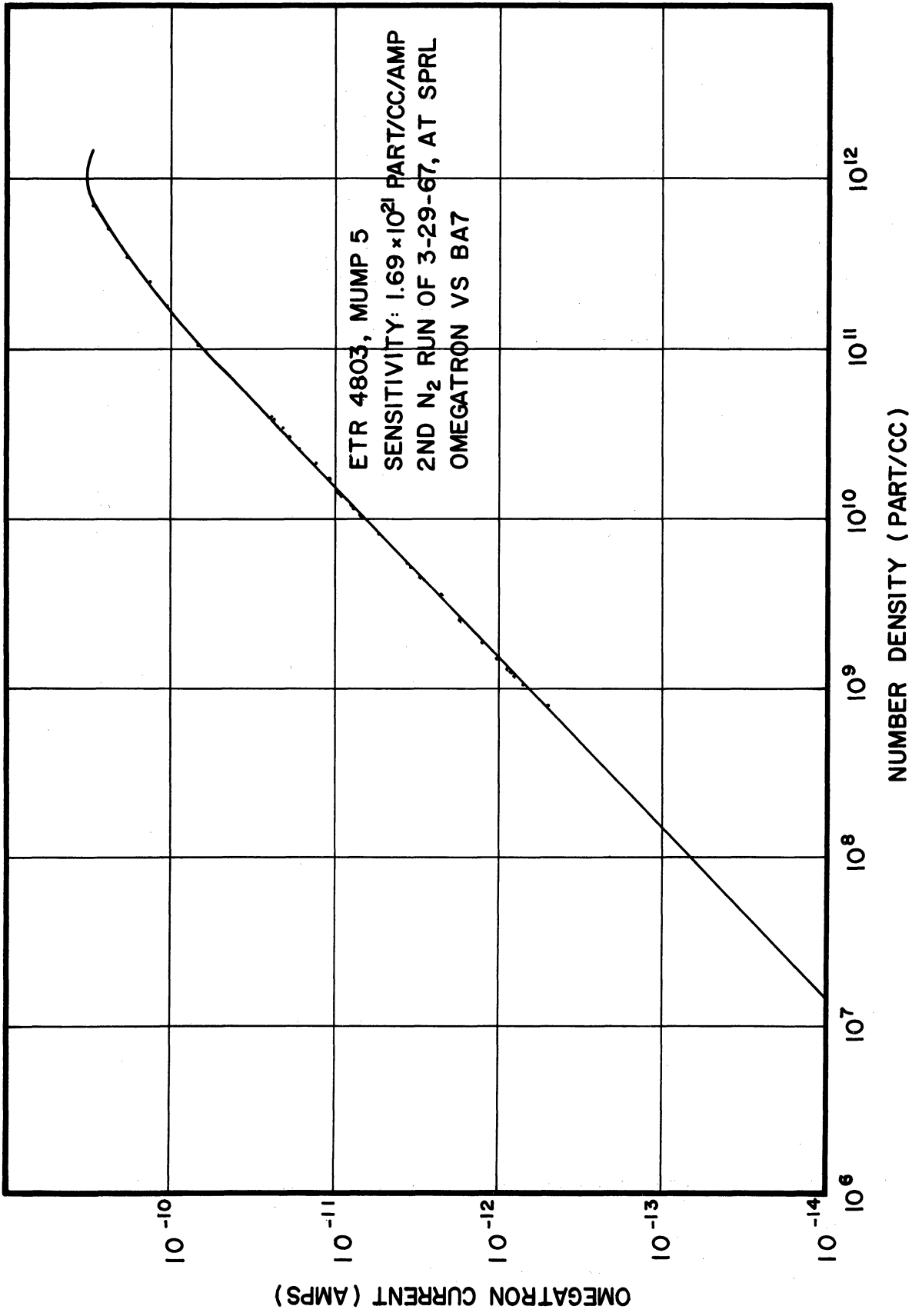
Figure 20. Omegatron calibration of MUMP 5.

Figure 21. Omegatron calibration of MUMP 6.

ETR 1828, MUMP 6

SENSITIVITY: $1.44 \times 10^{21} \dfrac{\text{PART./CC}}{\text{AMP}}$

2nd N RUN OF 12-1-66 AT SPRL
BA NO. 7 VS. OMEGATRON

3-31-67

NUMBER DENSITY (PART./CC)

OMEGATRON CURRENT (AMPS)

54
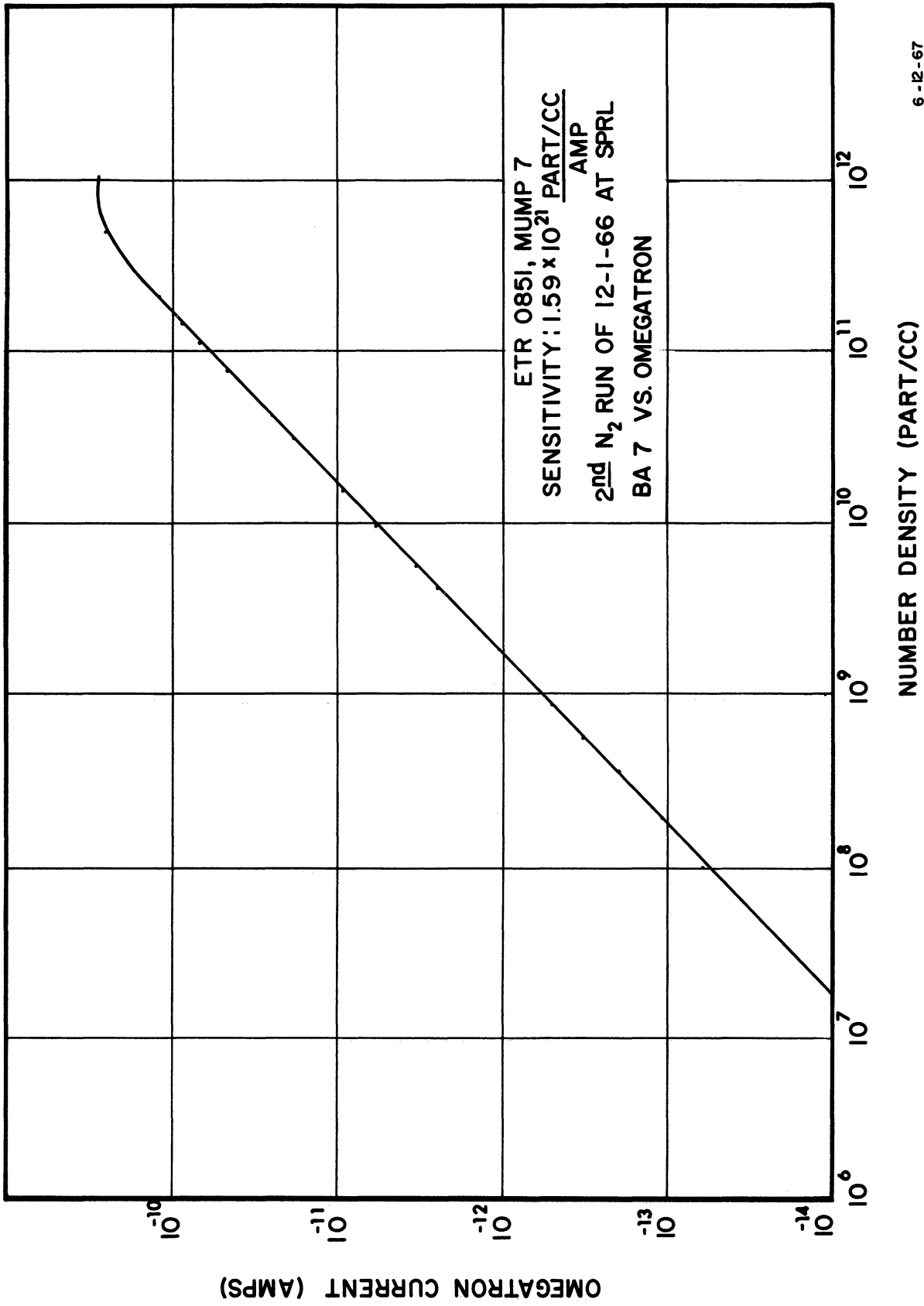
Figure 22. Omegatron calibration of MUMP 7.

NUMBER DENSITY (PART/CC)

OMEGATRON CURRENT (AMPS)

ETR 0851, MUMP 7
SENSITIVITY: 1.59×10^{21} $\dfrac{\text{PART/CC}}{\text{AMP}}$
$2\underline{\text{nd}}$ N_2 RUN OF 12-1-66 AT SPRL
BA 7 VS. OMEGATRON

6-12-67

55
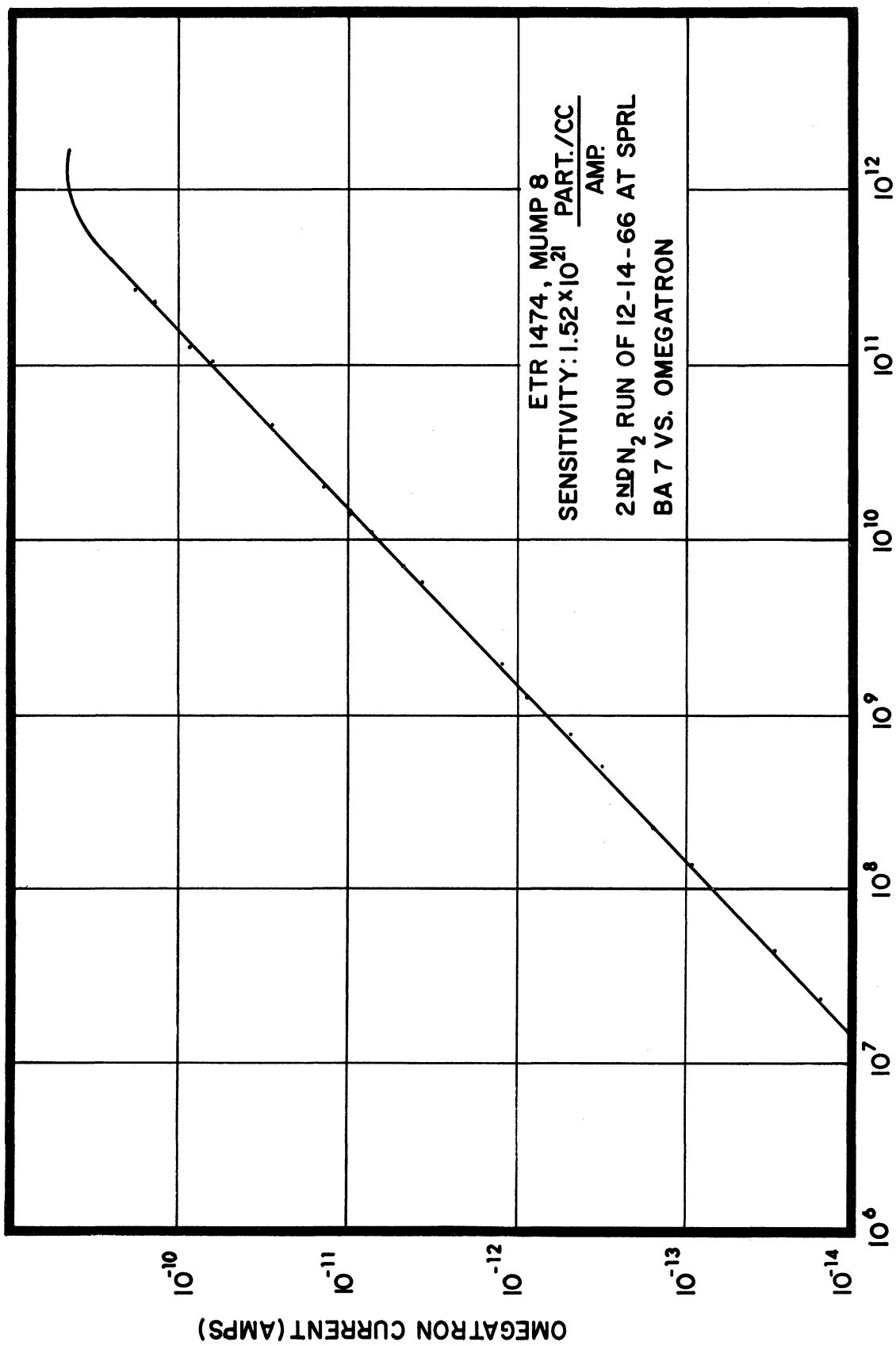
Figure 23. Omegatron calibration of MUMP 8.

3-30-67

56

6.2 ELECTROSTATIC PROBE (ESP)

The electrostatic probe (ESP) system described consists of a cylindrical Langmuir probe, shown in Figure 24, which is immersed in the plasma, and an electronics unit which measures the current collected by the probe.

The electronics unit consists of a dc-dc converter, a ramp voltage generator, a three-range current detector, range switching relays, and associated logic circuitry. The electronics unit has two output channels, a data channel, and a computer channel. The data channel output is a voltage proportional to the collected probe current. The computer channel contains information on detector ranges, system calibration, and ramp voltage levels which allows data reduction by computer methods. System timing and the computer channel format are given in Figure 25.

The following are the specifications of the ESP system for Mump 1 through 8:

(1) **Input Power**

1.54 watts at 28 volts

(2)

Sensitivity	Mumps 1, 2, 3, 5	Mumps 4, 6, 7, 8
Range 1	20 μa Full Scale*	10 μa Full Scale
Range 2	2.0 μa Full Scale	1.0 μa Full Scale
Range 3	0.2 μa Full Scale	0.1 μa Full Scale

*Full scale output is defined as the +4.0 v from the 0.5 v output bias level.

(3)

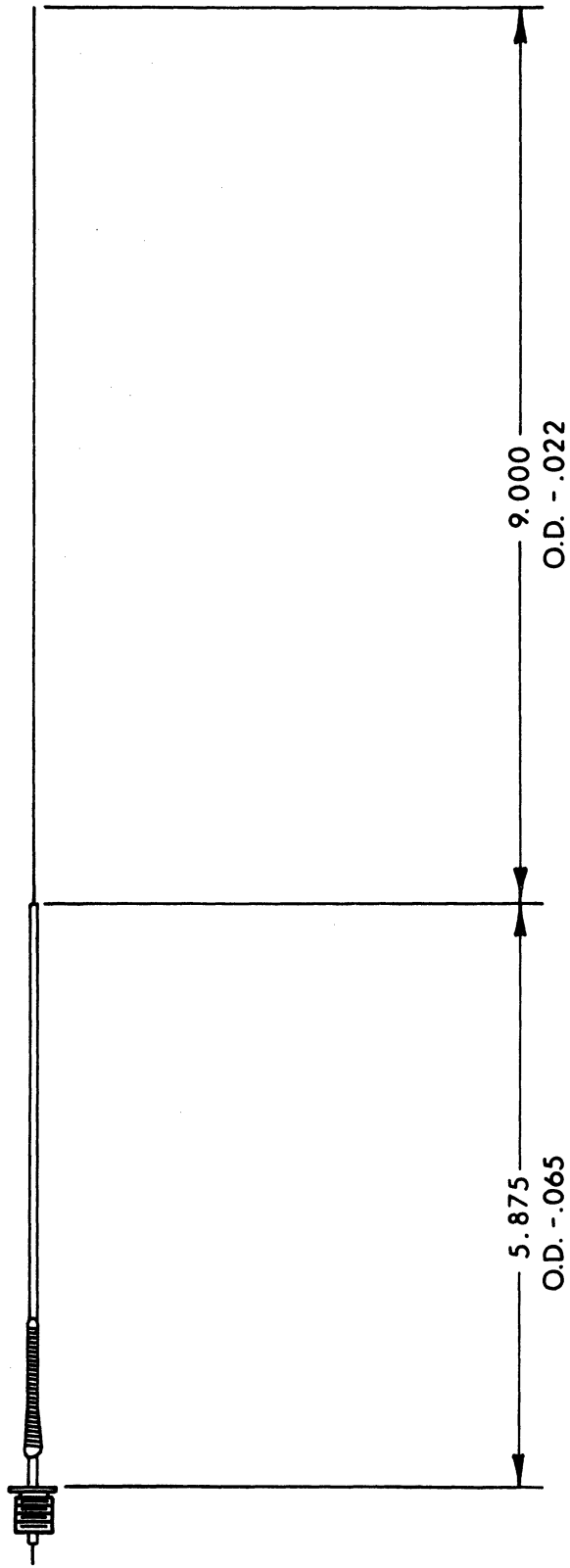| Ramp Voltage (ΔV)	Magnitude	Slope
High ΔV	-3 v TO +5 v	80 v/sec
Low ΔV	-1 v TO +1.8 v	28 v/sec

(4) **Output**

Voltage	-0.6 v TO +5.6 v
Resistance	less than 2 K
Bias Level	+0.5 v

(5) **Calibration**

ON-FOR 600 msec
Interval 28.8 sec
Synchronized with ΔV

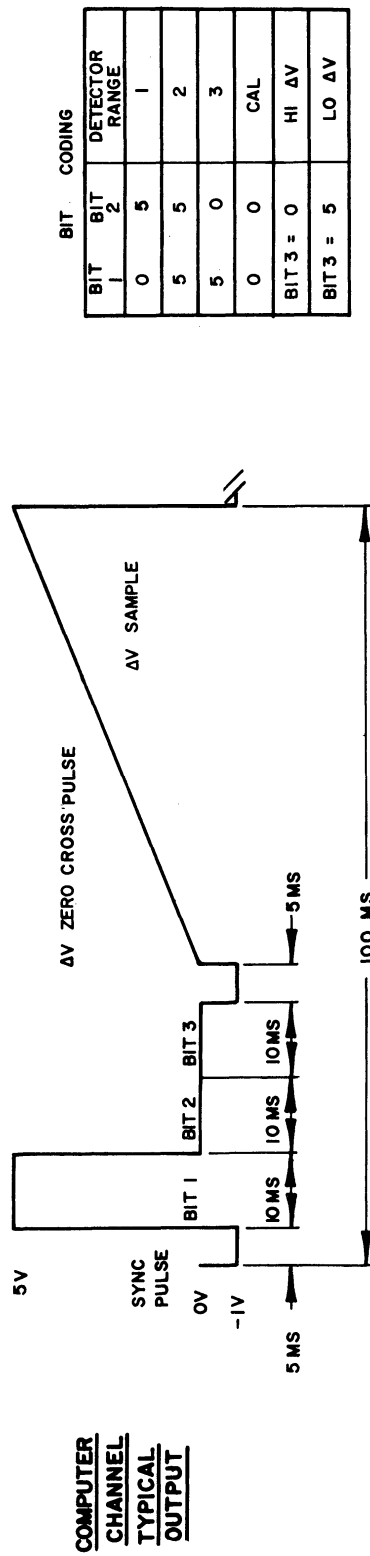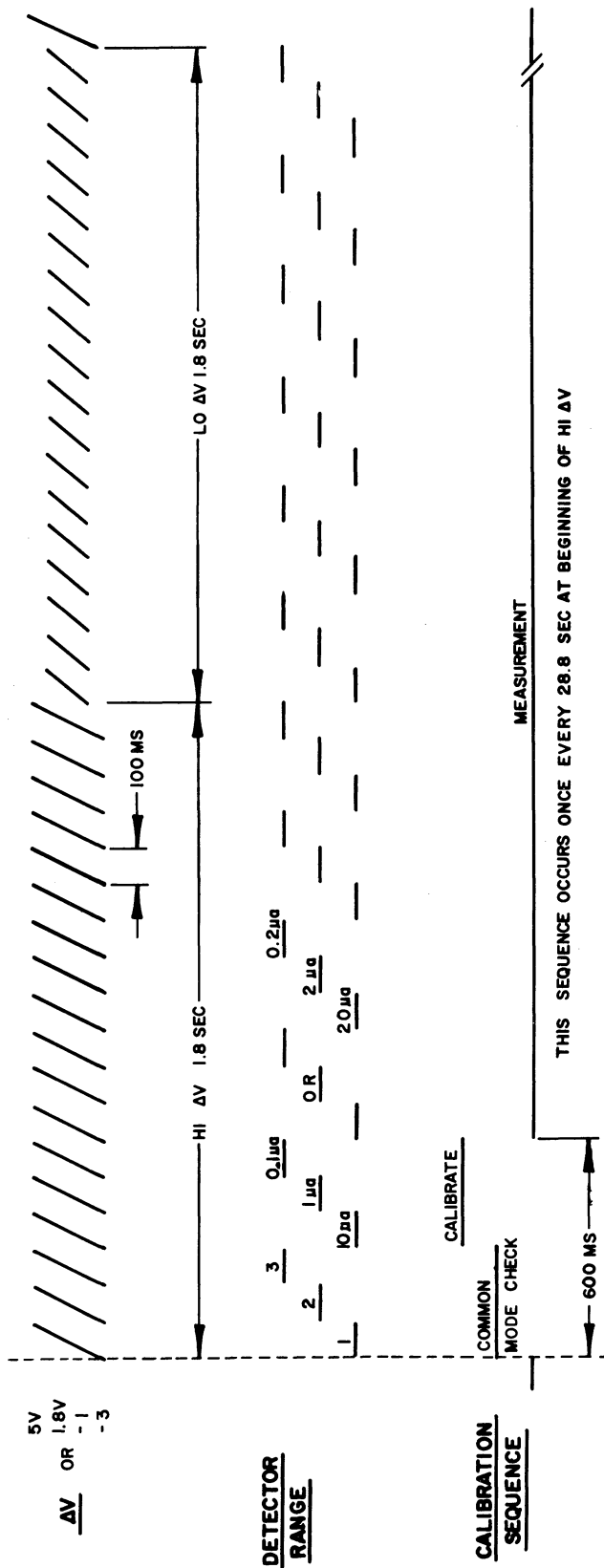(6) **Timing (see Figure 25)**

ΔV-High-Low alternated every 1.8 sec
Range - Sequential, 100 msec each range

ELECTROSTATIC PROBE

9.000
O.D. - .022

5.875
O.D. - .065

Figure 24. Electrostatic probe dimensions.

MUMP SYSTEM TIMING & COMPUTER CHANNEL FORMAT

ΔV
5V
OR 1.8V
-1
-3

HI ΔV 1.8 SEC

LO ΔV 1.8 SEC

100 MS

DETECTOR RANGE

2	3			
10μa	10μa	1μa	0.1μa	
		OR	0.1μa	
		20μa	2μa	0.2μa

CALIBRATE

CALIBRATION SEQUENCE

COMMON MODE CHECK

600 MS

MEASUREMENT

THIS SEQUENCE OCCURS ONCE EVERY 28.8 SEC AT BEGINNING OF HI ΔV

COMPUTER CHANNEL TYPICAL OUTPUT

5V

SYNC PULSE

0V
-1V

BIT 1 BIT 2 BIT 3

ΔV ZERO CROSS PULSE

ΔV SAMPLE

5 MS
10 MS 10 MS 10 MS
5 MS
100 MS

BIT CODING

BIT 1	BIT 2	DETECTOR RANGE
0	5	1
5	5	2
5	0	3
0	0	CAL
BIT 3 = 0		HI ΔV
BIT 3 = 5		LO ΔV

Figure 25. Electrostatic probe timing and computer channel format.

59

6.3 SUPPORT MEASUREMENT AND INSTRUMENTATION

6.3.1 Aspect Determination System

The aspect determination systems, utilized for the eight payloads described herein, were identical to those used on previous Thermosphere Probe payloads. The launches performed during the sunlit hours utilized the Adcole Corporation solar sensors with their shift register electronics package. The launches performed at night utilized the University of Michigan lunar sensor. Adequate information for the determination of payload aspect was received in all cases. However, one of the solar aspect sensors malfunctioned after operating properly for a short period during the initial part of the flight. Details of the malfunction are discussed in Section 7.

In all cases the data were analyzed by a technique which used the velocity vector as a reference (Taeusch, Carignan, Niemann, and Nagy, 1965). It was hoped that the use of Adcole Corporation earth sensors used for the sunlit flights would yield enough information to allow aspect solutions independent of the velocity vector technique. Such information would allow a study of atmospheric winds. However, the earth sensors did not provide adequately accurate data and will subsequently not be used in the future. Other techniques are being attempted to recover the atmospheric wind data. If the techniques are successful, the results will be reported in the future.

The minimum angles of attack versus flight time for each flight are given in Figures 26 through 33. These angles are believed accurate to better than ±5°.
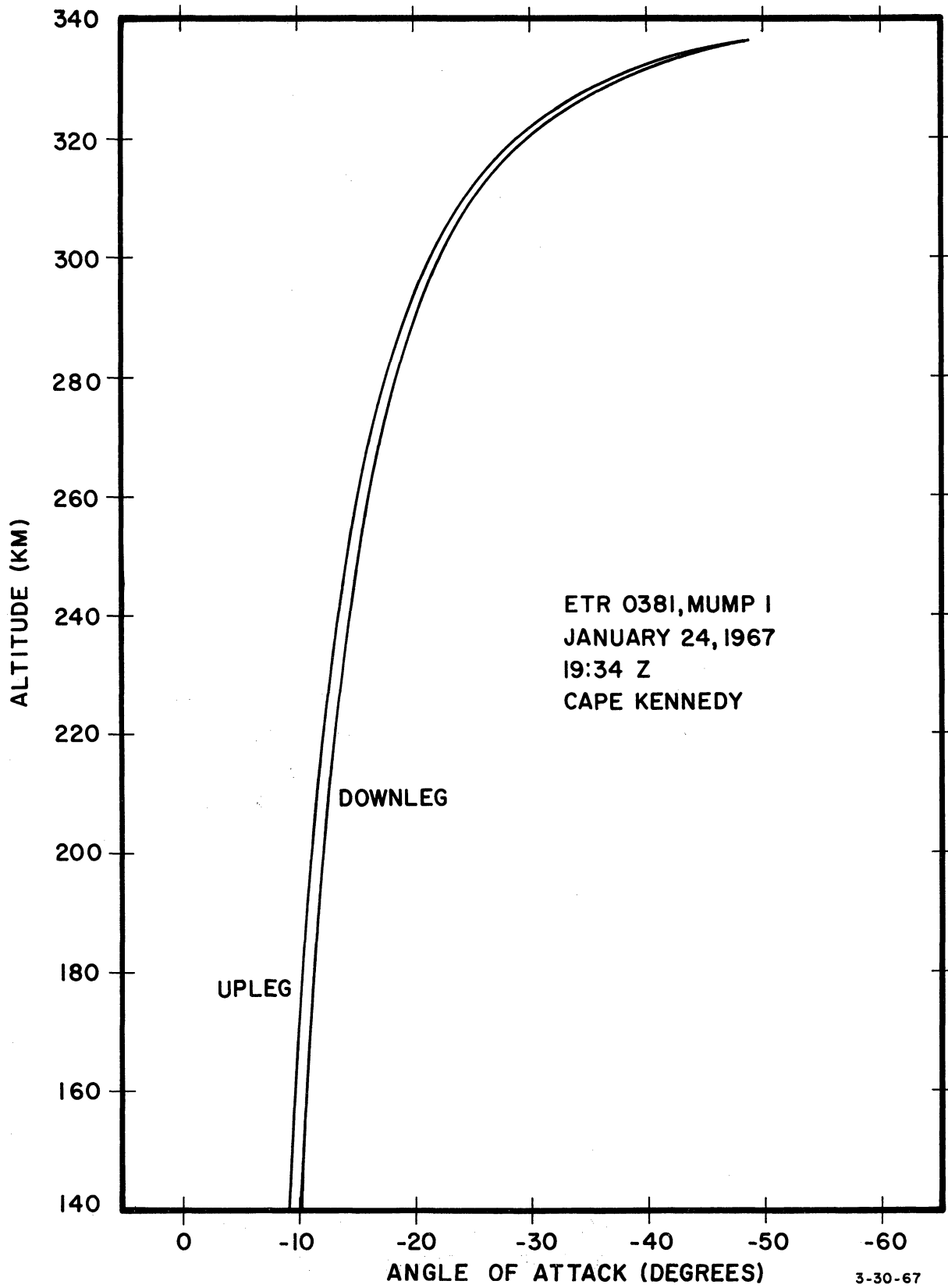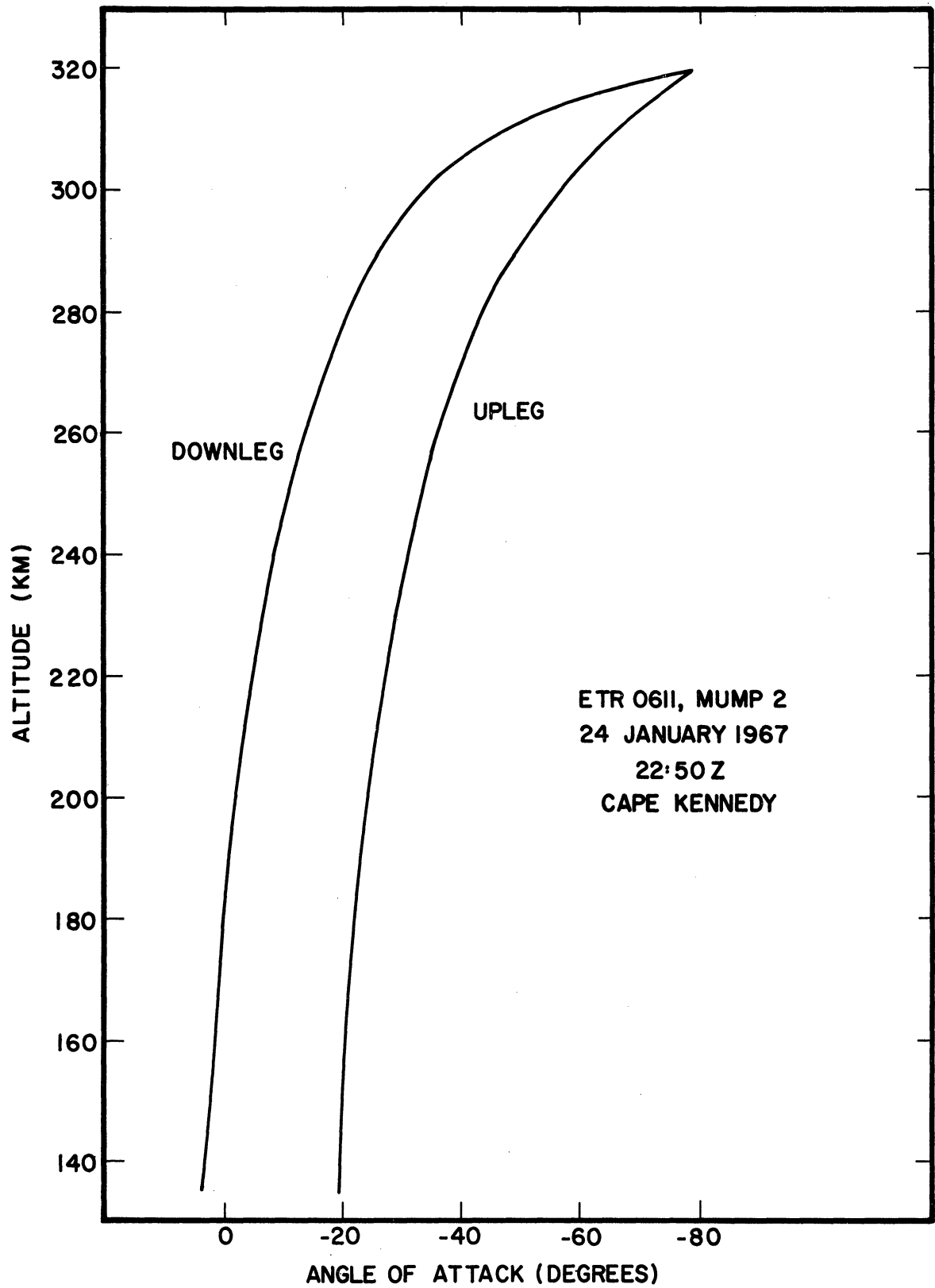
Figure 26.   Minimum angle of attack vs. altitude for MUMP 1.
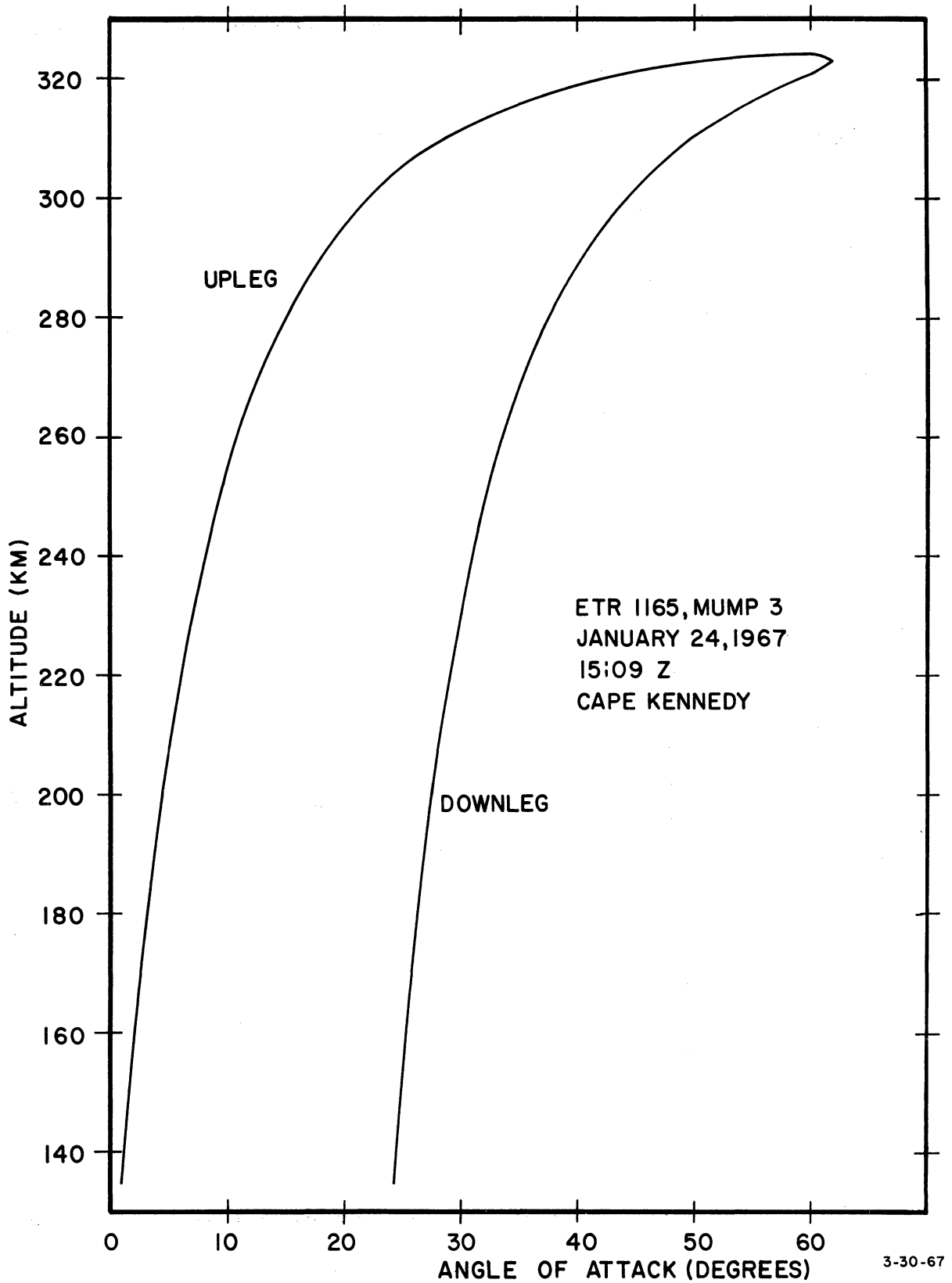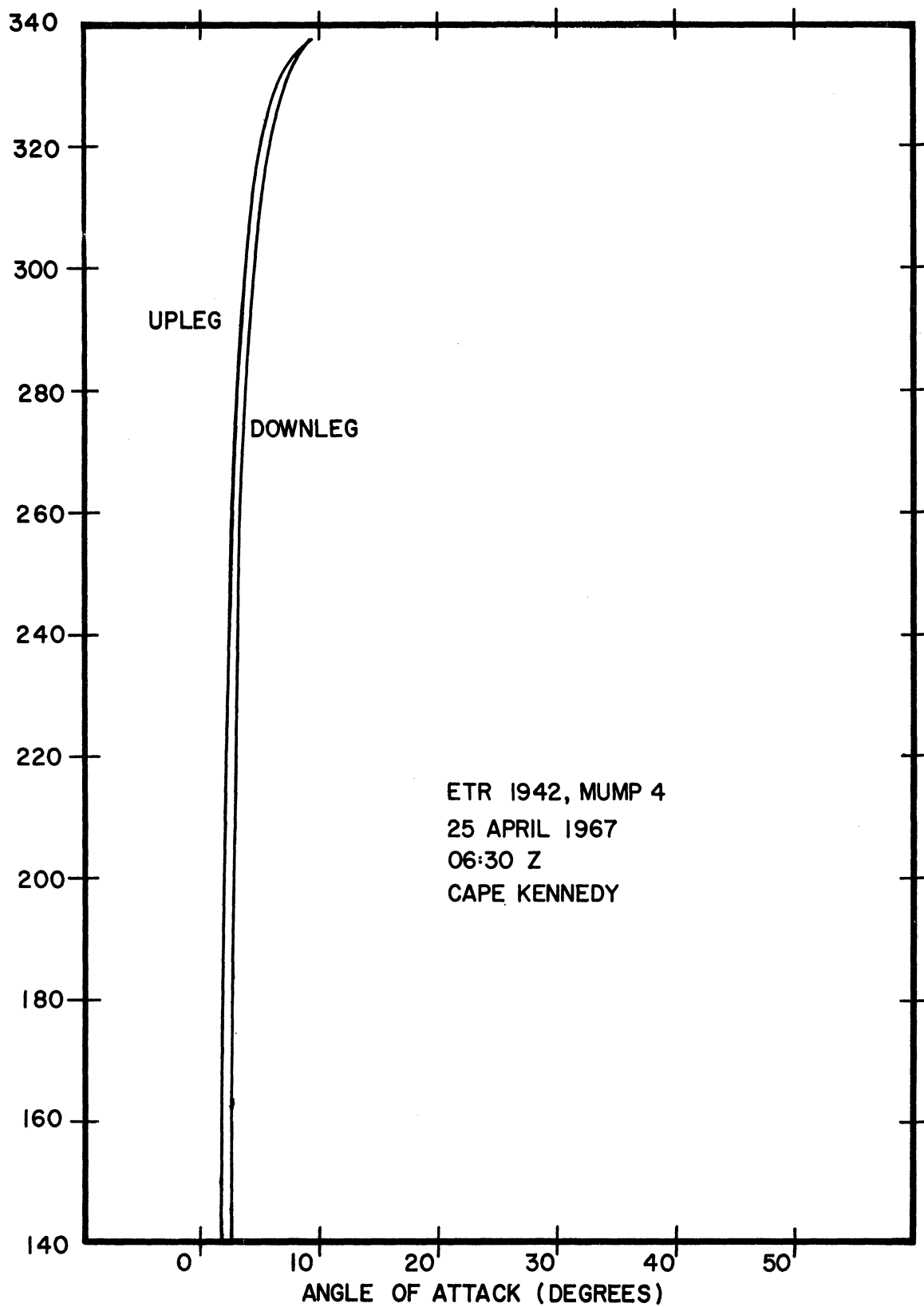
Figure 27. Minimum angle of attack vs. altitude for MUMP 2.

Figure 28. Minimum angle of attack vs. altitude for MUMP 3.

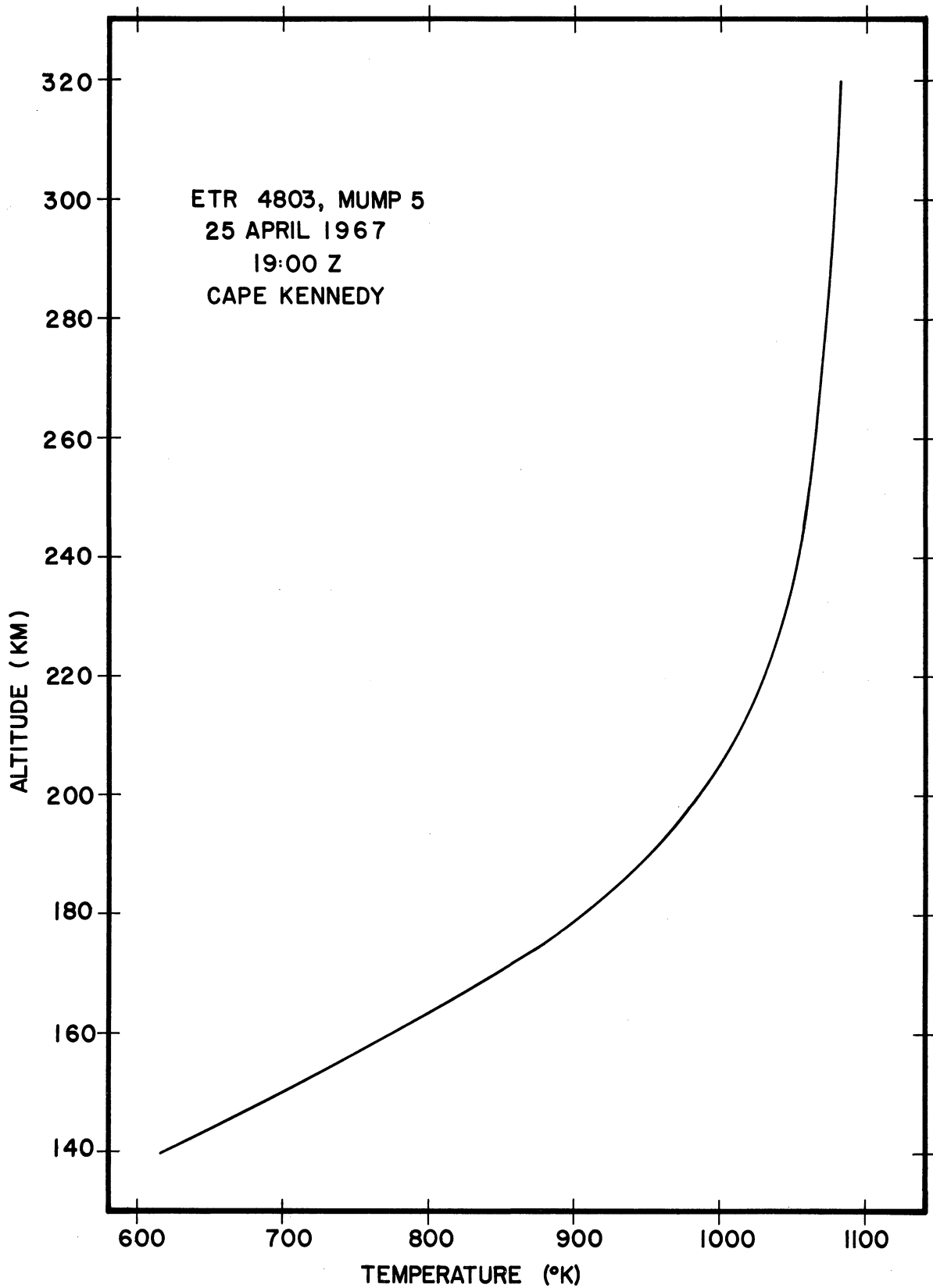Figure 29. Minimum angle of attack vs. altitude for MUMP 4.

Figure 30. Minimum angle of attack vs. altitude for MUMP 5.

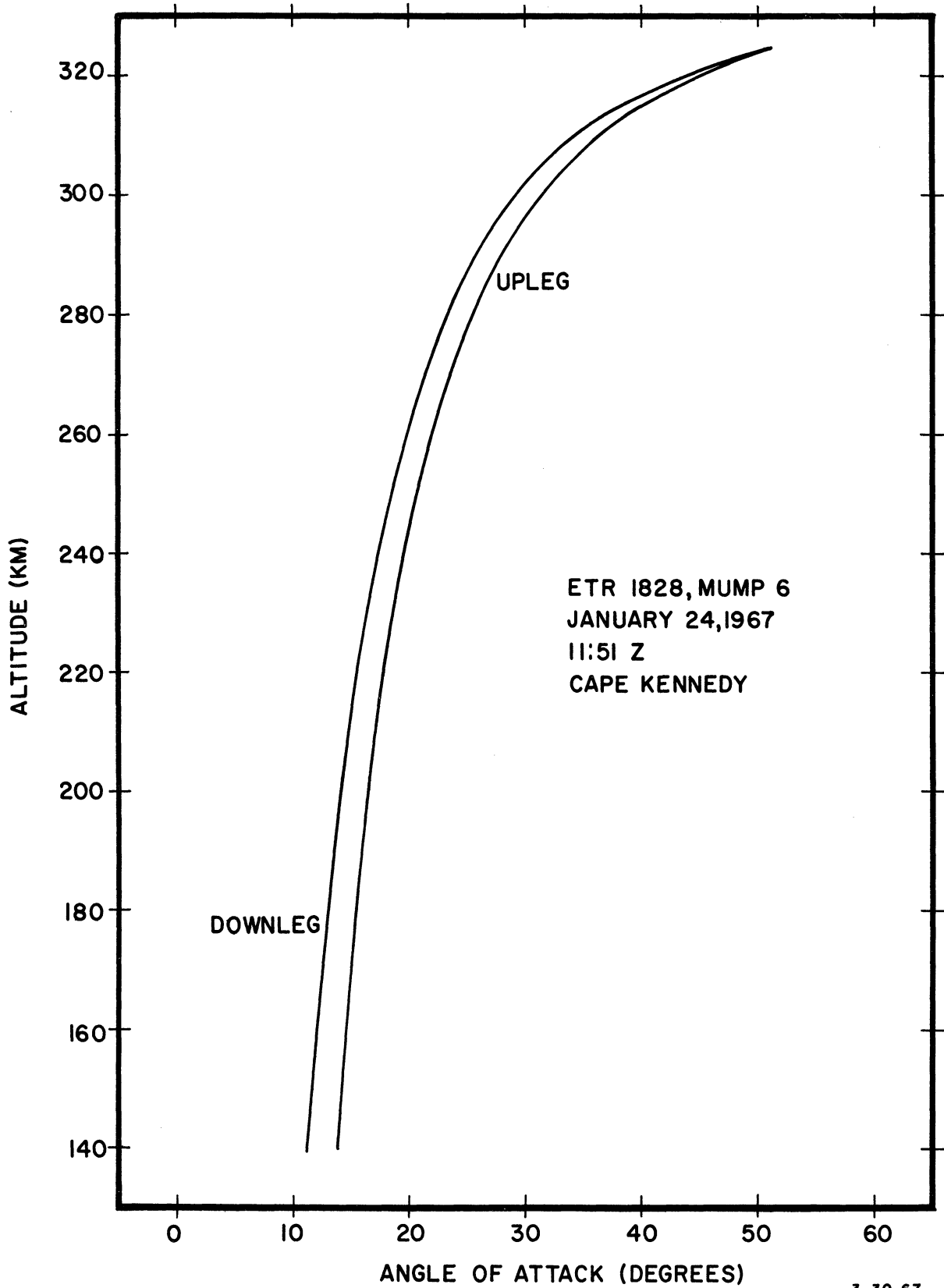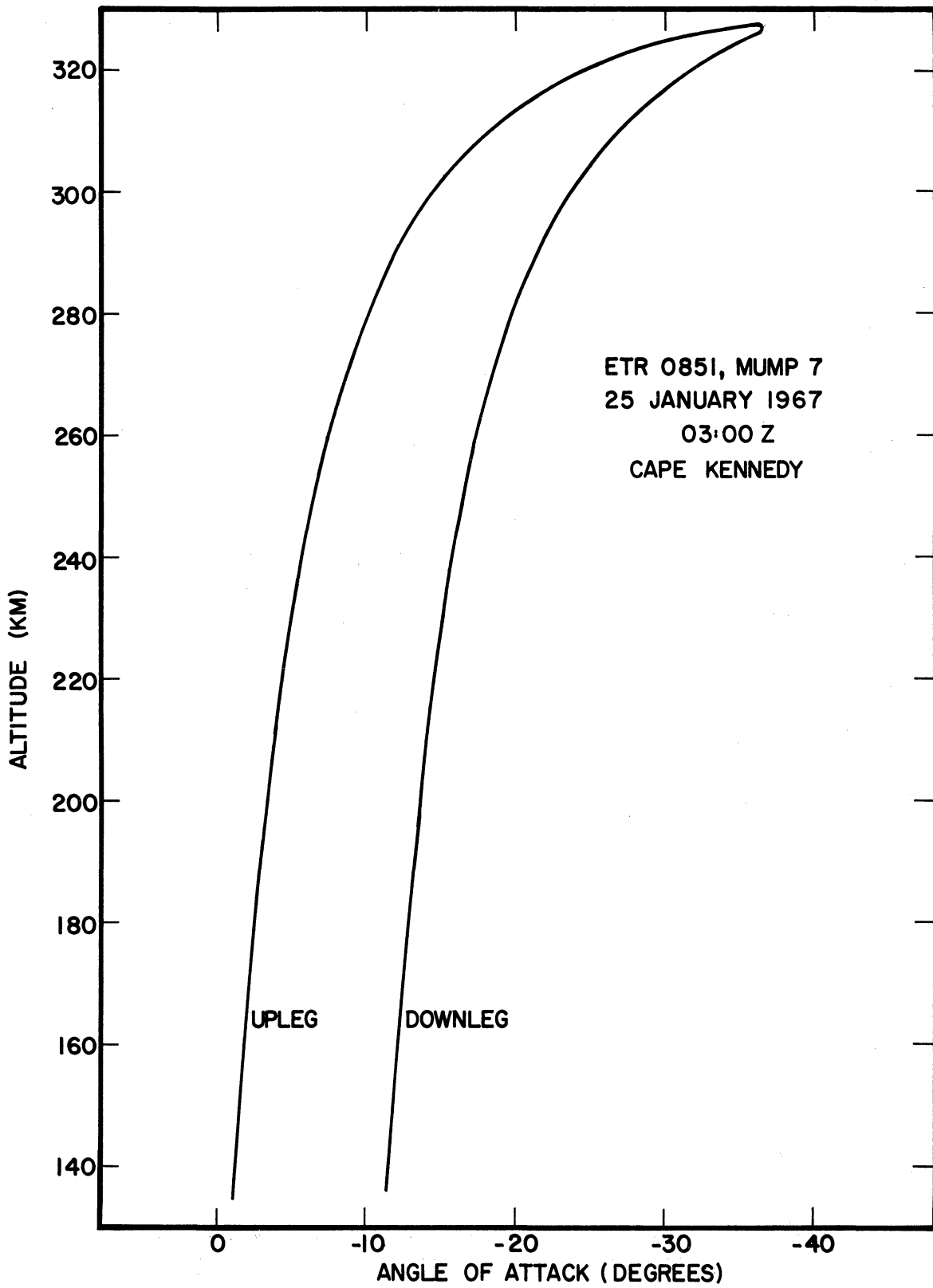Figure 31. Minimum angle of attack vs. altitude for MUMP 6.

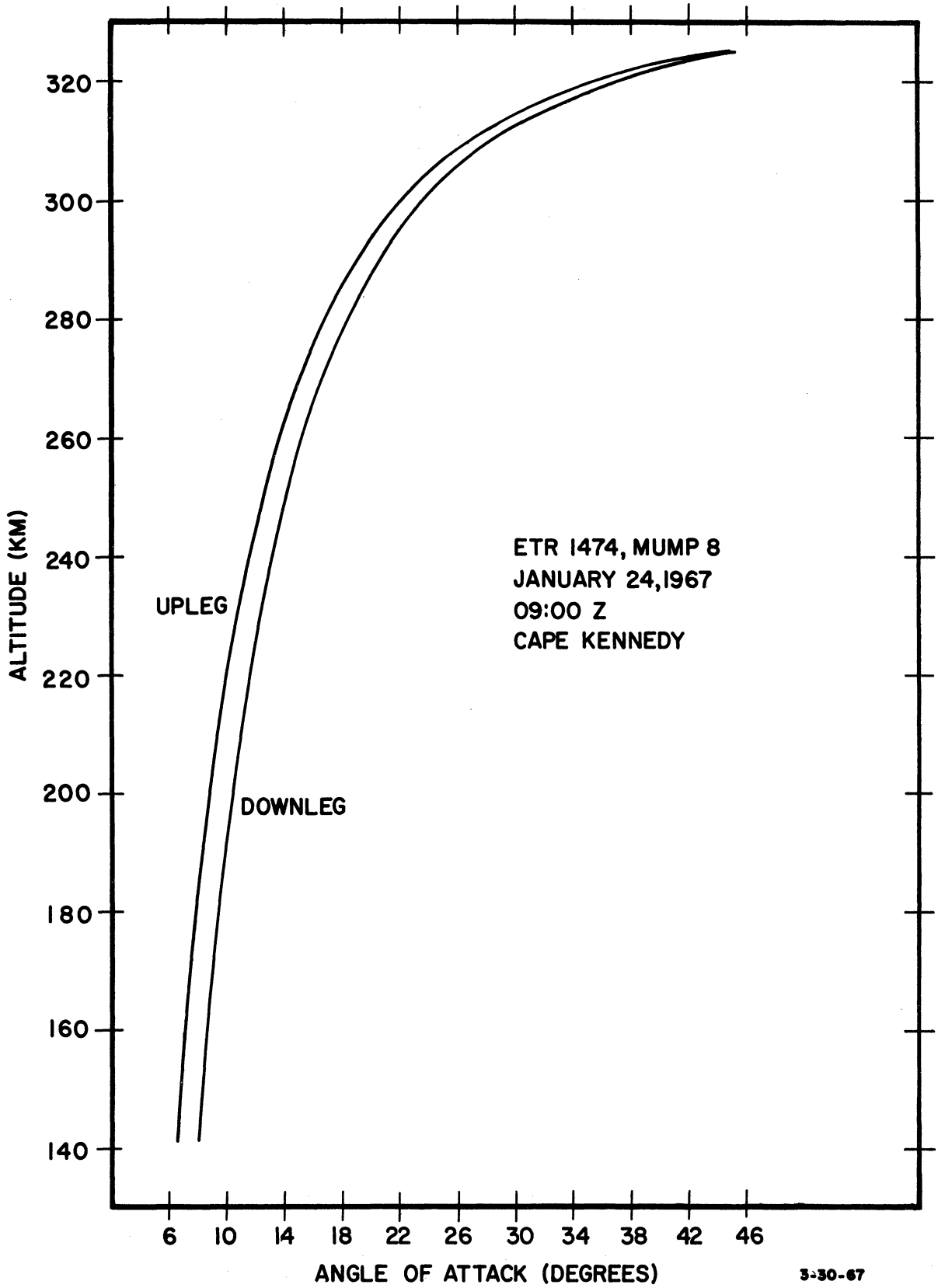Figure 32. Minimum angle of attack vs. altitude for MUMP 7.

Figure 33. Minimum angle of attack vs. altitude for MUMP 8.

6.3.2 Telemetry

The payload data were transmitted in real time by PAM/FM/FM telemetry systems at 231.4 M Hz. with a nominal output of 2.5 watts. The system used subcarrier channels assigned as outlined on the following pages.

MUMP 1

Subcarrier Channels (SCO-type TS58)

IRIG Band	Serial Number	Center Frequency		Nominal Frequency Response		Function
18	3113-25	70	kHz	1050	Hz	Omegatron
16	2499-25	40	kHz	600	Hz	ESP-Data
14	2497-25	22	kHz	330	Hz	ESP-Flag
12	2482-25	10.5	kHz	160	Hz	Aspect
11	2480-25	7.35	kHz	110	Hz	Commutator

Transmitter: Driver: TRPT-250 Serial Number: 2839
Power Amplifier: Type TRFP-2V-1 Serial Number: 521
Mixer Amplifier: Type TA58A Serial Number: 1063

Instrumentation power requirements totaled approximately 30 watts, which was supplied by a Yardney HR-1 Silvercell battery pack of a nominal 27 volt output.

MUMP 2

Subcarrier Channels (SCO-type TS58)

IRIG Band	Serial Number	Center Frequency		Nominal Frequency Response		Function
18	2503-25	70	kHz	1050	Hz	Omegatron
16	2498-25	40	kHz	600	Hz	ESP-Data
14	2495-25	22	kHz	330	Hz	ESP-Flag
12	3102-25	10.5	kHz	160	Hz	Aspect
11	2478-25	7.35	kHz	110	Hz	Commutator

Transmitter: Driver: TRPT-250   Serial Number: 2846
              Power Amplifier: Type TRFP-2V-1 Serial Number: 522
              Mixer Amplifier: Type TA58A   Serial Number: 1066

Instrumentation power requirements totaled approximately 30 watts, which was supplied by a Yardney HR-1 Silvercell battery pack of a nominal 27 volt output.

MUMP 3

Subcarrier Channels (SCO-type TS58)

IRIG Band	Serial Number	Center Frequency		Nominal Frequency Response		Function
18	3111-25	70	kHz	1050	Hz	Omegatron
16	2542-25	40	kHz	600	Hz	ESP-Data
14	2493-25	22	kHz	330	Hz	ESP-Flag
12	2487-25	10.5	kHz	160	Hz	Aspect
11	2476-25	7.35	kHz	110	Hz	Commutator

Transmitter: Driver: Type TRPT-250   Serial Number: 2845
             Power Amplifier: Type TRFP-2V-1   Serial Number: 523
             Mixer Amplifier: Type TA58A   Serial Number: 1065

Instrumentation power requirements totaled approximately 30 watts, which was supplied by a Yardney HR-1 Silvercell battery pack of a nominal 27 volt output.

ETR 1942

MUMP 4

Subcarrier Channels (SCO-type TS58)

IRIG Band	Serial Number	Center Frequency		Nominal Frequency Response		Function
18	2506-25	70	kHz	1050	Hz	Omegatron
16	3108-25	40	kHz	600	Hz	ESP-Data
14	3107-25	22	kHz	330	Hz	ESP-Flag
12	1985-25	10.5	kHz	160	Hz	Aspect
11	3100-25	7.35	kHz	110	Hz	Commutator

Transmitter: Driver: Type TRPT-250   Serial Number: 2844
              Power Amplifier: Type TRFP-2V-1   Serial Number: 524
              Mixer Amplifier: Type TA58A   Serial Number: 1123

Instrumentation power requirements totaled approximately 30 watts, which was supplied by a Yardney HR-1 Silvercell battery pack of a nominal 27 volt output.

Subcarrier Channels (SCO-type TS58)

IRIG Band	Serial Number	Center Frequency		Nominal Frequency Response		Function
18	2504-25	70	kHz	1050	Hz	Omegatron
16	2502-25	40	kHz	600	Hz	ESP-Data
14	2494-25	22	kHz	330	Hz	ESP-Flag
12	2483-25	10.5	kHz	160	Hz	Aspect
11	2477-25	7.35	kHz	110	Hz	Commutator

Transmitter: Driver: Type TRPT-250   Serial Number: 2848
             Power Amplifier: Type TRFP-2V-1 Serial Number: 525
             Mixer Amplifier: Type TA58A   Serial Number: 1122

Instrumentation power requirements totaled approximately 30 watts, which was supplied by a Yardney HR-1 Silvercell battery pack of a nominal 27 volt output.

ETR 1828

MUMP 6

Subcarrier Channels (SCO-type TS58)

IRIG Band	Serial Number	Center Frequency		Nominal Frequency Response		Function
18	3112-25	70	kHz	1050	Hz	Omegatron
16	3109-25	40	kHz	600	Hz	ESP-Data
14	3106-25	22	kHz	300	Hz	ESP-Flag
12	3104-25	10.5	kHz	160	Hz	Aspect
11	3101-25	7.35	kHz	110	Hz	Commutator

Transmitter: Driver: Type TRPT-250   Serial Number: 2490
              Power Amplifier: Type TRFP-2V-1   Serial Number: 428
              Mixer Amplifier: Type TA58A   Serial Number: 1124

Instrumentation power requirements totaled approximately 30 watts, which was supplied by a Yardney HR-1 Silvercell battery pack of a nominal 27 volt output.

MUMP 7

Subcarrier Channels (SCO-type TS58)

IRIG Band	Serial Number	Center Frequency		Nominal Frequency Response		Function
18	2505-25	70	kHz	1050	Hz	Omegatron
16	3110-25	40	kHz	600	Hz	ESP-Data
14	3105-25	22	kHz	330	Hz	ESP-Flag
12	3103-25	10.5	kHz	160	Hz	Aspect
11	3099-25	7.35	kHz	110	Hz	Commutator

Transmitter:	Driver:	Type TRPT-250	Serial Number:	2974
	Power Amplifier:	Type TRFP-2V-1	Serial Number:	535
	Mixer Amplifier:	Type TA58A	Serial Number:	1060

Instrumentation power requirements totaled approximately 30 watts, which was supplied by a Yardney HR-1 Silvercell battery pack of a nominal 27 volt output.

MUMP 8

Subcarrier Channels (SCO-type TS58)

IRIG Band	Serial Number	Center Frequency		Nominal Frequency Response		Function
18	2560-25	70	kHz	1050	Hz	Omegatron
16	2010-25	40	kHz	600	Hz	ESP-Data
14	1891-25	22	kHz	330	Hz	ESP-Flag
12	1689-25	10.5	kHz	160	Hz	Aspect
11	1977-25	7.35	kHz	110	Hz	Commutator

Transmitter: Driver: Type TRPT-250   Serial Number   2973
              Power Amplifier: Type TRFP-2V-1   Serial Number   536
              Mixer Amplifier: Type TA58A   Serial Number   1057

Instrumentation power requirements totaled approximately 30 watts, which was supplied by a Yardney HR-1 Silvercell battery pack of a nominal 27 volt output.

6.3.3 Housekeeping Monitors

Outputs from various monitors throughout the instrumentation provide information bearing on the operations of the electronic components during flight. These outputs are fed to a thirty-segment commutator which runs at one rps. The commutator assignments are as follows:

	COMMUTATOR FORMAT FOR MUMP		9-7-66
SEG. NO.	SEGMENT ASSIGNMENT	EXPECTED READING	ACTUAL READING
1	RANGE	4.9/8 0/1	
2	OUT	4.95/OFF .83/CAL	
3	FIL	3.1/ON .11/OFF	
4	BEAM	3.2/ON .46/OFF	
5	BIAS	3.95	
6	RF	3.1/N_2 2.3/O_2 2.1/0	
7	PRESS	1.8/OFF	
8	TH-GAGE	3.8/20° 3.5/25° 3.1/30°	
9	TH-AMP	" " "	
10	TH-REG	" " "	
11	TH-NO	" " "	
12	TH-XTMR	" " "	
13	OPEN		
14	OPEN		
15	28/5	E_0/E = 1/6.11 OR 4.5/27.5	
16	POS	5.0/7 4.2/8 2.7/10 2.0/11	
17	CAL V	5.0	
18	TH-CM	3.8/20° 3.5/25° 3.1/30°	
19	"	"	
20	"	"	
21	"	"	
22	"	"	
23	"	"	
24	0 CAL	0.00	
25	1 CAL	1.00	
26	2 CAL	2.00	
27	3 CAL	3.00	
28	4 CAL	4.00	
29 & 30	5 CAL	5.00 (FRAME SYNC)	

7. ENGINEERING RESULTS

Because of the nature of program objectives, no engineering innovations of consequence were introduced into the instrumentation. Rather, every effort was made to use previously flight-tested designs. The three night shots were identical to the Thermosphere Probe launched by NASA 18:22, and the day shots differed only in their use of a solar aspect sensor and in the sensitivity of the Langmuir probe current detector.

A great deal of laboratory effort was devoted to an attempt to find a surface treatment for the omegatron gauge and envelope which would permit a measurement of atomic oxygen abundance. The results of the laboratory studies, insofar as permitting the atomic oxygen measurement to be made, were negative, and the measurement was reluctantly abandoned. The circuitry required for the measurement had already been incorporated into the instrument and was merely disabled. As a consequence, measurement of complete N_2 density profiles on both up and downleg was permitted.

The recovery of 100% data was realized from all eight shots. With two known exceptions all eight instruments performed completely as designed. On flight # 1165, solar sensor outputs were erratic (spurious readouts plus many normal readouts) until 135 seconds of flight time. After 135 seconds of flight time, no useful solar data were obtained. The early normal behavior permitted an orientation determination, which then permitted a sorting out of the normal from the spurious outputs. No loss of information resulted from this failure.

On flight 611, the usual method of aspect determination which assumes a constant angular momentum vector for the probe and then tests the assumption, failed to confirm its validity. Further analysis of the data showed that consistent interpretation of the aspect data could be obtained only by permitting the angular momentum vector to move at a rate of approximately 2° per second. It has been concluded that the most likely explanation for this situation was that a small leak developed such that a thrust perpendicular to the cylindrical axis existed. A second possible explanation offered is that the cable attached between the negator motor and the probe for imparting tumble failed to release from the probe, thus resulting in a complex non-rigid system. Other explanations are possible, but the leak theory seems best to fit the observations. At any rate, no known loss or deterioration of data were experienced as a result of this problem.

Since no new engineering concepts were tested on these flights, little can be identified as engineering results. The success, however, of eight of eight shots seems to indicate that the Thermosphere Probe in the configuration used is a reliable space flight instrument.

8. ANALYSIS OF DATA

The telemetered data were recorded on magnetic-tape at the Station 1 (Tel 4) facility. One set of real time paper records, run at one inch per second, were obtained for "quick look" evaluation of the performance of each payload. Other paper records were obtained as required for data reduction as stipulated in the Operations Directives.

Tracking data for trajectory information were obtained from the 0.18 and 19.18 radar facilities.

8.1 TRAJECTORY AND MINIMUM ANGLE OF ATTACK

The trajectory and the velocity information used for the reduction of the data and for the interpretation was obtained by fitting a smooth theoretical trajectory to the radar data. The theoretical trajectory is programmed for computer solution similar to that described by Parker (1962). The output format is shown in Figure 34. The analysis of minimum angle of attack (α) as described by Taeusch, et al. (1965), is also incorporated in the program and the output of the computer furnishes α and $\cos \alpha$ versus time, altitude, etc. Plots of α versus altitude for each of the payloads are given in Figures 26 through 33.

8.2 AMBIENT N_2 DENSITY AND TEMPERATURE

The neutral molecular nitrogen densities for each of the flights were determined from the measured gauge partial densities as described by Spencer, et al. (1965, 1966), by using the basic relationship:

$$na_{N_2} = \left(\frac{\Delta n_i \, u_i}{2\sqrt{\pi} \, V\cos \alpha} \right)_{N_2} K(S,\alpha)$$

where

na_{N_2} = Ambient N_2 number density

Δn_i = Maximum minus minimum gauge number density during one tumble

$u_i = \sqrt{\dfrac{2kT_i}{m}}$ most probable thermal speed of particle inside gauge.

T_i = Gauge wall temperature.

V = Vehicle velocity with respect to earth.

80

α = Minimum angle of attack for one tumble.

K(S,α) = Correction factor required because of imperfect gauge geometry. (See Spencer, Taeusch, Carignan, 1966).

ΔI_i, the difference between the maximum (peak) omegatron gauge current[1] and the minimum (background) gauge current versus flight time is shown for a typical flight in Figure 35. The background current is also shown in the figure. The background current is the result of the outgassing of the gauge walls, and the inside density due to atmospheric particles which have enough translational energy to over-take the payload and enter the gauge. In contrast to reports by Moe and Moe (1967), there is laboratory evidence that the background of N_2, due to outgassing of the gauge walls, is constant for at least one tumble period, and effects both the peak reading and the background reading and therefore does not effect the difference. From calibration data, obtained as discussed in a previous section, the inside number density difference, Δn_i, is computed for the measured current. As described by Spencer, Taeusch and Carignan (1965), the uncertainty in these data is believed to be ±5% relative to other gauges calibrated at the same time on the same system. Much could be written concerning the absolute accuracy which cannot be proved or disproved to anything better than ±25% to date.

By using the thermistor measured gauge wall temperature, u_i, the most probable thermal speed of the particles inside the gauge, is computed. The uncertainty in this measuring is believed to be about ±2% absolute.

V, the vehicle velocity with respect to the earth, is believed known to better than ±1% absolute. It is obtained from the trajectory curve fitting described previously and is the most accurately known quantity obtained from the analysis.

Cos α is obtained from the aspect analysis described by Taeusch, et al. (1965). Since the uncertainty in cos α depends upon α, for any given uncertainty in α, each particular case and altitude range must be considered separately. However, the upleg angle of attack is typically less than 10°. With an assumed maximum uncertainty in α of ±5°, this results in less than a ±2% uncertainty in cos α. The low angle of attack data were used as control data in all cases.

K(S,α) for each flight was determined from theoretical and empiri-cal results gathered over a four-year period utilizing data obtained from about ten payloads similar to the ones described herein. Several researchers have contributed to this work (Pearl, John, and Vogel, U., Space Physics Research Laboratory, The University of Michigan, to be published; and Ballance, 1967). In general, the maximum correction to the data is approximately 15%, or K(S,α) = .85. These corrections are believed known to better than 2%.

The ambient N_2 number densities versus altitude obtained from the measured quantities described above are given in Figures 36 through 43, and are tabulated with the derived kinetic temperature in Tables 17 through 24.

The ambient neutral particle temperature profiles shown in Figures 44 through 51 were obtained by integrating the density profiles, which gives the ambient N_2 pressure. The densities and the resulting pressures are then related to the temperatures through the ideal gas law. The assumption that the gas is in hydrostatic equilibrium and behaves as an ideal gas is implicit. Since the temperatures derived depend only on the shape of the density profile and not its magnitude, it is believed that the uncertainty in its magnitude is less than ±5% absolute.

TABLE XVII

ETR 0381, MUMP 1

January 24, 1967

19:34 Z

14:34 Local (EST)

Cape Kennedy, Florida

ALTITUDE (km)	TEMPERATURE (°K)	DENSITY (part/cc)
140	640	3.70×10^{10}
145	693	2.61
150	744	1.94
155	792	1.49
160	838	1.16×10^{10}
165	877	9.24×10^{9}
170	913	7.47
175	942	6.08
180	969	5.03
185	991	4.19
190	1010	3.51
195	1026	2.97
200	1041	2.51
205	1054	2.14
210	1065	1.82
215	1074	1.57
220	1081	1.35
225	1086	1.16
230	1090	1.01×10^{9}
235	1093	8.76×10^{8}
240	1096	7.60
245	1099	6.60
250	1102	5.72
255	1104	4.99
260	1106	4.32
265	1108	3.76
270	1110	3.27
275	1112	2.85
280	1114	2.50
285	1115	2.17
290	1116	1.89
295	1117	1.65
300	1118	1.44
305	1120	1.25
310	1122	1.10×10^{8}
315	1123	9.58×10^{7}
320	1124	8.33×10^{7}

TABLE XVIII

ETR 0611, MUMP 2

January 24, 1967

22:50 Z

17:50 Local (EST)

Cape Kennedy, Florida

ALTITUDE (km)	TEMPERATURE (°K)	DENSITY (part/cc)
140	657	3.53×10^{10}
145	677	2.72
150	696	2.10
155	715	1.64
160	735	1.27
165	754	1.00×10^{10}
170	772	7.99×10^{9}
175	791	6.40
180	809	5.13
185	828	4.13
190	846	3.37
195	864	2.74
200	881	2.25
205	898	1.85
210	914	1.54
215	928	1.28
220	940	1.07×10^{9}
225	951	9.02×10^{8}
230	959	7.60
235	967	6.41
240	974	5.43
245	981	4.61
250	988	3.92
255	994	3.34
260	999	2.85
265	1004	2.43
270	1009	2.08
275	1014	1.78
280	1018	1.52
285	1022	1.31
290	1026	1.12×10^{8}
295	1030	9.61×10^{7}

TABLE XIX

ETR 1165, MUMP 3

January 24, 1967

15:09 Z

10:09 Local (EST)

Cape Kennedy, Florida

ALTITUDE (km)	TEMPERATURE (°K)	DENSITY (part/cc)
140	632	3.52×10^{10}
145	662	2.65
150	684	2.02
155	704	1.57
160	722	1.22×10^{10}
165	739	9.56×10^{9}
170	755	7.57
175	769	6.03
180	784	4.85
185	797	3.90
190	810	3.18
195	823	2.59
200	835	2.12
205	846	1.74
210	857	1.43
215	869	1.18×10^{9}
220	880	9.80×10^{8}
225	890	8.16
230	900	6.77
235	910	5.63
240	919	4.70
245	929	3.95
250	938	3.32
255	946	2.80
260	952	2.36
265	959	2.00
270	965	1.70
275	972	1.44
280	977	1.23
285	982	1.04×10^{8}
290	988	8.97×10^{7}
295	992	7.64
300	997	6.56
305	1002	5.61
310	1006	4.81
315	1011	4.12
320	1015	3.55×10^{7}

TABLE XX

ETR 1942, MUMP 4

April 25, 1967

06:30 Z

01:30 Local (EST)

Cape Kennedy, Florida

ALTITUDE (km)	TEMPERATURE (°K)	DENSITY (part/cc)
145	591	3.70×10^{10}
150	628	2.74
155	658	2.04
160	690	1.55
165	720	1.18×10^{10}
170	747	9.19×10^{9}
175	774	7.22
180	796	5.77
185	816	4.61
190	831	3.74
195	846	3.07
200	860	2.51
205	875	2.06
210	887	1.70
215	898	1.41
220	906	1.18×10^{9}
225	915	9.82×10^{8}
230	922	8.27
235	927	7.00
240	931	5.92
245	935	5.00
250	937	4.23
255	939	3.60
260	940	3.06
265	941	2.60
270	941	2.21
275	942	1.88
280	942	1.60
285	942	1.36
290	942	1.17×10^{8}
295	942	9.90×10^{7}
300	942	8.45
305	942	7.20
310	942	6.08
315	942	5.19
320	942	4.41×10^{7}

TABLE XXI

ETR 4803, MUMP 5

April 25, 1967

19:00 Z

14:00 Local (EST)

Cape Kennedy, Florida

ALTITUDE (km)	TEMPERATURE (°K)	DENSITY (part/cc)
140	616	4.81×10^{10}
145	654	3.56
150	693	2.65
155	736	2.00
160	777	1.54
165	814	1.20×10^{10}
170	848	9.54×10^{9}
175	880	7.69
180	907	6.24
185	931	5.13
190	951	4.26
195	969	3.55
200	983	2.99
205	997	2.52
210	1010	2.14
215	1021	1.81
220	1030	1.54
225	1037	1.32
230	1044	1.13×10^{9}
235	1049	9.66×10^{8}
240	1053	8.34
245	1057	7.20
250	1060	6.21
255	1062	5.38
260	1065	4.63
265	1067	4.01
270	1069	3.47
275	1071	3.01
280	1072	2.61
285	1073	2.27
290	1075	1.97
295	1076	1.70
300	1077	1.48
305	1078	1.29
310	1080	1.12×10^{8}
315	1081	9.60×10^{7}
320	1082	8.29×10^{7}

TABLE XXII

ETR 1828, MUMP 6

January 24, 1967

11:51 Z

06:51 Local (EST)

Cape Kennedy, Florida

ALTITUDE (km)	TEMPERATURE (°K)	DENSITY (part/cc)
140	576	3.25×10^{10}
145	630	2.29
150	672	1.68
155	703	1.28×10^{10}
160	727	9.90×10^{9}
165	745	7.80
170	762	6.20
175	774	5.00
180	786	4.02
185	795	3.27
190	804	2.64
195	812	2.16
200	819	1.76
205	826	1.45
210	832	1.19×10^{9}
215	838	9.85×10^{8}
220	844	8.13
225	849	6.75
230	853	5.61
235	857	4.67
240	861	3.87
245	866	3.25
250	869	2.71
255	872	2.26
260	875	1.88
265	878	1.58
270	881	1.33
275	884	1.12×10^{8}
280	886	9.35×10^{7}
285	889	7.90
290	890	6.65
295	892	5.65
300	894	4.72
305	896	3.98
310	898	3.35
315	899	2.82
320	901	2.38×10^{7}

TABLE XXIII

ETR 0851, MUMP 7

January 24, 1967

03:00 Z

22:00 Local (EST)

Cape Kennedy, Florida

ALTITUDE (km)	TEMPERATURE (°K)	DENSITY (part/cc)
140	597	3.59×10^{10}
145	635	2.60
150	666	1.95
155	688	1.50
160	706	1.16×10^{10}
165	722	9.18×10^{9}
170	737	7.27
175	750	5.78
180	762	4.63
185	773	3.73
190	784	3.00
195	794	2.42
200	803	1.97
205	812	1.61
210	821	1.31
215	829	1.07×10^{9}
220	837	8.79×10^{8}
225	844	7.20
230	852	5.97
235	859	4.96
240	865	4.11
245	870	3.43
250	875	2.85
255	879	2.39
260	883	2.00
265	886	1.68
270	889	1.41
275	892	1.18
280	894	1.00×10^{8}
285	896	8.41×10^{7}
290	898	7.10
295	900	6.00
300	902	5.07×10^{7}

TABLE XXIV

ETR 1474, MUMP 8

January 24, 1967

09:00 Z

04:00 Local (EST)

Cape Kennedy, Florida

ALTITUDE (km)	TEMPERATURE (°K)	DENSITY (part/cc)
140	502	3.80×10^{10}
145	550	2.57
150	596	1.81
155	635	1.32×10^{10}
160	669	9.90×10^{9}
165	700	7.51
170	726	5.78
175	750	4.51
180	771	3.55
185	790	2.82
190	807	2.28
195	821	1.84
200	834	1.50
205	846	1.22
210	855	1.00×10^{9}
215	864	8.29×10^{8}
220	871	6.87
225	878	5.73
230	883	4.77
235	889	3.98
240	893	3.32
245	897	2.80
250	901	2.37
255	905	1.99
260	908	1.68
265	911	1.41
270	913	1.19
275	916	1.00×10^{8}
280	918	8.43×10^{7}
285	920	7.19
290	922	6.08
295	924	5.18
300	925	4.40
305	926	3.74
310	928	3.20
315	929	2.73
320	930	2.35×10^{7}

ETR 4803 MUMP 5

LAUNCH TIME (GMT)

```
        YEAR    1967
        DAY      115
        HOUR      19
        MINUTE     0
        SECOND      .000
```

INITIAL CONDITIONS

```
               TIME        70.000 SECONDS FROM LAUNCH
           ALTITUDE     416538.7 FT
              RANGE      88146.3 FT
           VELOCITY       6536.1 FT/SEC
  FLIGHT PATH ANGLE      76.6289 DEGREES UP FROM LOCAL HORIZONTAL PLANE
            AZIMUTH      76.1700 DEGREES EAST OF LOCAL NORTH
          LONGITUDE     -80.2596 DEGREES (+EAST)
           LATITUDE      28.5122 DEGREES (+NORTH)
```

NO WIND SPECIFIED

CONE CORRECTION   -.70

MOMENTUM VECTOR INPUT BY SPECIFYING PHI LS = 62.0 AND THETA LS = 129.6
COMPUTED MOMENTUM VECTOR IN EARTH FIXED COORDINATES IS   .299509   .883184   -.360943

MOMENTUM VECTOR INPUT BY SPECIFYING PHI LS = 172.0 AND THETA LS = 129.6
COMPUTED MOMENTUM VECTOR IN EARTH FIXED COORDINATES IS   -.401072   -.008207   -.916010

PEAK PARAMETERS

TIME	ALTITUDE F / ALTITUDE M	ALPHA / V*COS ALPHA	PHI / V	RANGE F VELOCITY F / RANGE M VELOCITY M	VXFX / VYFX	VZFX	AZIMUTH / ELEVATION	LATITUDE / LONGITUDE
286.79	1098205 / 334733	30.90 / -21.10	360.09 / 391.50	103.66 / -177.20	384318 1376.80 / 117140 419.65	1339.35 / 317.15	-31.17	77.387 / -.000	28.699 / -79.360

Figure 34. Trajectory program output format.
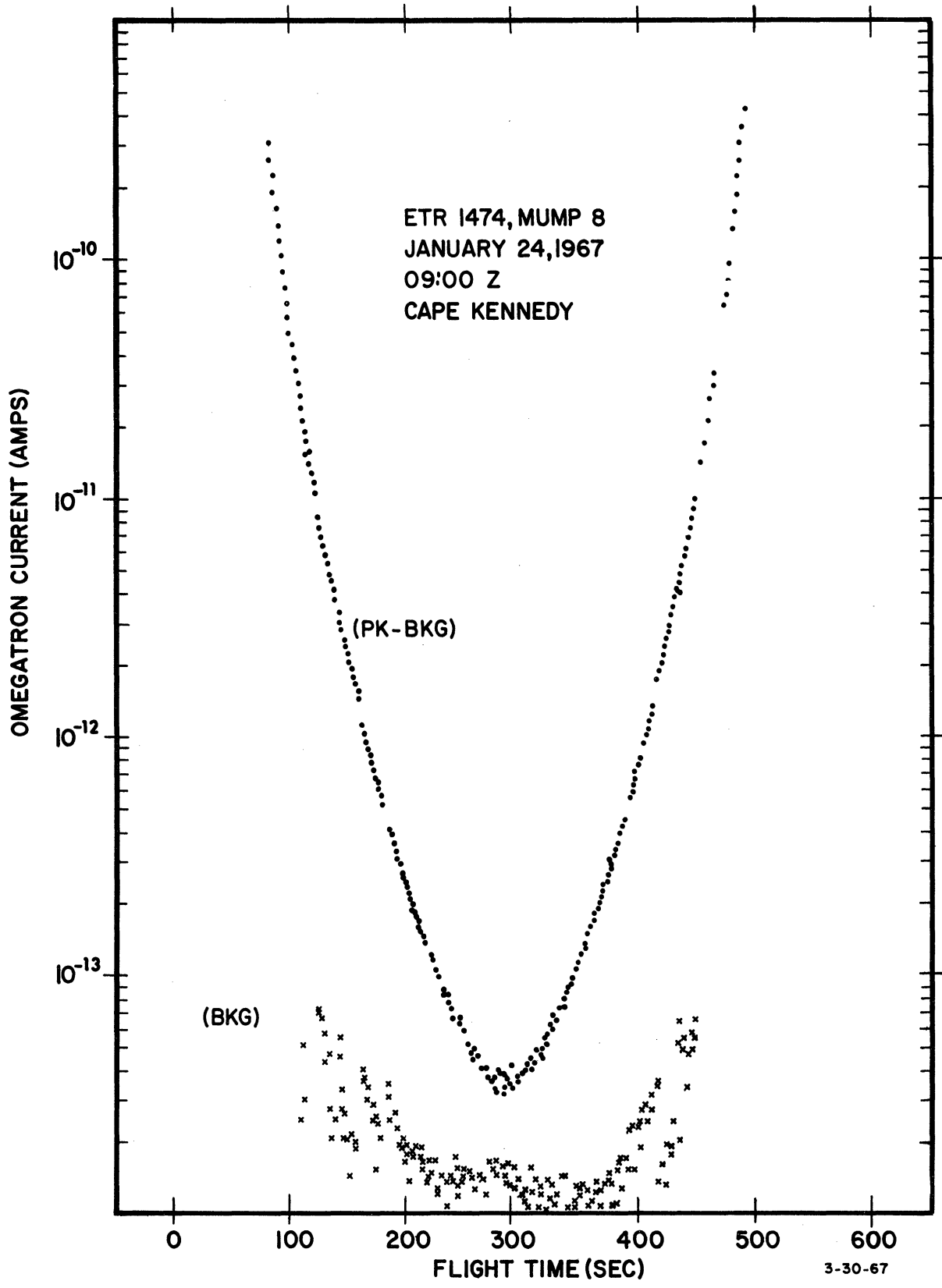
Figure 35. Omegatron current vs. flight time.

Figure 36. Ambient N_2 density for MUMP 1.

ETR 0381, MUMP 1
JANUARY 24, 1967
19:34 Z
CAPE KENNEDY

AMBIENT N_2 DENSITY (PART/CC)

ALTITUDE (KM)

3-30-67

93
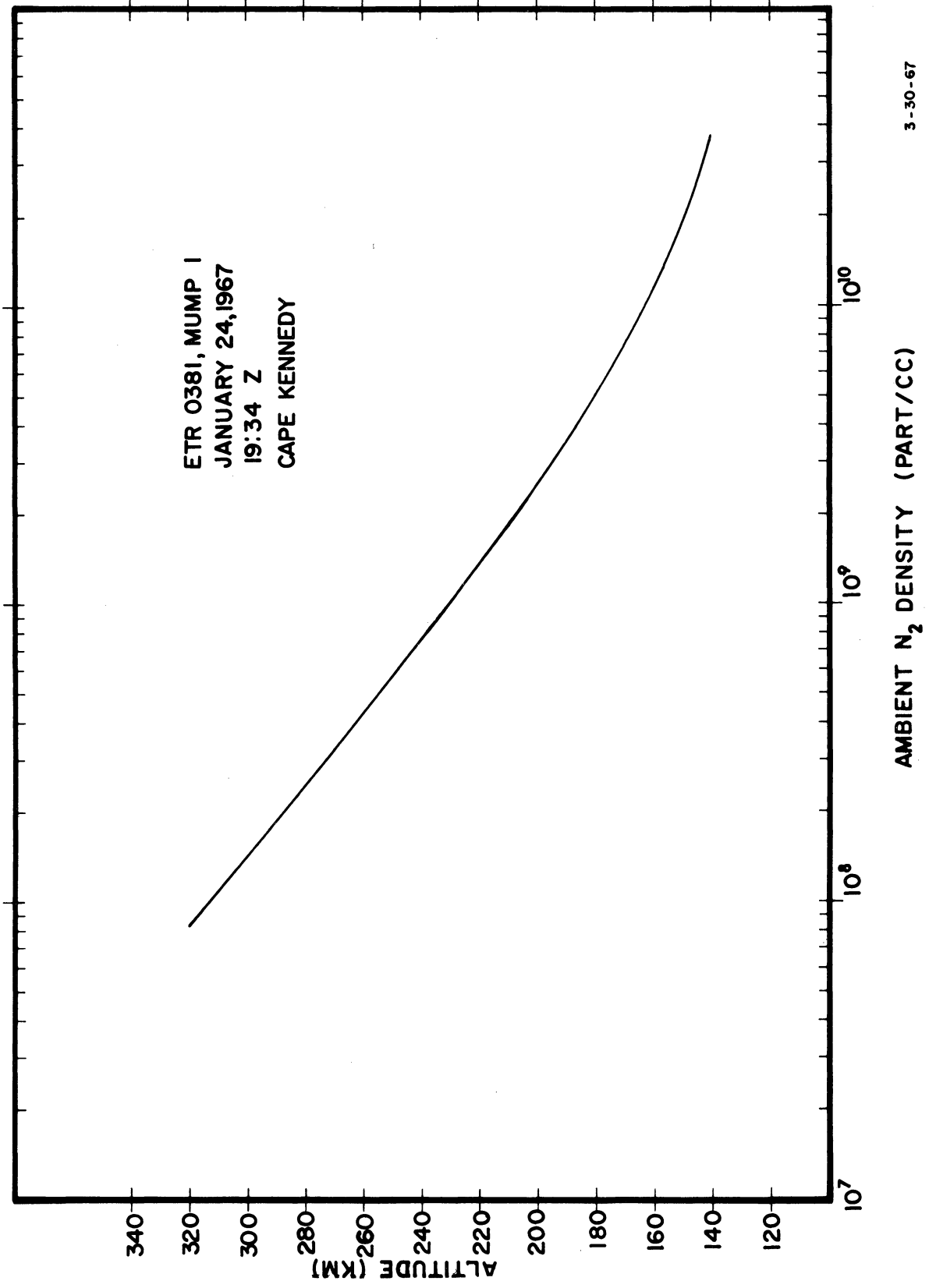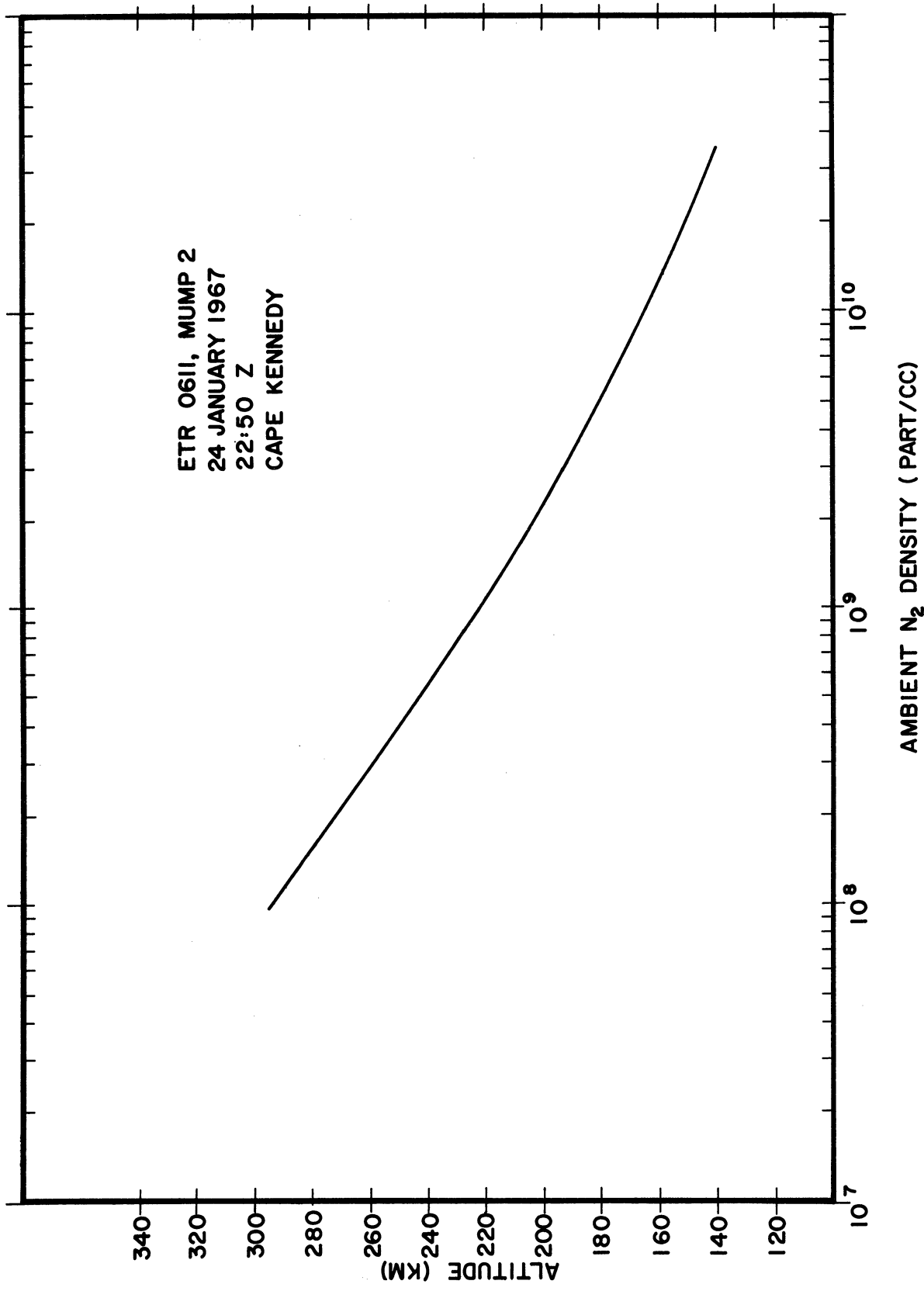
Figure 37. Ambient N_2 density for MUMP 2.

6-12-67

94
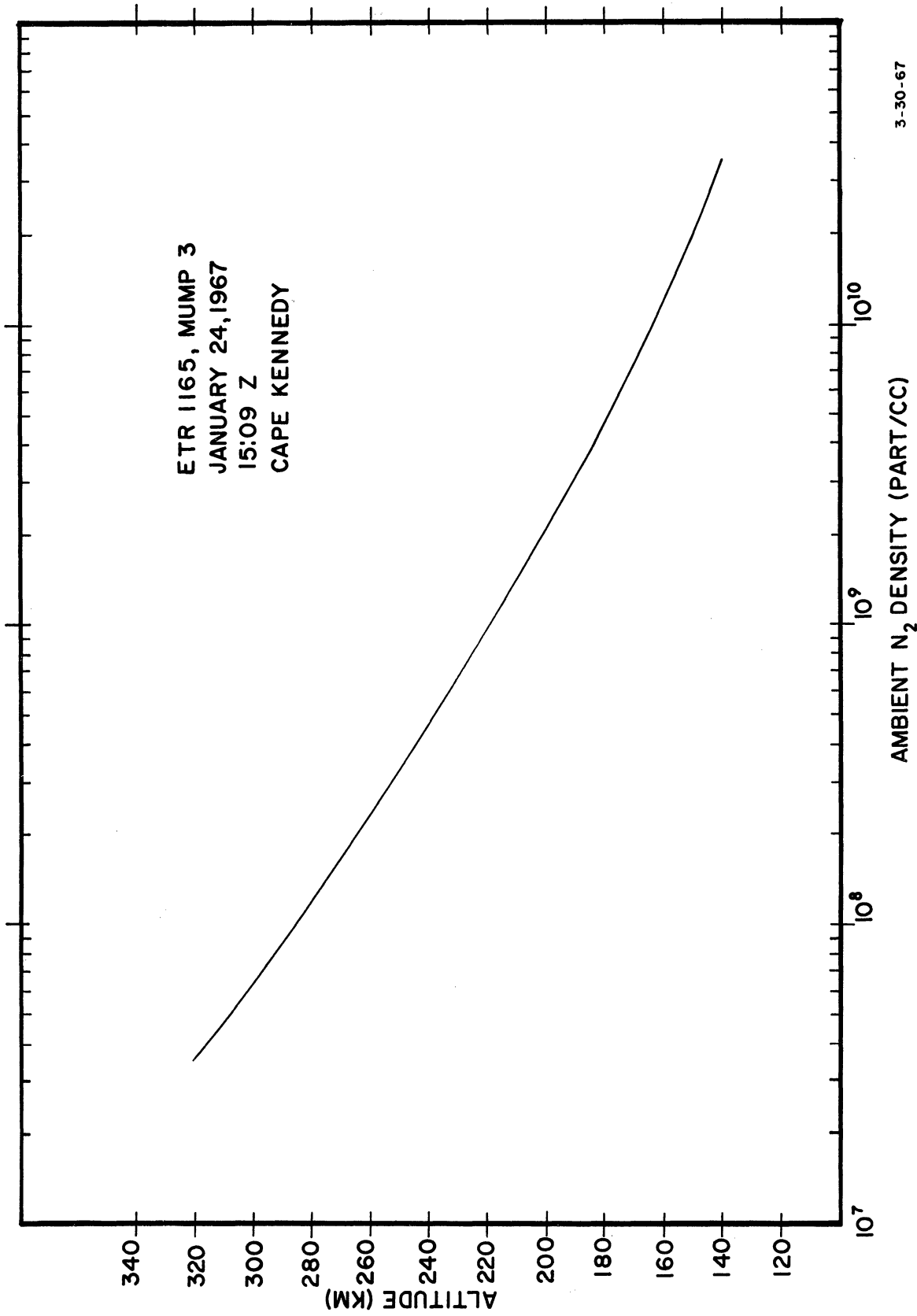
Figure 38. Ambient N_2 density for MUMP 3.
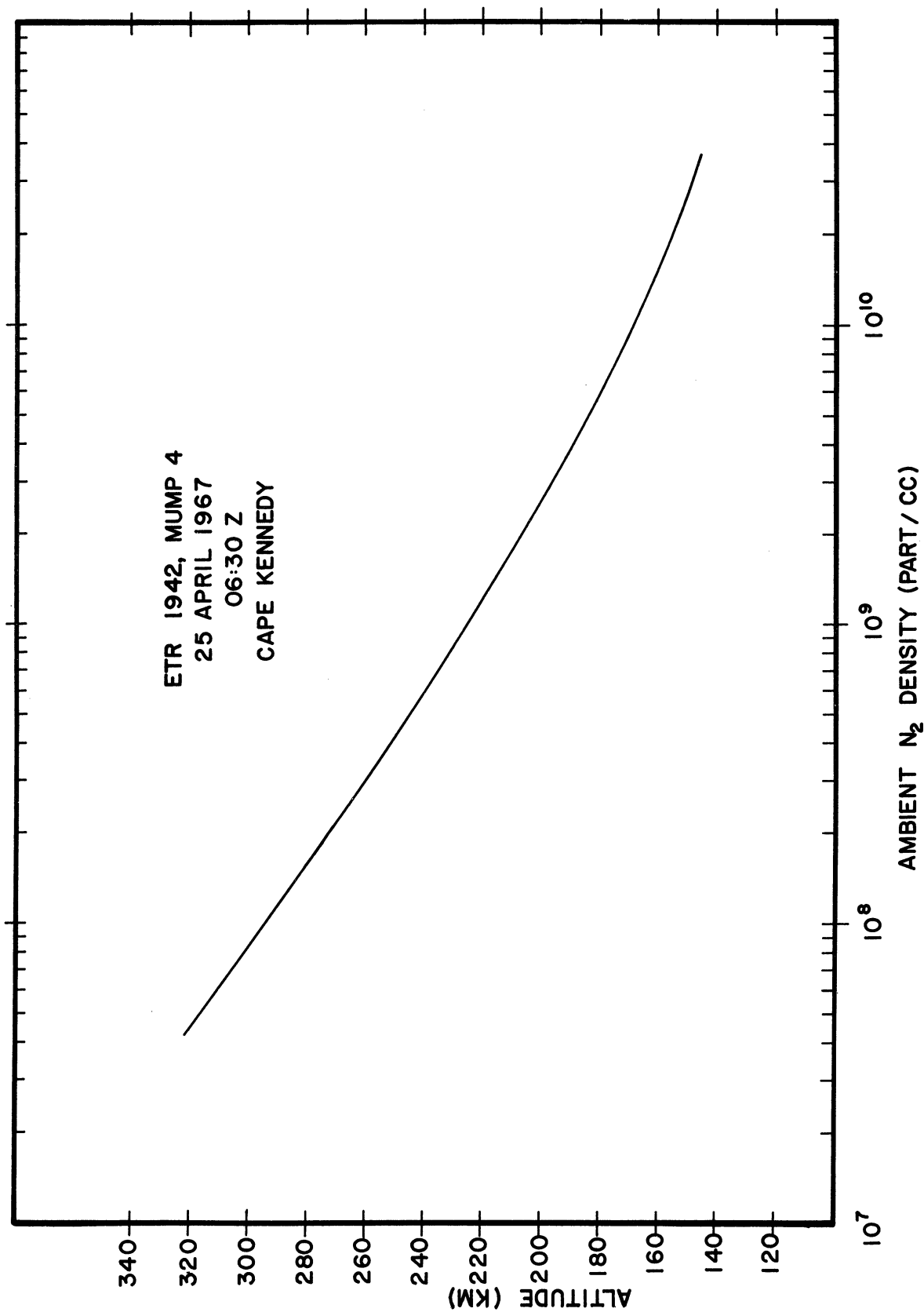
Figure 39. Ambient N_2 density for MUMP 4.

6-2-67
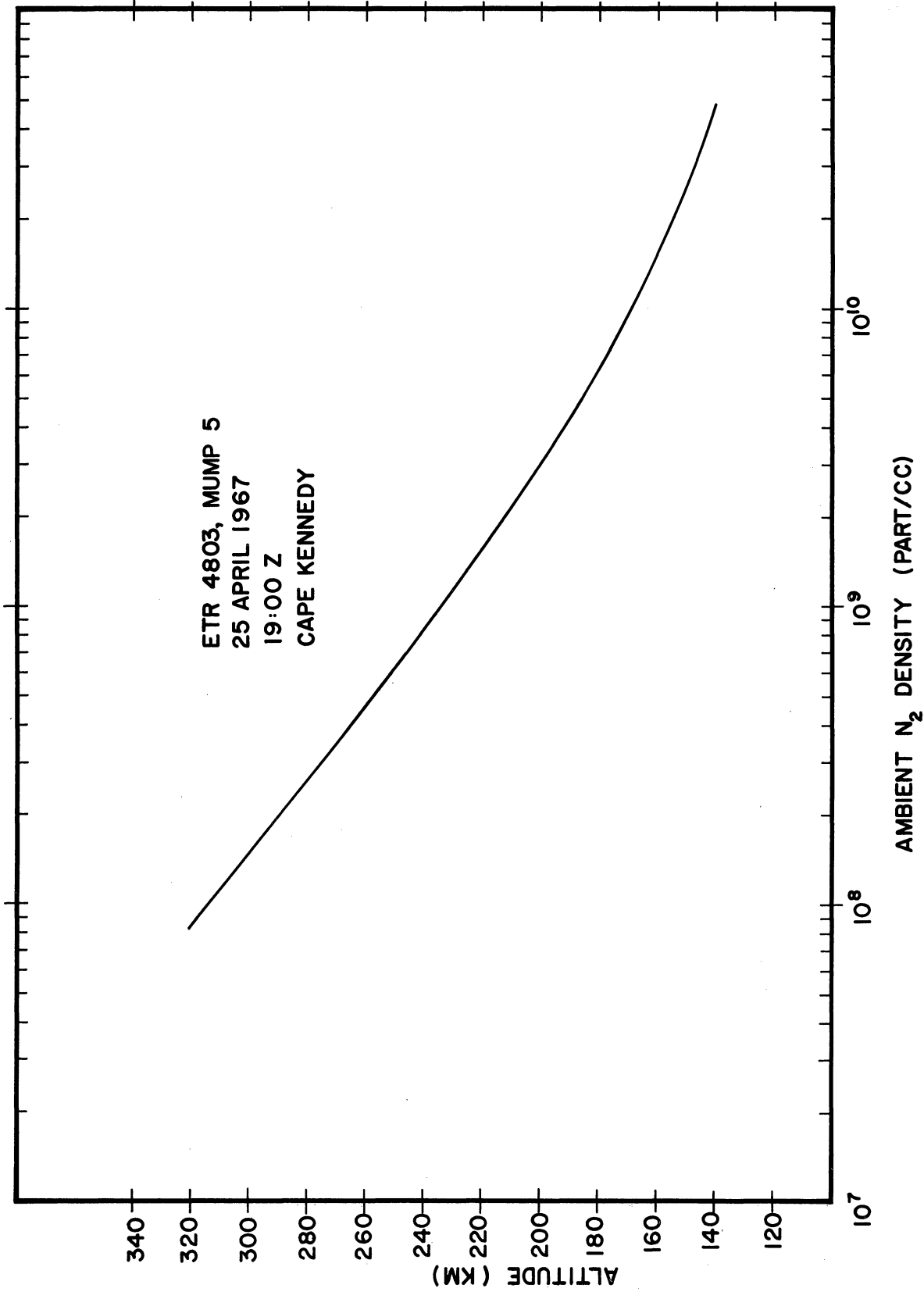
6-2-67

Figure 40. Ambient N_2 density for MUMP 5.
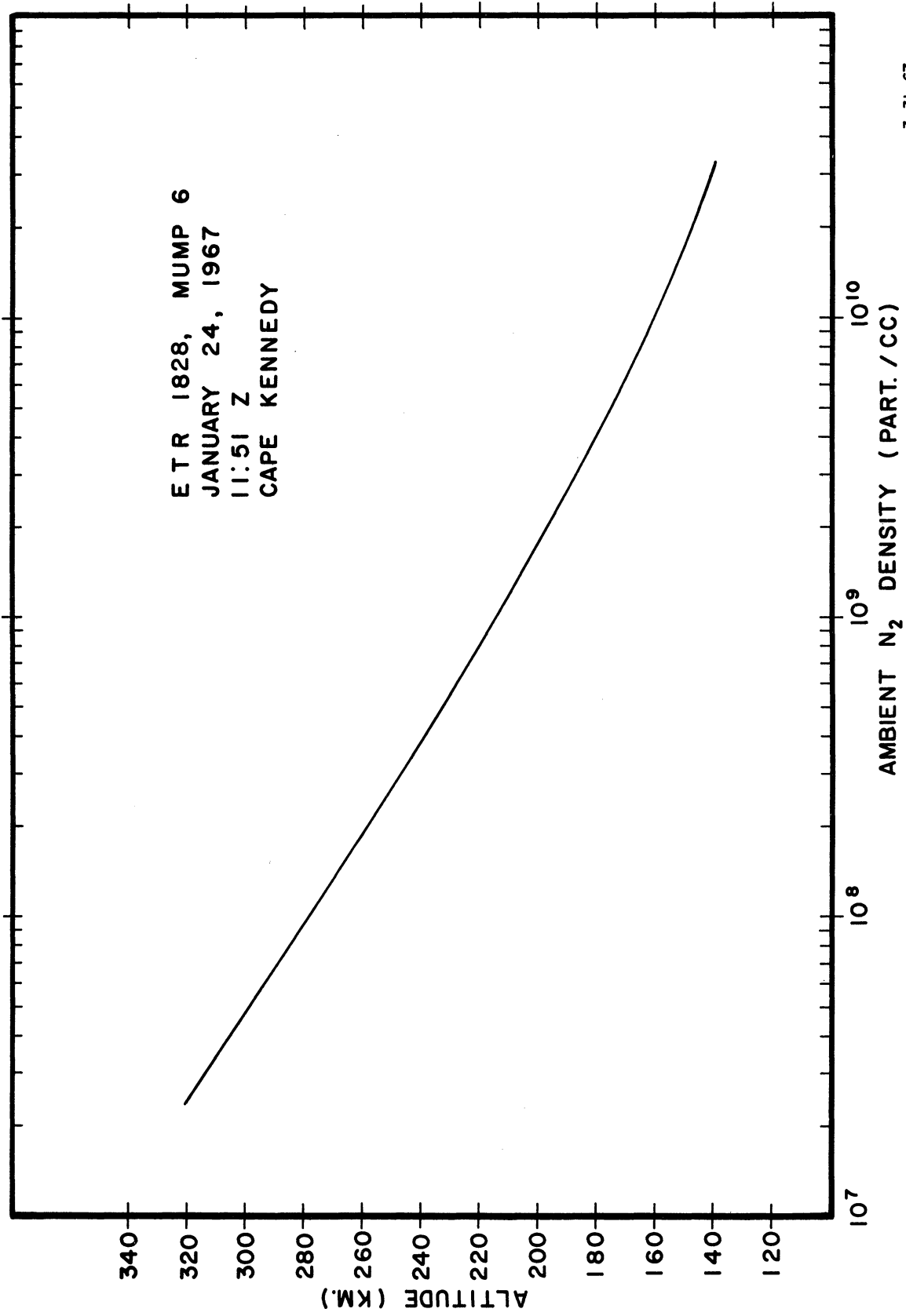
Figure 41. Ambient N_2 density for MUMP 6.
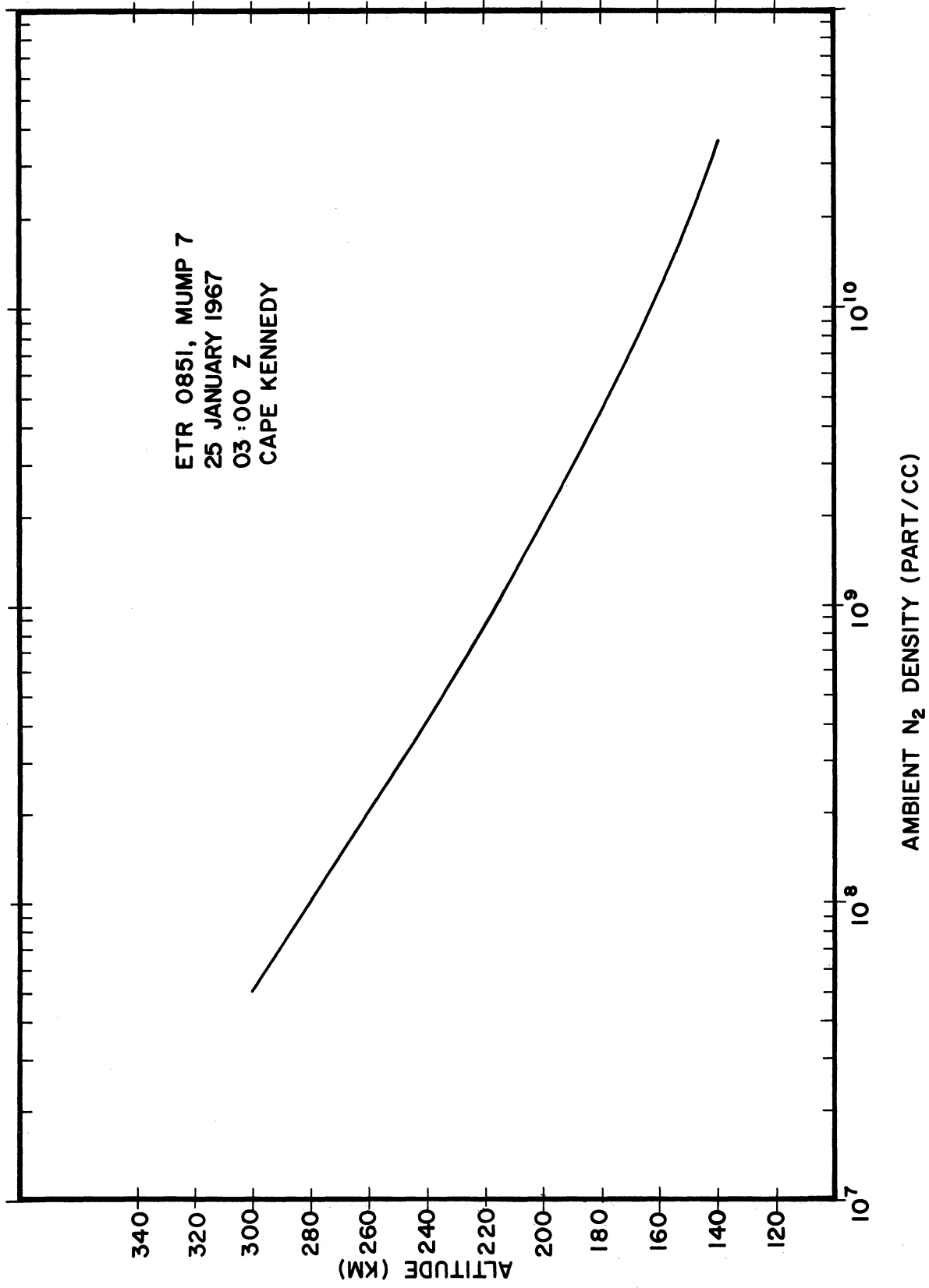
Figure 42. Ambient N_2 density for MUMP 7.

ETR 0851, MUMP 7
25 JANUARY 1967
03:00 Z
CAPE KENNEDY

AMBIENT N_2 DENSITY (PART/CC)
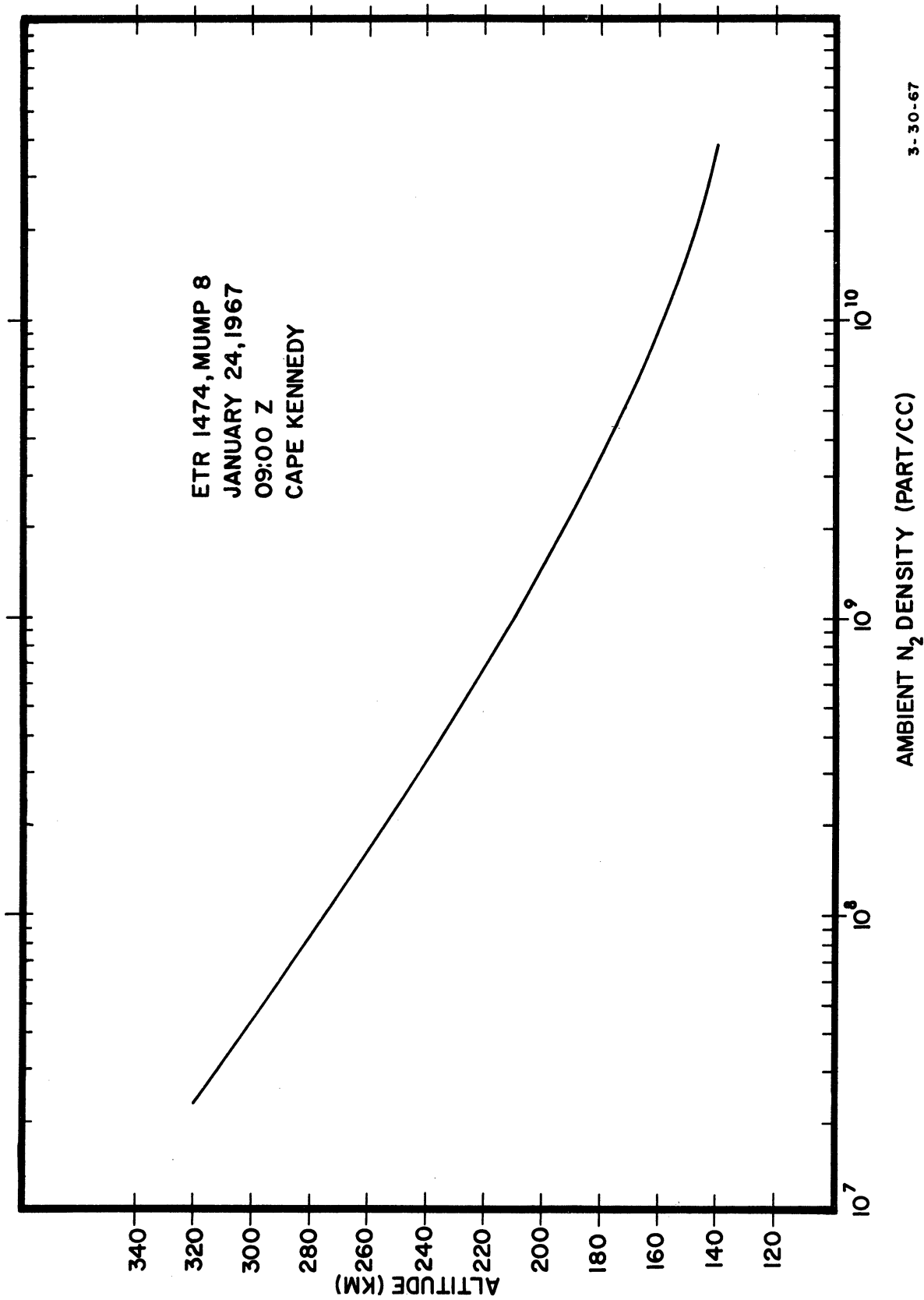
ALTITUDE (KM)

6-12-67

Figure 43. Ambient N_2 density for MUMP 8.

ETR 0381, MUMP 1
JANUARY 24, 1967
19:34 Z
CAPE KENNEDY

3-30-67
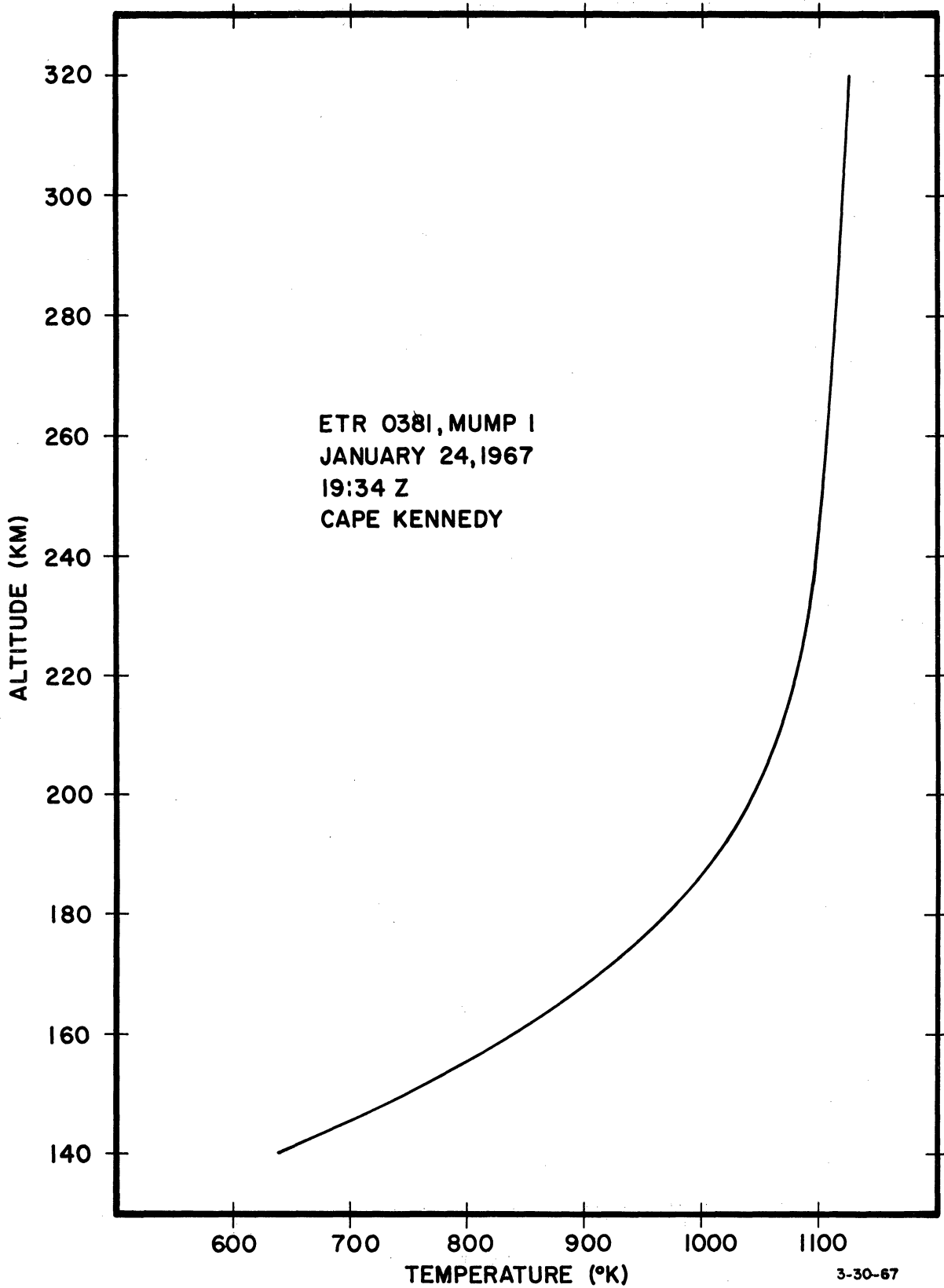
Figure 44. Neutral particle temperature vs. altitude for MUMP 1.

ETR 0611, MUMP 2
24 JANUARY 1967
22:50 Z
CAPE KENNEDY
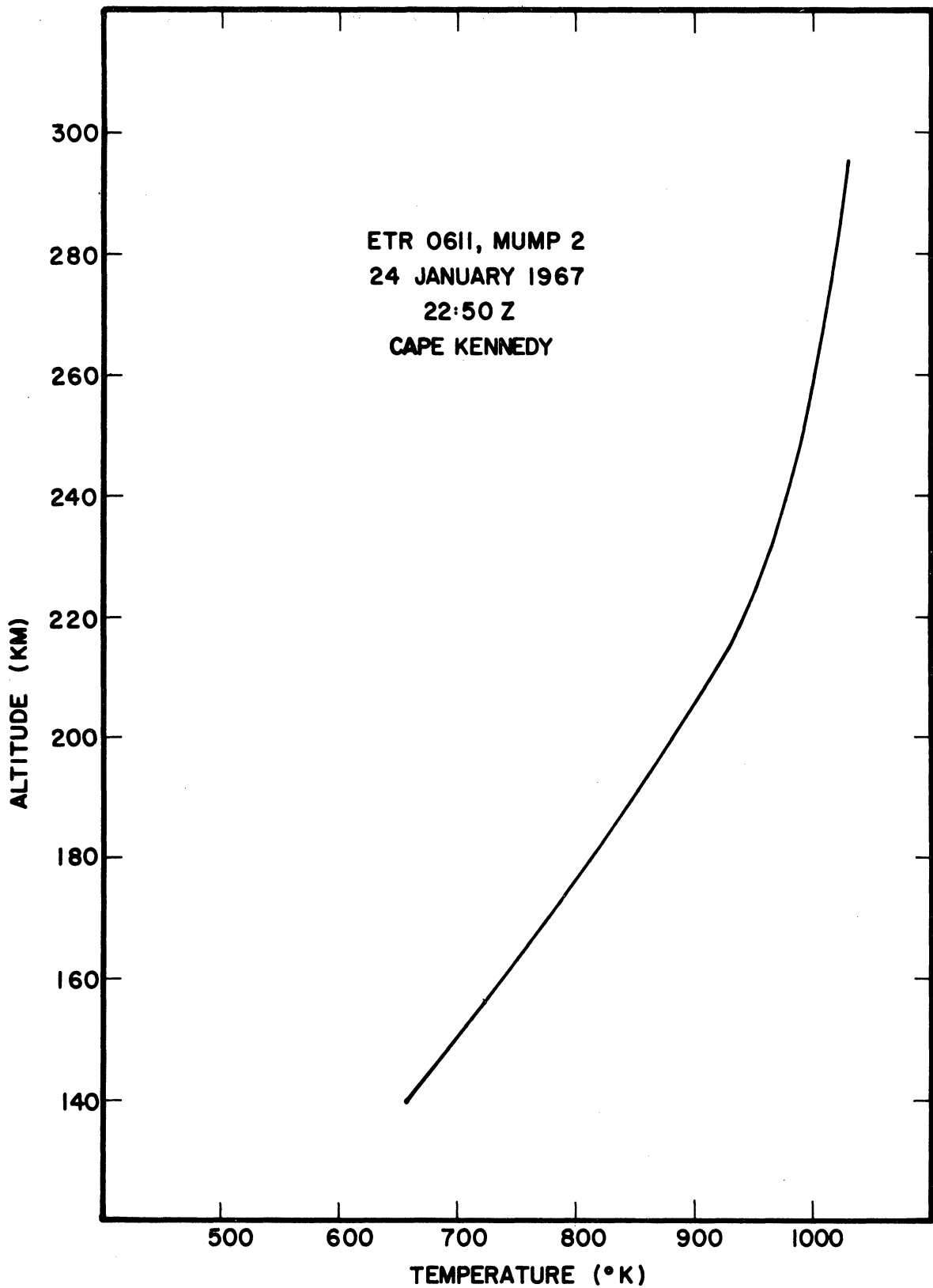
6-12-67

Figure 45. Neutral particle temperature vs. altitude for MUMP 2.
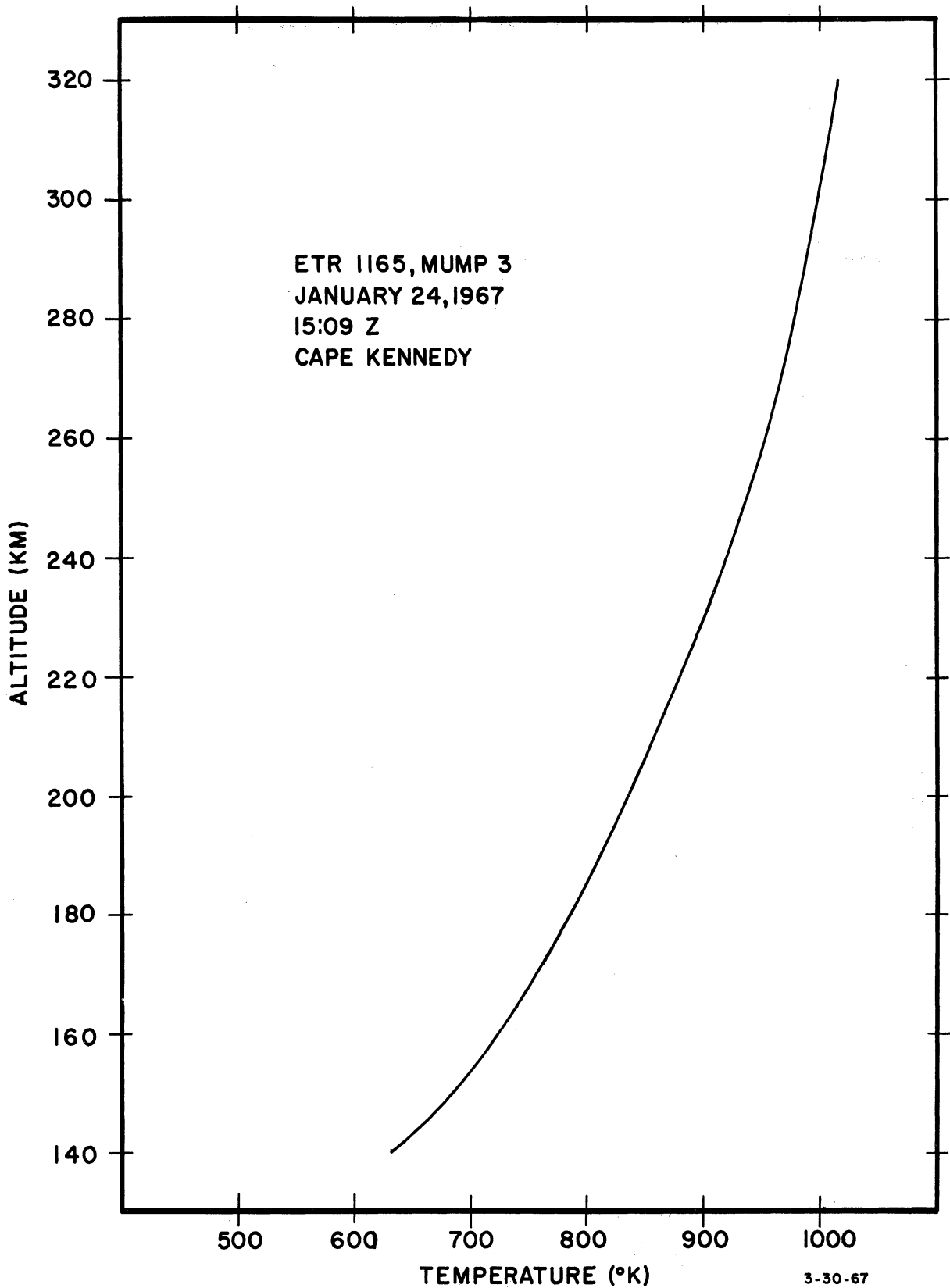
Figure 46. Neutral particle temperature vs. altitude for MUMP 3.
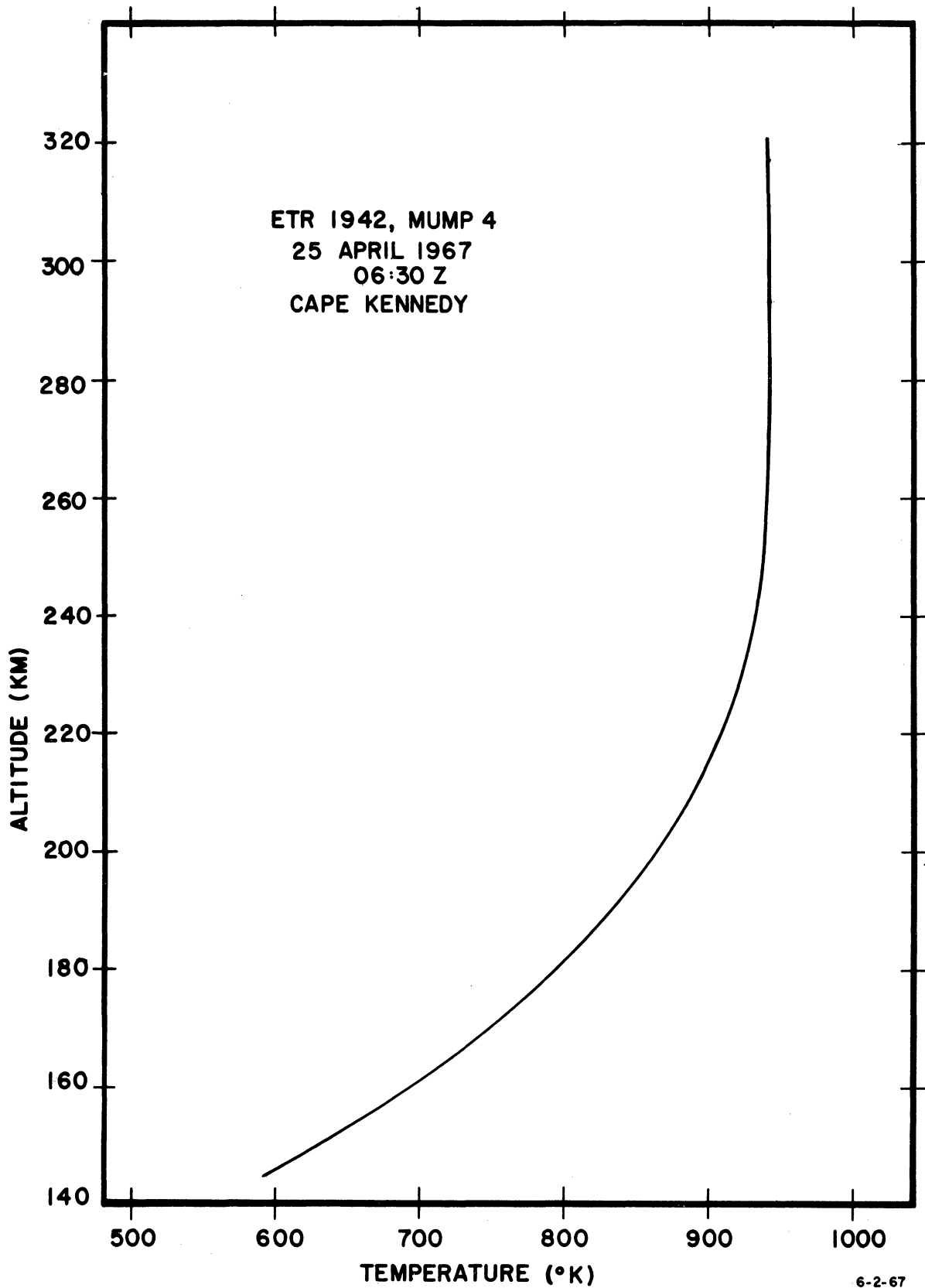
Figure 47. Neutral particle temperature vs. altitude for MUMP 4.
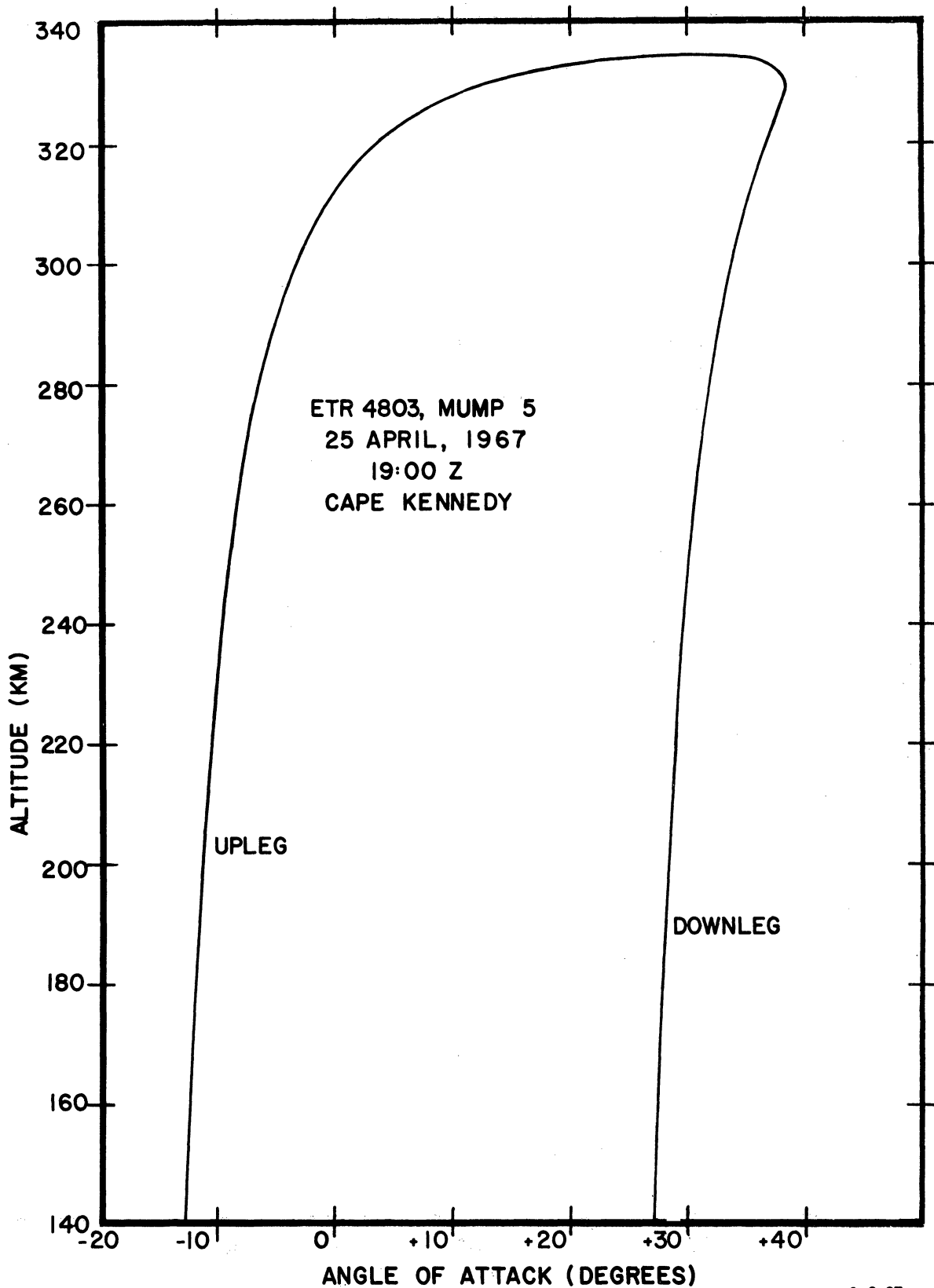
Figure 48. Neutral particle temperature vs. altitude for MUMP 5.
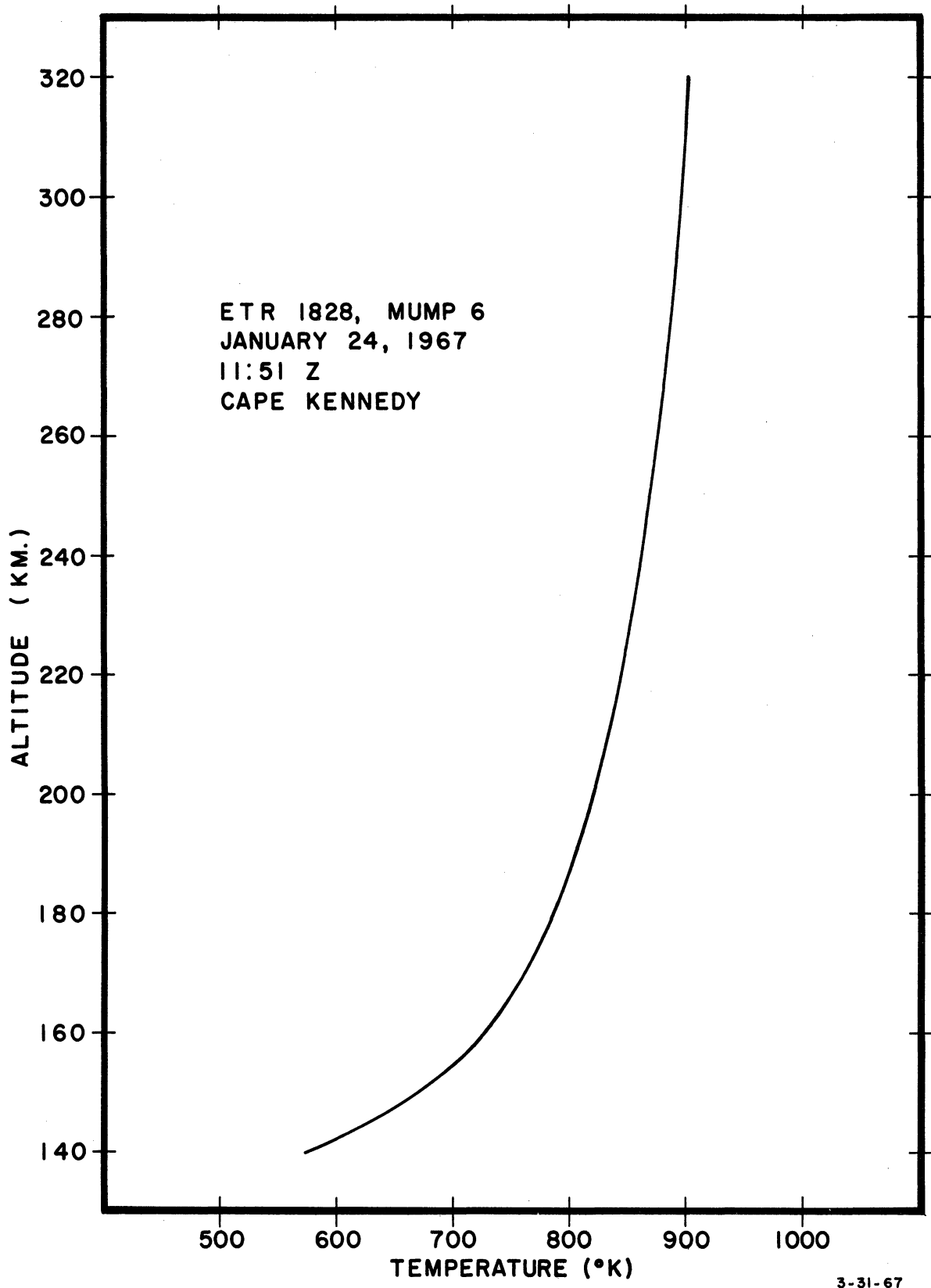
Figure 49. Neutral particle temperature vs. altitude for MUMP 6.

ETR 0851, MUMP 7
25 JANUARY 1967
03:00 Z
CAPE KENNEDY
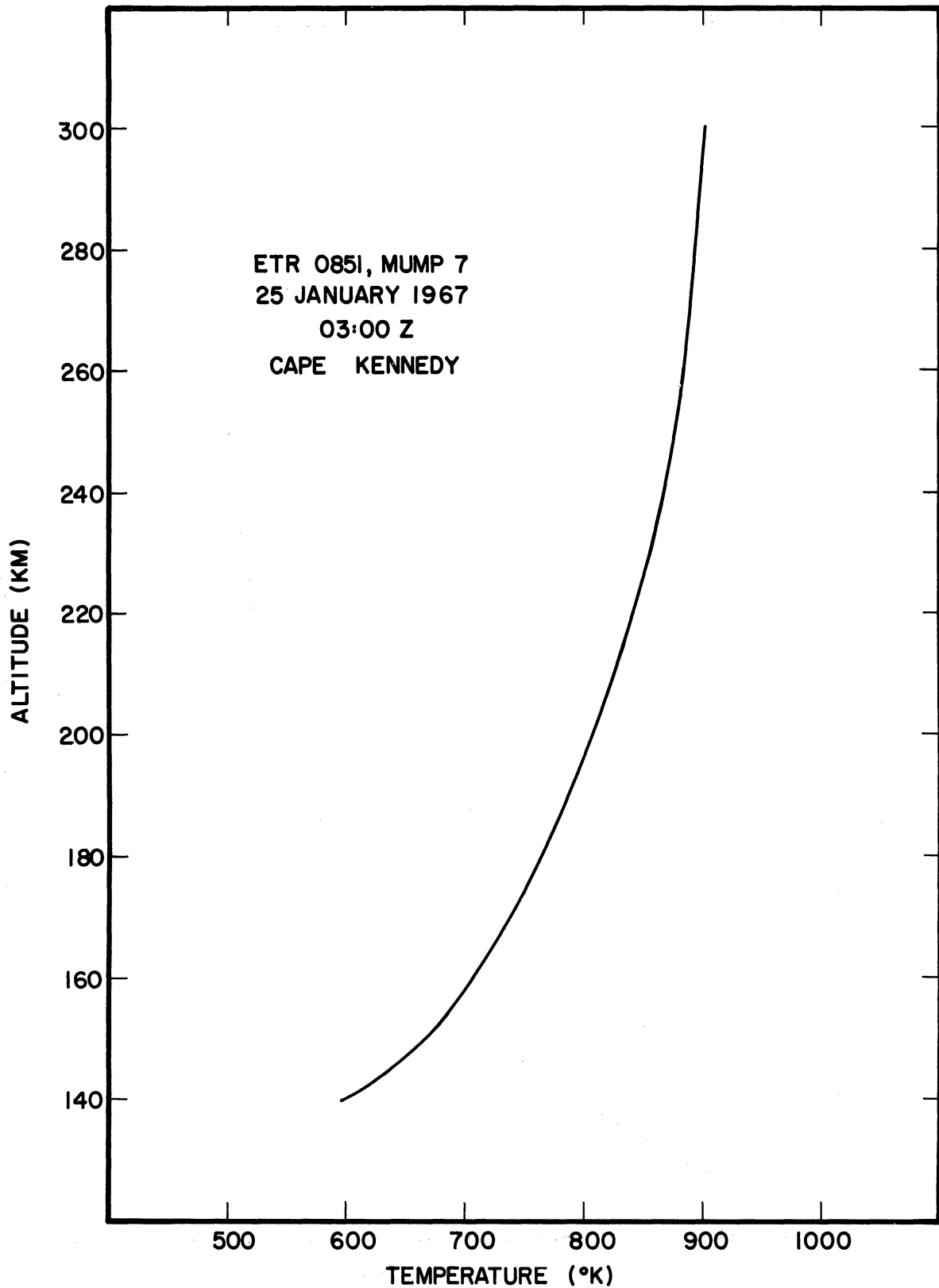
6-12-67

Figure 50. Neutral particle temperature vs. altitude for MUMP 7.

ETR 1474, MUMP 8
JANUARY 24, 1967
09:00 Z
CAPE KENNEDY

3-30-67
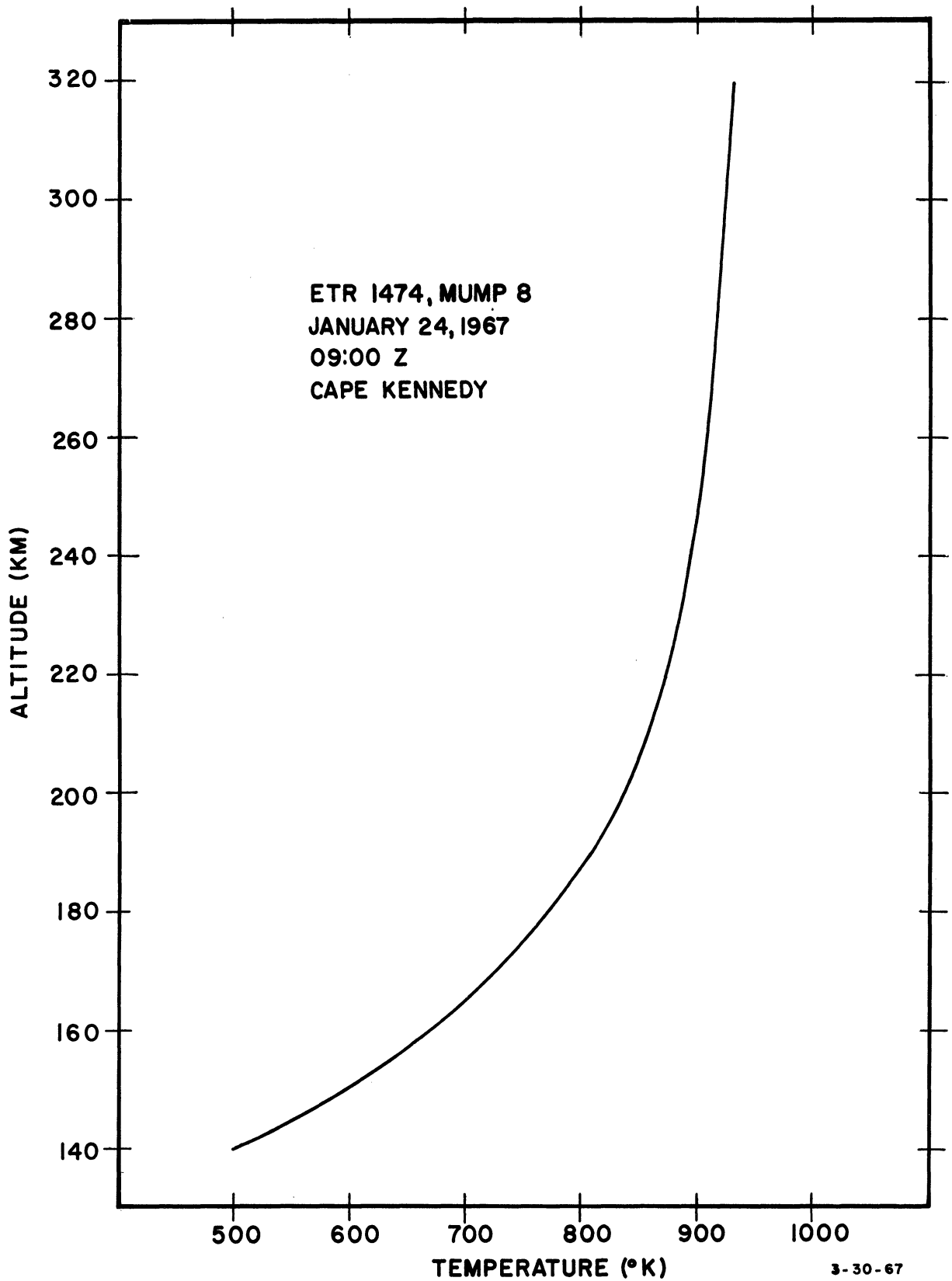
Figure 51. Neutral particle temperature vs. altitude for MUMP 8.

8.3 ELECTRON TEMPERATURE AND DENSITY

The cylindrical Langmuir probe technique which was used in this series of experiments has been described a number of times before (e.g., Brace, et al., 1963; Nagy, et al., 1963; Spencer, et al., 1965); therefore only a brief review of the data reduction technique will be given here. The equations for the current collected by a stationary cylindrical probe immersed in a plasma were derived by Mott-Smith and Langmuir (1926). Recently Kanal (1964) extended this work to moving cylindrical probes. The thermal velocity of the electrons is very large in comparison with typical rocket velocities; therefore, if the effect of sheath distortion is neglected, the probe can be considered stationary for electron current calculations. The dimension of the sheath which surrounded the collector is of the order of the Debye length, which is inversely proportional to the electron density and therefore the sheath will be the smallest in the daytime F region. The Debye length corresponding to typical daytime F region conditions is of the order of 0.3 cm; since the radius of the collector used in this experiment is only 0.027 cm, a large a/r ratio (sheath radius to probe radius) results. The retarded and accelerated electron current equations under these conditions are, respectively

$$I_r = \left(\frac{kT_e}{2\pi m_e}\right)^{1/2} N_e q A \exp\ (V_o) \tag{1}$$

$$I_a = \left(\frac{kT_e}{2\pi m_e}\right)^{1/2} N_e q A$$

$$\cdot \left[2\left(\frac{V_o}{\pi}\right)^{1/2} + \exp\ (V_o)\ \mathrm{erfc}\ (V_o^{1/2})\right] \tag{2}$$

where

k = Boltzmann's constant.
T_e = electron temperature.
m_e = mass of an electron.
N_e = number density of electrons.
q = electronic charge.
A = collector area.
V_o = qV_{pp}/kT.
V_{pp} = potential difference between the probe and the ambient plasma = $V_{ap} + V_r$.
V_{ap} is applied voltage.
V_r is potential of the reference with respect to the plasma.
erfc (x) = complementary error function = $1 - (2/\pi^{1/2}) \int_o^x \exp\ [-\beta^2]\ d\beta$.

The method of electron temperature reduction from the retarding potential current characteristics, used on previous occasions, was outlined in the report by Taeusch, et al., (1965). In this method the retarded electron current is plotted on a semilog paper, and the temperature is obtained from the slope of the resulting straight line; such a typical plot from flight ETR 1474 is shown in Figure 52. Since this technique is very cumbersome and time consuming and the computerized system for reduction of the data was not yet operational, the following "template method" was used to reduce the bulk of the data.

The natural logarithm of the ratio of two points on the retarded electron current characteristics is:

$$\ln C = \frac{q}{k} \frac{\Delta V_{ap}}{T_e}$$

$$C = \frac{I_{e2}}{I_{e1}} = \text{ratio of electron currents}$$

$$\Delta V_{ap} = V_{ap2} - V_{ap1}$$

V_{ap2} = applied voltage corresponding to I_{e2}

V_{ap1} = applied voltage corresponding to I_{e1}

Since the retarded electron current is exponential (Equation 1), ΔV_{ap} will be the same for all points having the same ratio C. Given a C we can therefore determine ΔV_{ap} for different temperatures and draw a grid as shown in Figure 53.

The current collected by the probe is not the electron but the total current, so we have to apply the same corrections as used on previous occasions. The ion saturation current is extrapolated by a straight line and it is assumed that the difference between the net current and the straight line is the electron current. This leads to the con struction of a template as shown in Figure 54. Here instead of calibrating the grids in terms of ΔV_{ap} we did it in terms of temperature allowing direct determination of the electron temperatures. The templates were made of transparent paper by allowing them to be used directly on the paper record of the telemetered data. The majority of the temperature information was obtained in this manner. Numerous data curves were also reduced by using the conventional semi-log method for the sake of comparison, but no detectable difference in the results was observed.

The accelerated electron current is two orders of magnitude higher than the retarded ion current; therefore, the effect of the latter on the total current is negligible. The two unknown quantities in the accelerated electron current, Equation (2), are the electron density, N_e, and the reference potential, V_r. Any two points from this portion of the curve are, therefore, sufficient to solve for the unknowns (Nagy and Faruqui, 1965). Templates based on this method were used to obtain the electron density results from the series of flights discussed here.

When $V_O >> 1$ Equation (2) simplifies to

$$ I_{ea} \approx \left(\frac{kT_e}{2\pi m_e} \right)^{1/2} N_e qA \ \frac{2}{\pi^{1/2}} \ V_O^{1/2} \tag{3} $$

For typical ionospheric conditions (e.g., $T_e = 2000°$ K) V_O is 5.79 V when V_{ap} is 1 V; therefore, Equation (3) is applicable when $V_{ap} > 1$ V. Let us consider two points on the accelerated electron current characteristics corresponding to $(V_{ap} - V_r)$ equal to 2 V and 1 V respectively. The ratio of the currents corresponding to these two voltages is $\sqrt{2}$ according to Equation (3). Two vertical lines, separated by a distance, corresponding to a difference of 1 V in the applied voltage, as shown in Figure 55, provides a template which can be used to determine the electronic density directly from the characteristic curves. The density is obtained by placing the template on the data curve and shifting it horizontally until the curve crosses the vertical lines at the points which correspond to the same electron density (see Figure 56). This value then corresponds to the solution of Equation (3) for N_e.

The charged particle results obtained from the electrostatic probe experiments of MUMPS 1, 2, 3, 4, 5, 6, 7, and 8 are shown in Figures 57 through 64, respectively.

8.4   GEOPHYSICAL INDICES

The 10.7 cm solar flux ($F_{10.7}$) and the geomagnetic activity indices (a_p) for the appropriate periods during launch day are shown in Figures 65, 66, and 67.

LOG CURRENT vs. POTENTIAL FOR ESP

ETR 1474   MUMP 8   TIME FROM LAUNCH: 114.9 SEC.

SCALED ELECTRON CURRENT

SCALED POTENTIAL

$T_e = 1,262 \ ^\circ K$
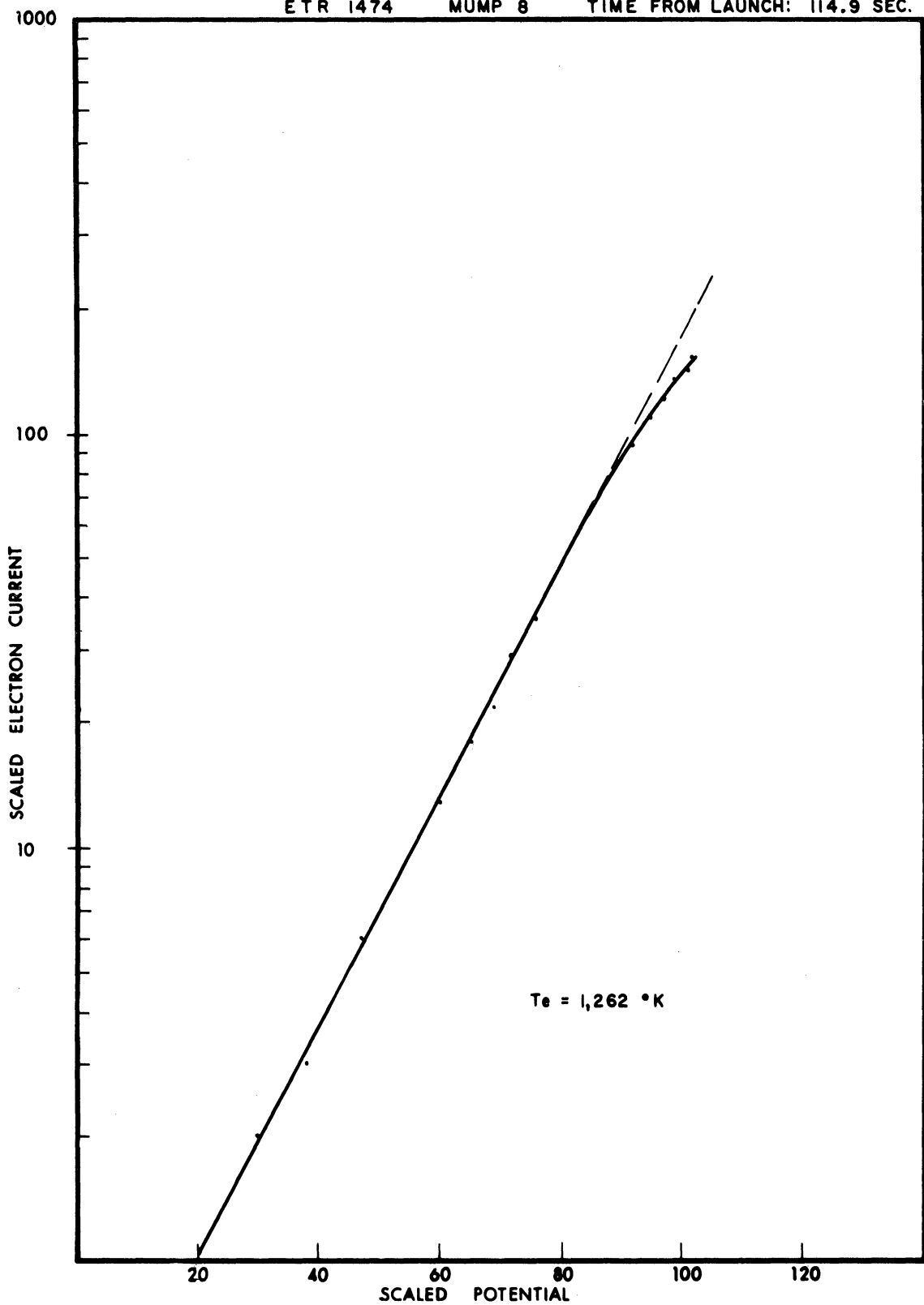
Figure 52. Typical log current vs. potential plot
from the electrostatic probe experiment of MUMP 8.

Figure 53. Electron temperature template with no ion current correction.

Figure 54. Electron temperature template with ion current correction.
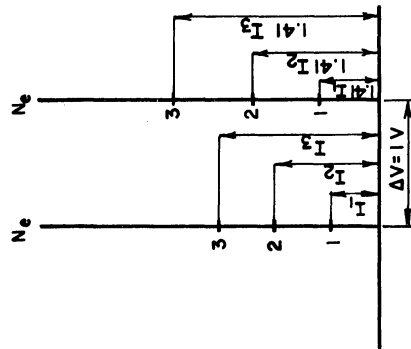
Figure 55. Basic electron density template.
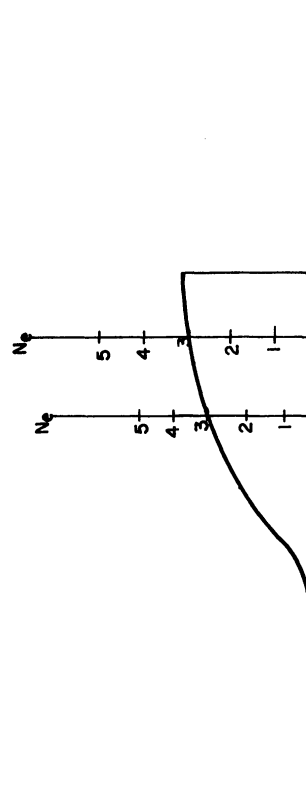
Figure 56. Electron density template superimposed on data curve.

113
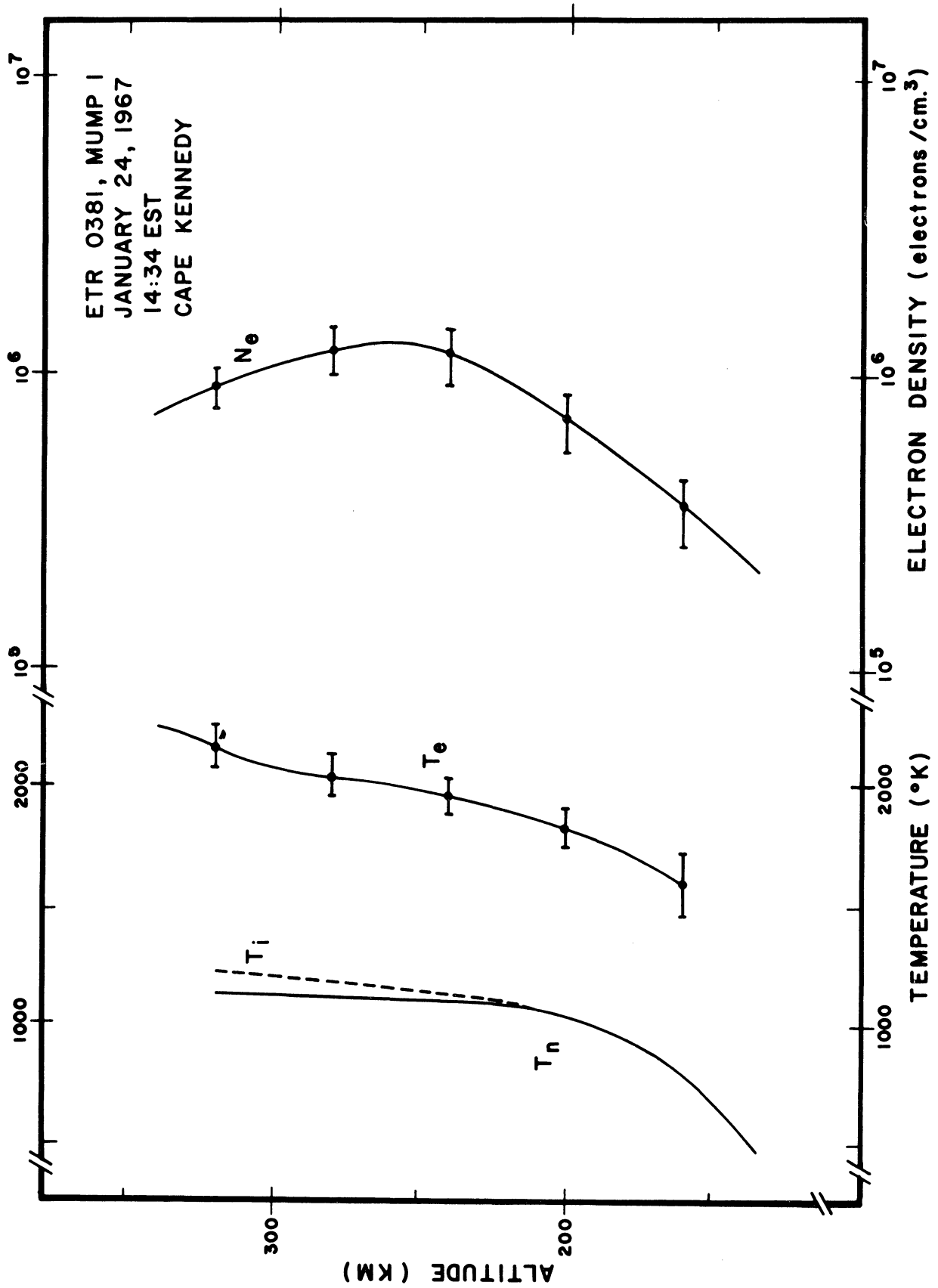
Figure 57. Charged particle results from the electrostatic probe experiment of MUMP 1.
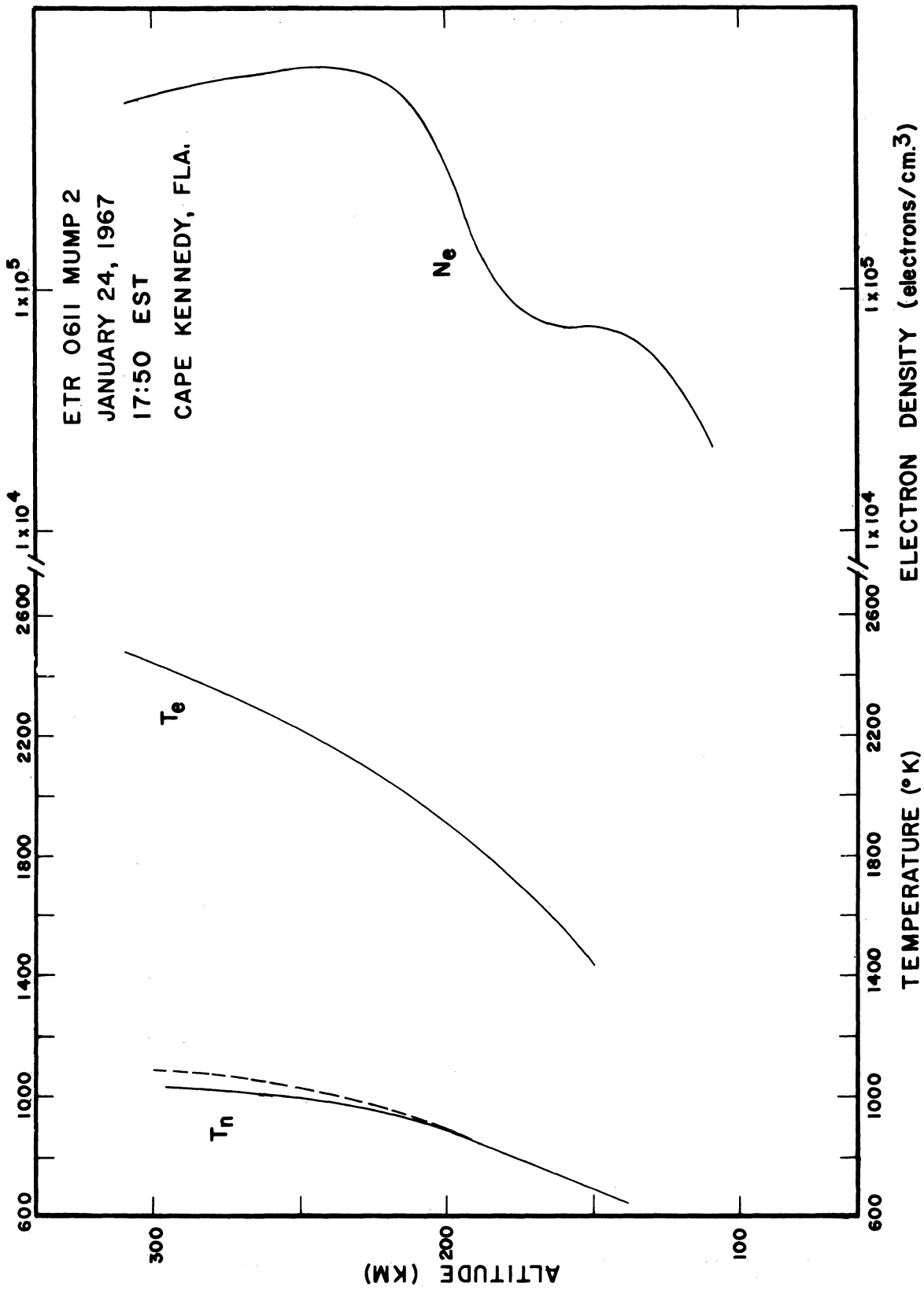
Figure 58. Charged particle results from the electrostatic probe experiment of MUMP 2.
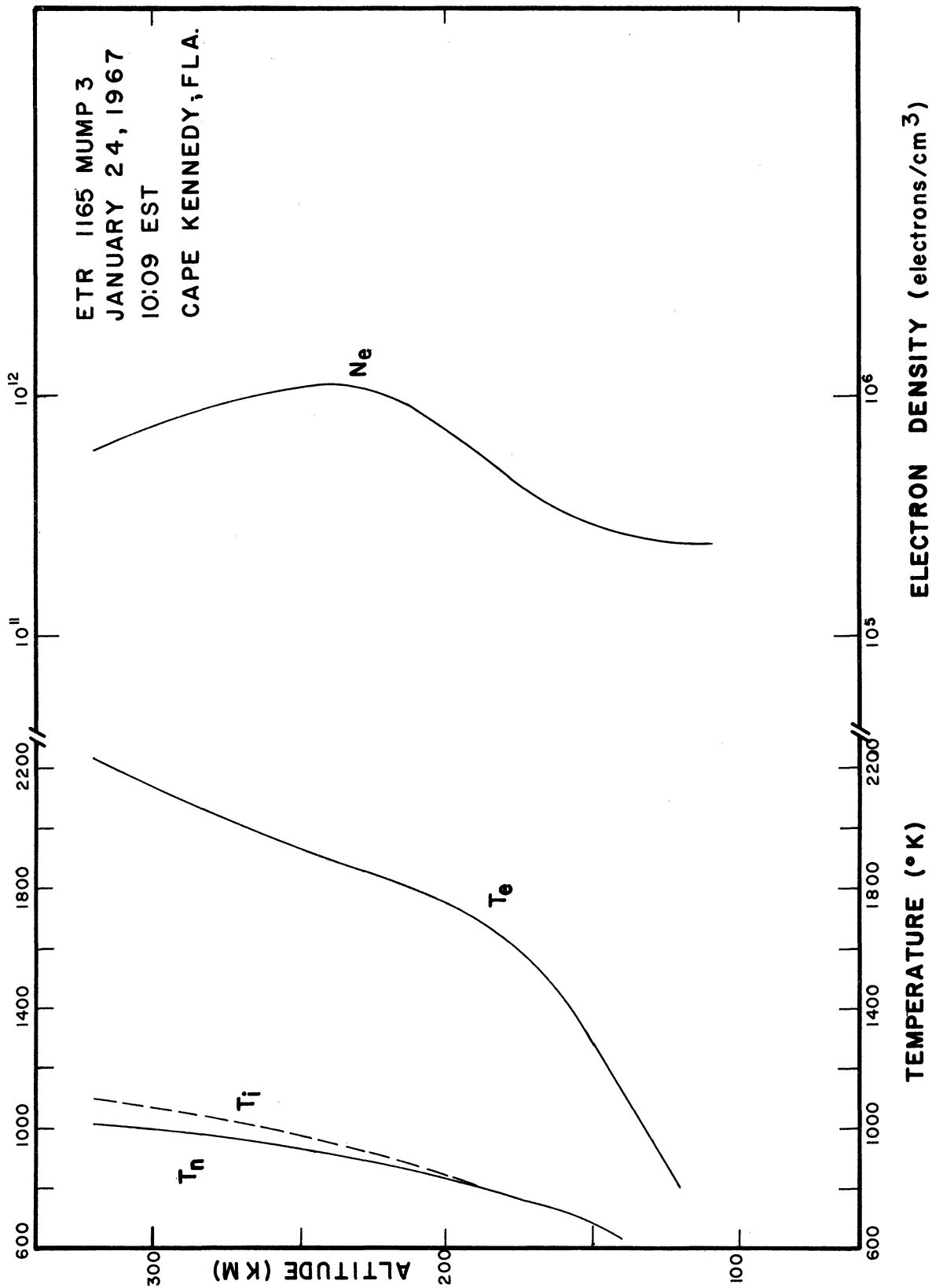
Figure 59. Charged particle results from the electrostatic probe experiment of MUMP 3.
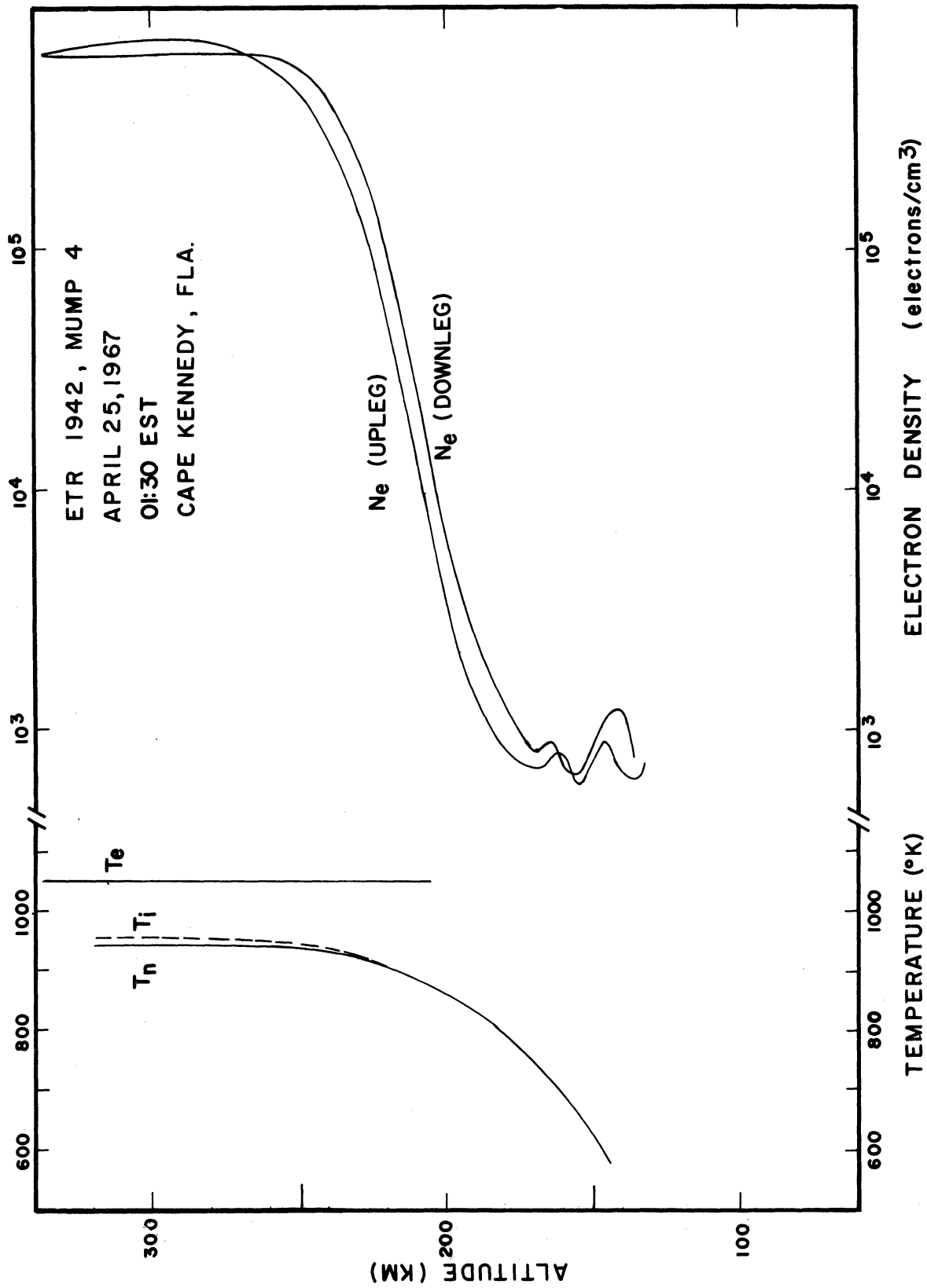
Figure 60. Charged particle results from the electrostatic probe experiment of MUMP 4.
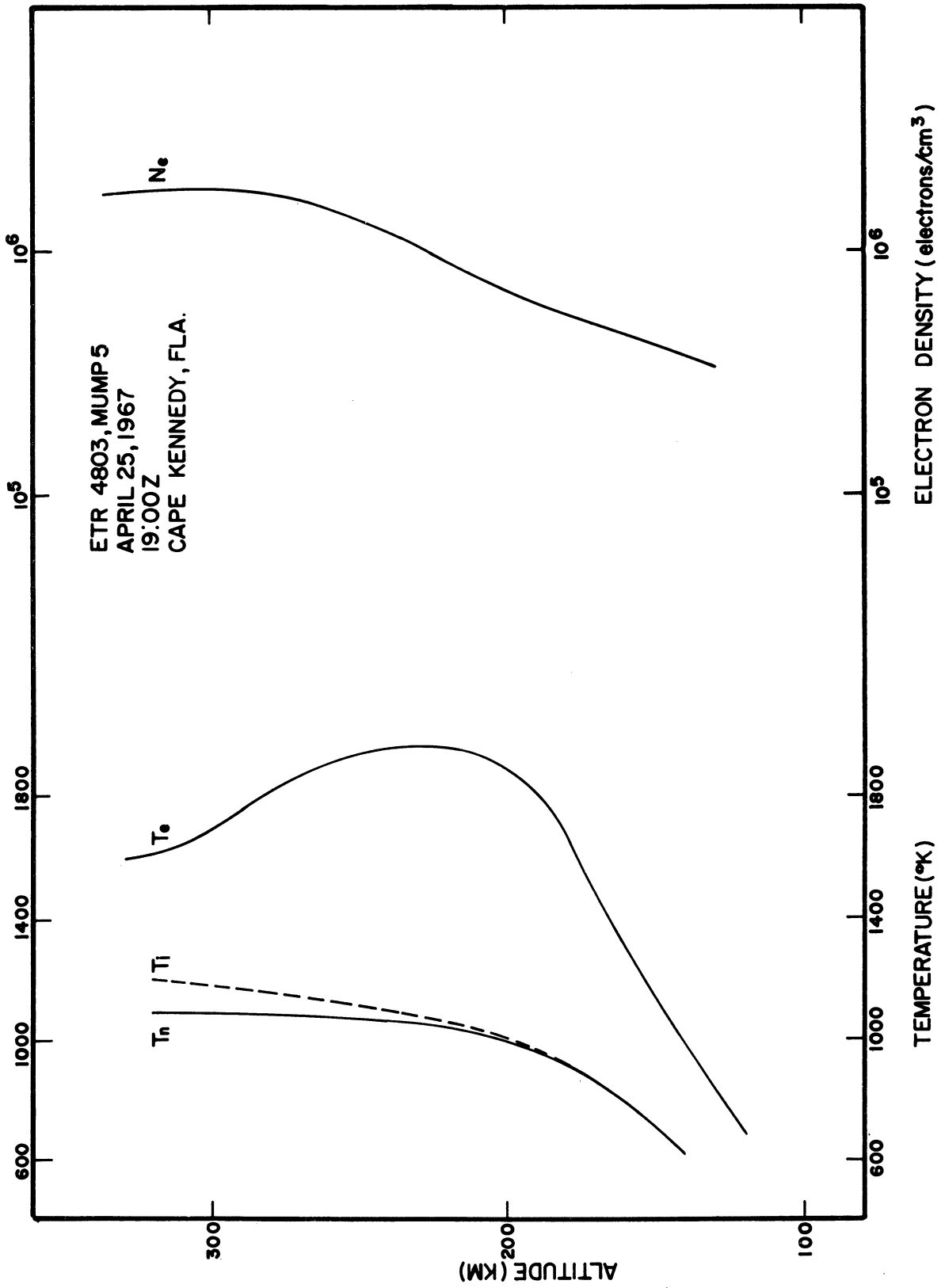
Figure 61. Charged particle results from the electrostatic probe experiment of MUMP 5.
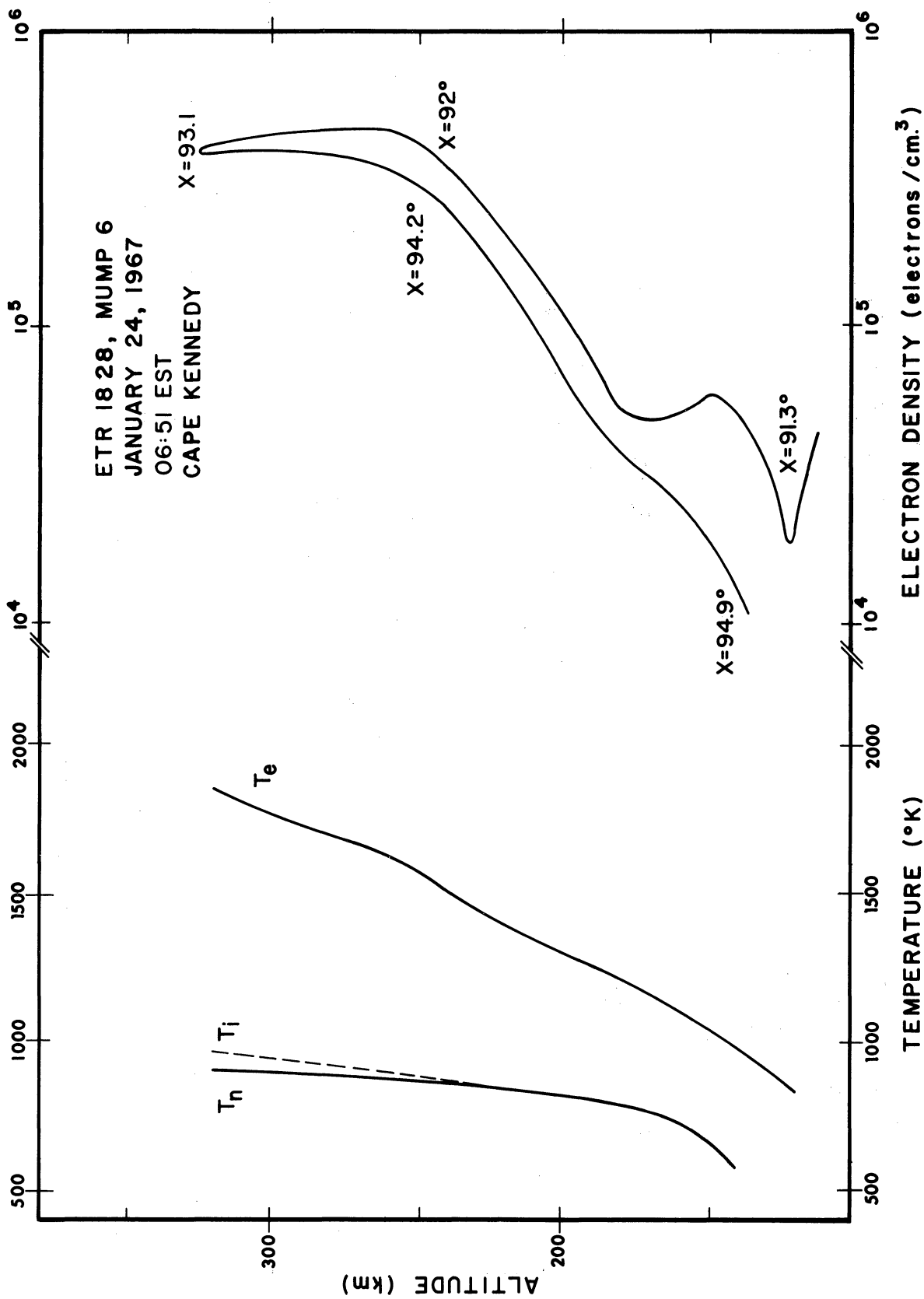
Figure 62. Charged particle results from the electrostatic probe experiment of MUMP 6.
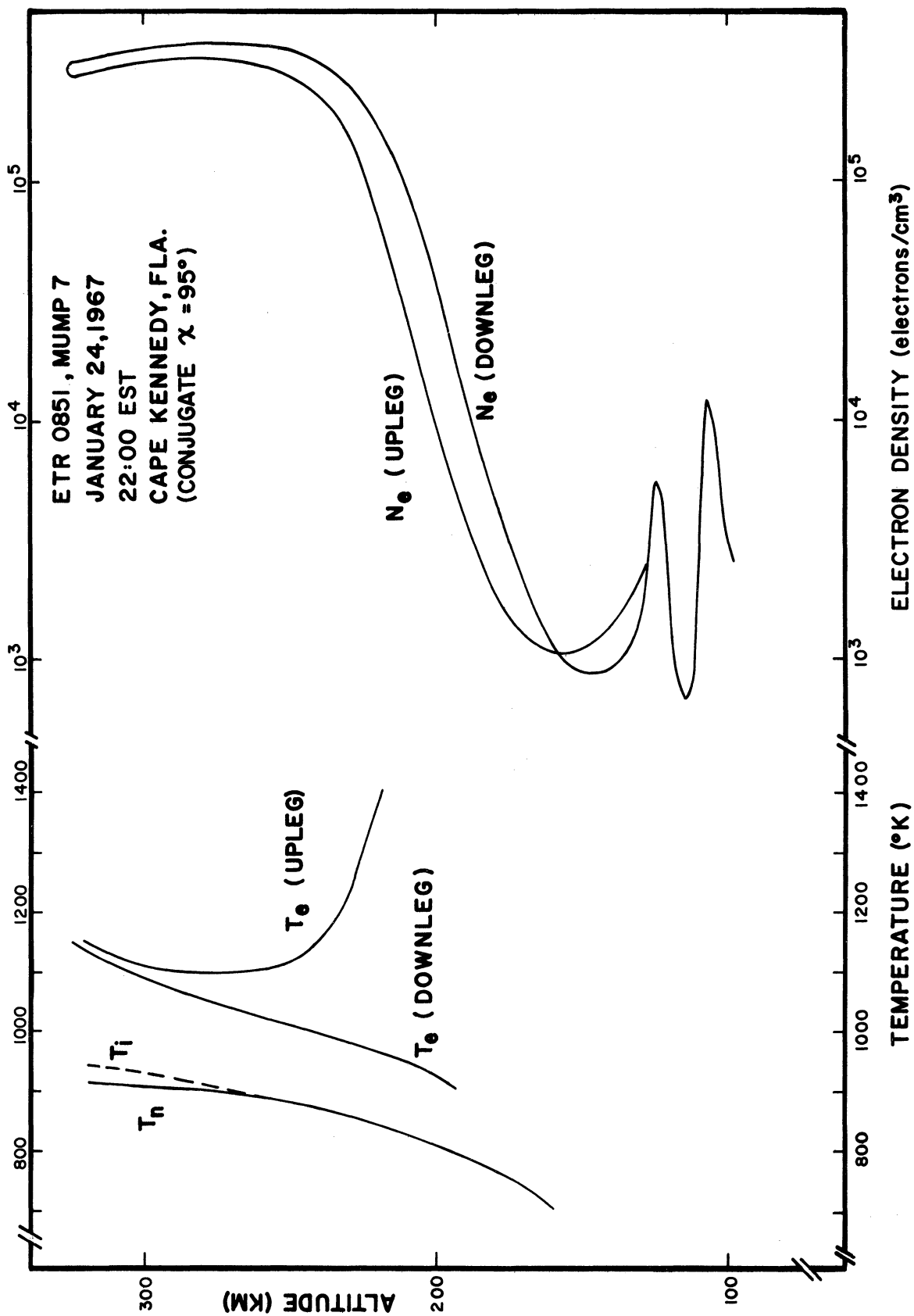
Figure 63. Charged particle results from the electrostatic probe experiment of MUMP 7.
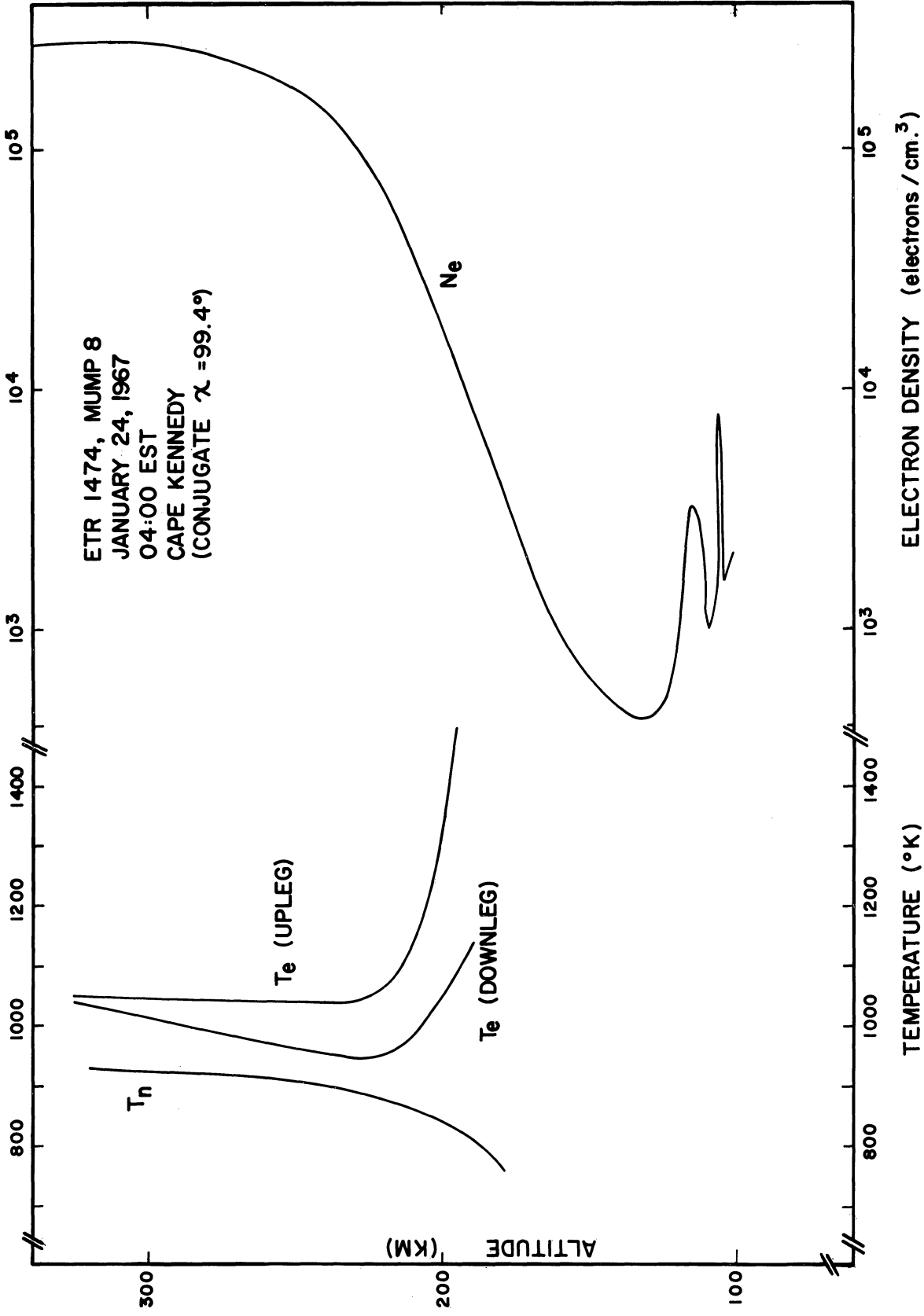
Figure 64. Charged particle results from the electrostatic probe experiment of MUMP 8.
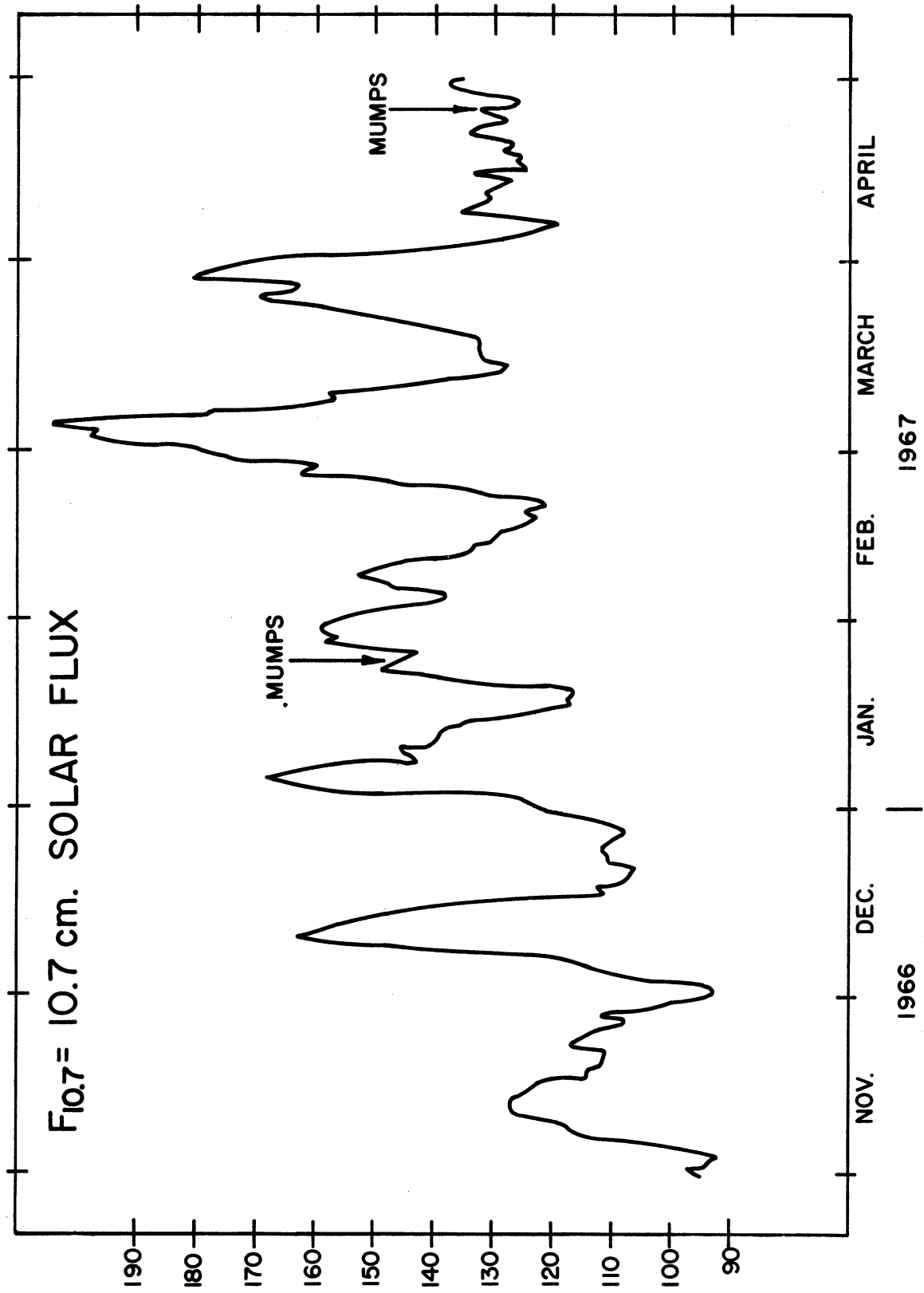
Figure 65. The solar flux at 10.7 cm wavelength.
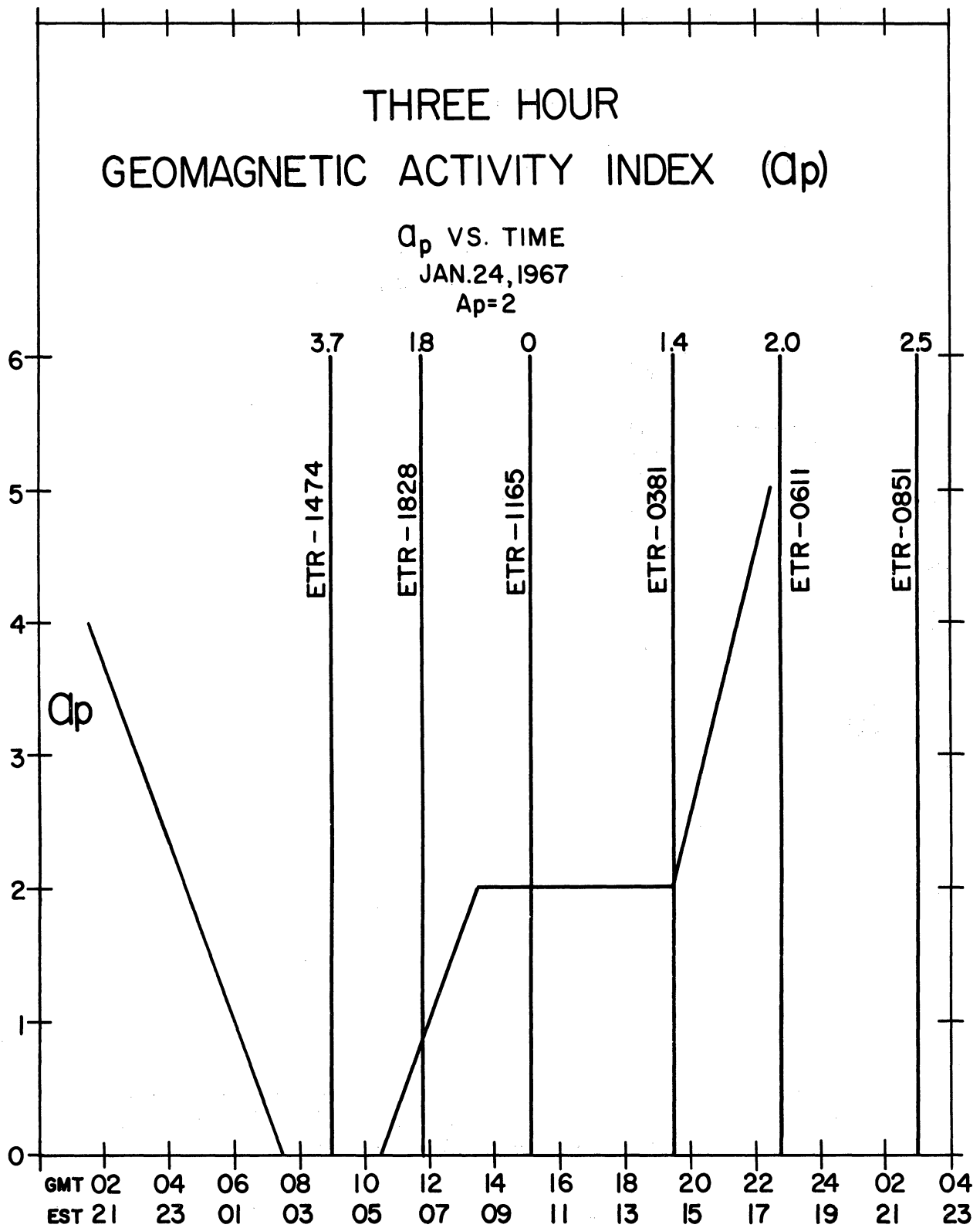
Figure 66. Three-hour geomagnetic activity index (a_p) (January 24, 1967).
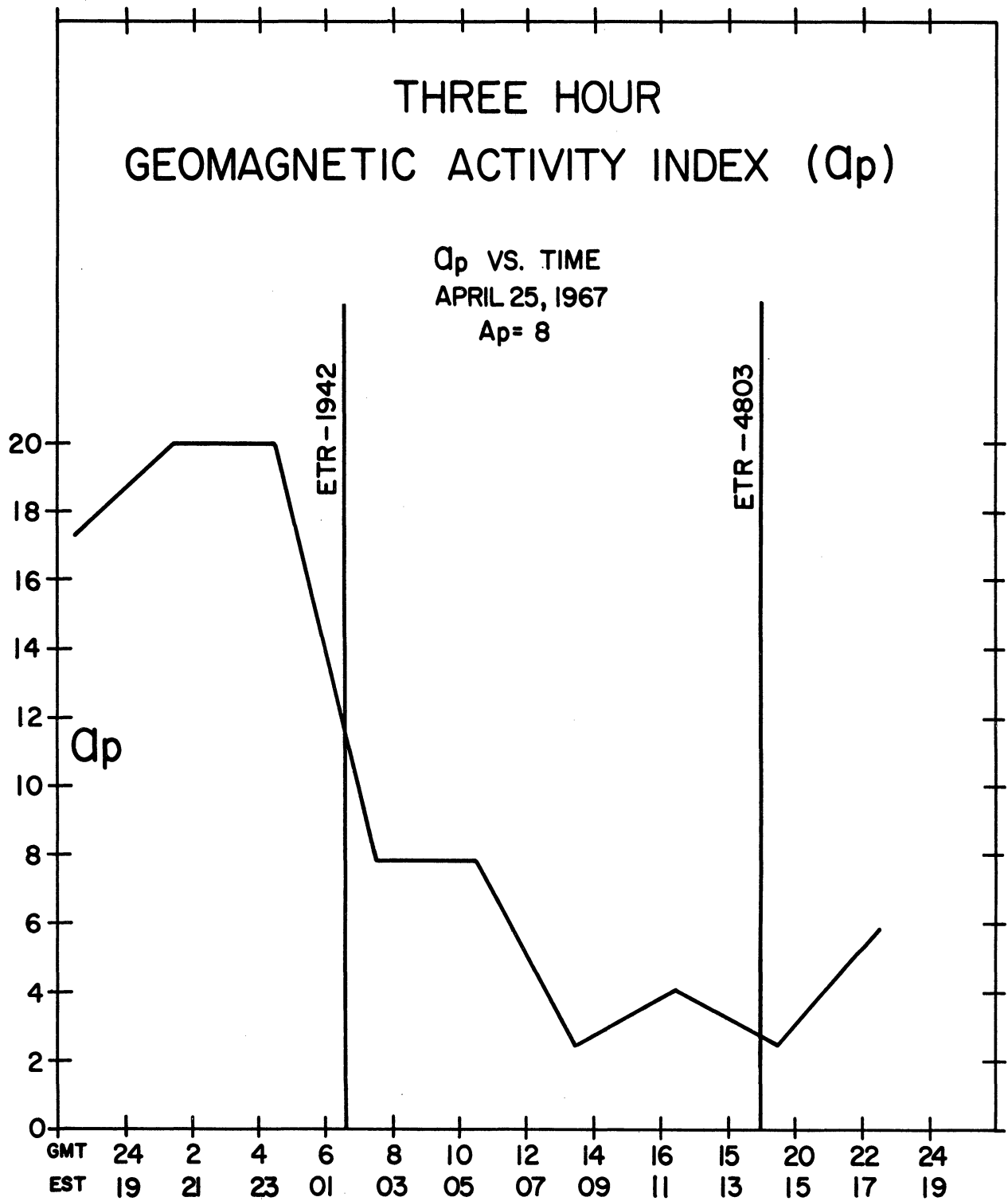
Figure 67. Three-hour geomagnetic activity index (a_p) (April 25, 1967).

9. CONCLUSIONS

The payload design and successful launching of eight Marshall-University of Michigan probes have been described in the present report. These probes provided data which permitted the determination of the neutral molecular nitrogen density and temperature and the electron density and temperature in the altitude region between approximately 140 and 320 km. Six of the payloads provided data during one diurnal cycle on January 24, 1967. Two additional payloads provided data on the maximum and on the minimum of the diurnal variation on April 25, 1967. The purpose of the two sets of launches was to obtain data which would bear on the diurnal variation of the atmospheric parameters, and consequently be of value in the development of future model atmospheres. The data have been reported at the July meeting of COSPAR in London, England, and the paper has been accepted for publication in Space Research VIII. A summary discussion of the preliminary findings and significant points of interest are included in the following subsections.

9.1 NEUTRAL MOLECULAR NITROGEN DENSITY AND TEMPERATURE

The theory of the measurement, of the reduction of raw data, and of the probable errors for each of the nitrogen, density, and temperature altitude profiles was discussed in the previous section. Figures 68 and 69 give the congeries of these data. Of more interest here, however, are the variations with time of day as given in Figures 70 and 71. The figures also show several data points taken from the CIRA 1965 model 4 and also show the variation as is predicted by Jacchia (1964, 1965a,b) for the appropriate 10.7 cm solar flux and geomagnetic activity levels. As can be seen, the density values predicted by the two models are approximately a factor of two greater than the measured values. This discrepancy between gauge measurements and drag measurements has persisted for many years. However, the temperature predictions made by Jacchia (1964, 1965a,b) are in excellent agreement with the temperature values determined from the measured density profiles.

Even though these data are relatively new and much work remains to be done, some preliminary conclusions are as follows:

1. Densities determined by satellite drag techniques are typically on the order of a factor of two higher than those determined by density gauge and mass spectrometer techniques.

2. CIRA 1965 model nighttime temperatures are in good agreement with those derived by direct measurements, but the daytime model temperatures are consistently too high at the level of solar activity used for the comparison.

125

3. The atmospheric temperatures and densities below 200 km are more variable than current models predict.

4. The Jacchia empirical formulae, which predict exospheric temperatures as a function of geomagnetic activity, solar flux, and time of day and year, are consistent with the mass spectrometer results.
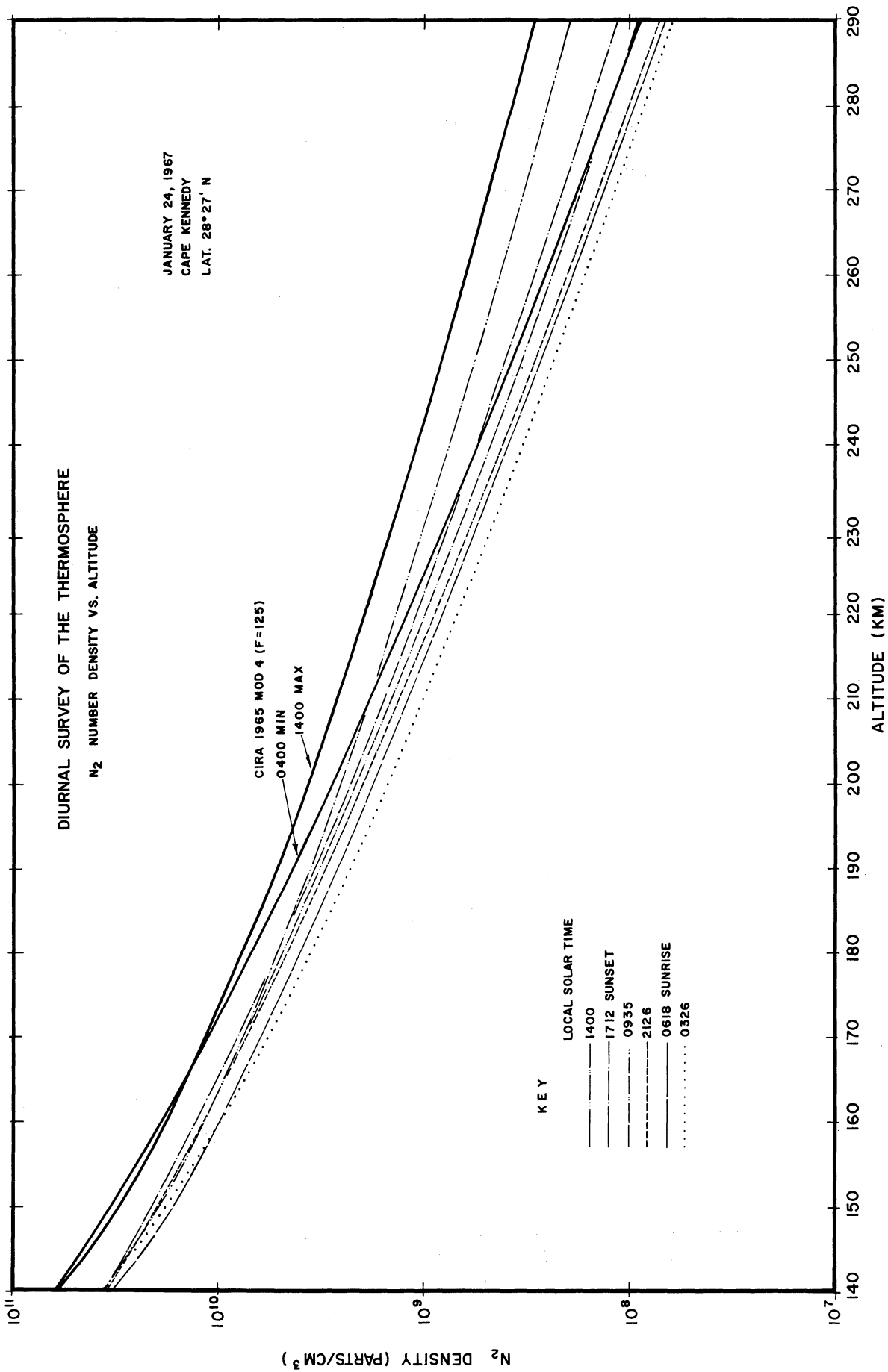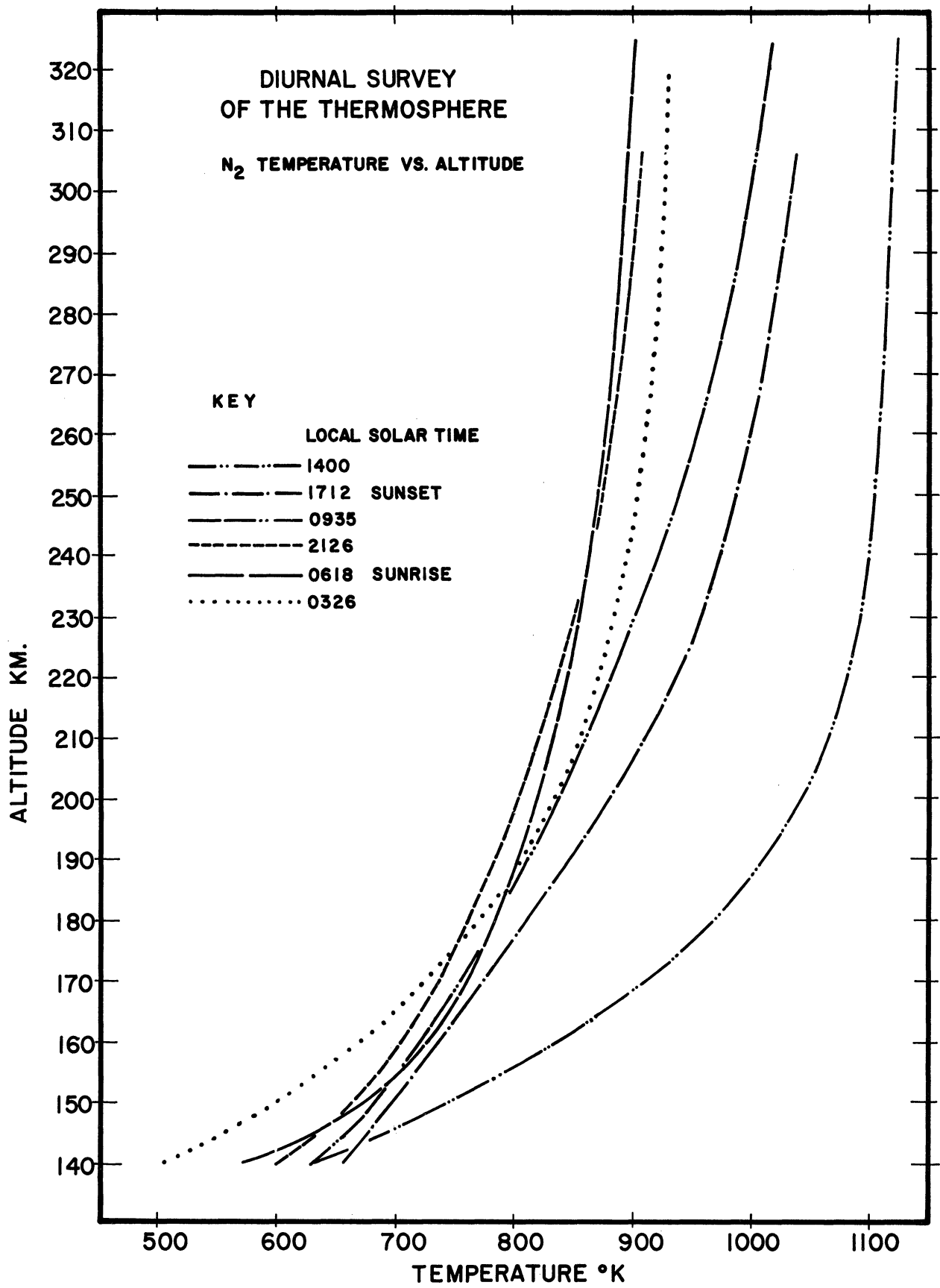
Figure 68. N_2 density vs. altitude.

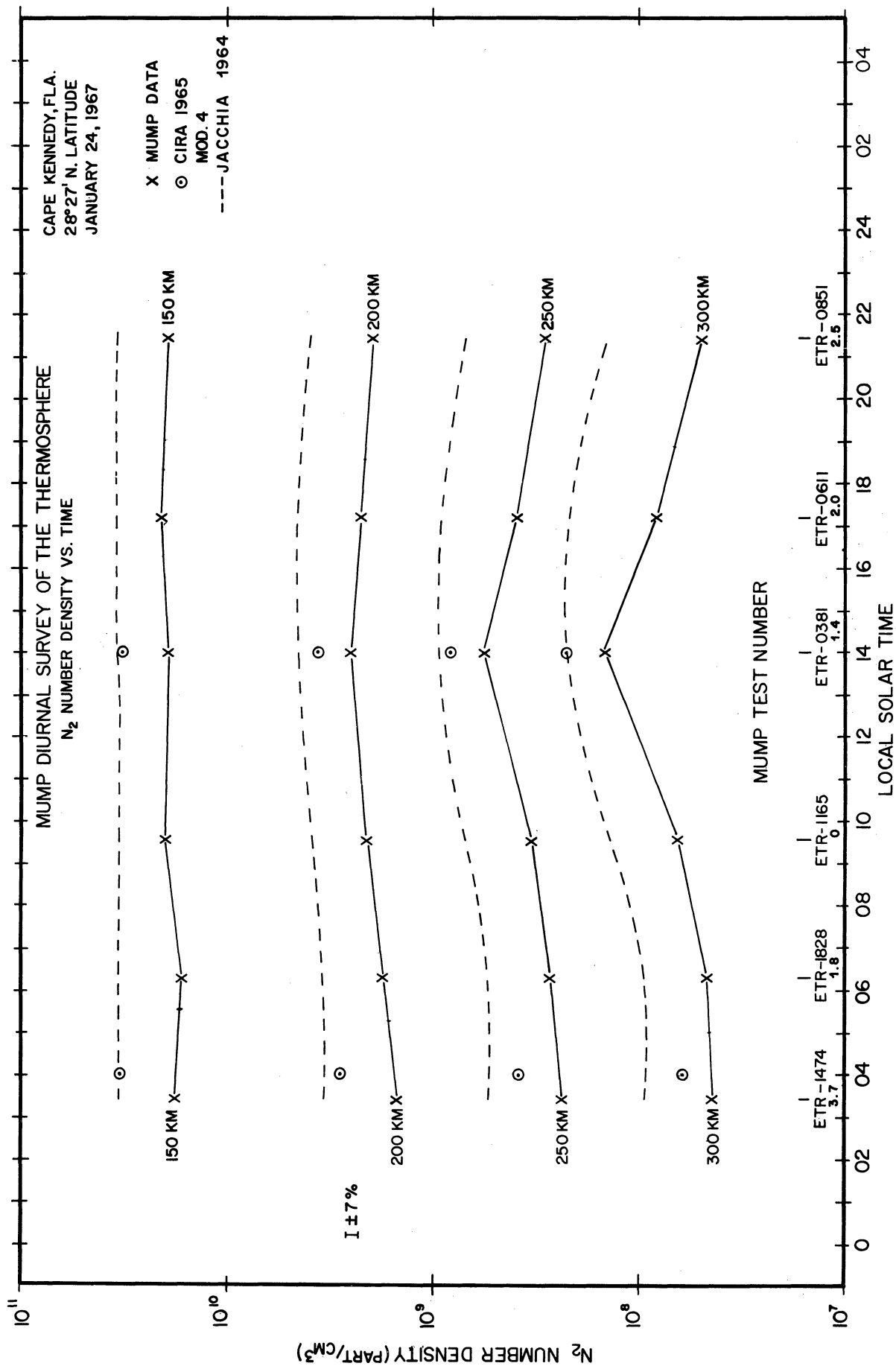127

Figure 69. N_2 temperature vs. altitude.

Figure 70. N_2 density vs. local solar time.
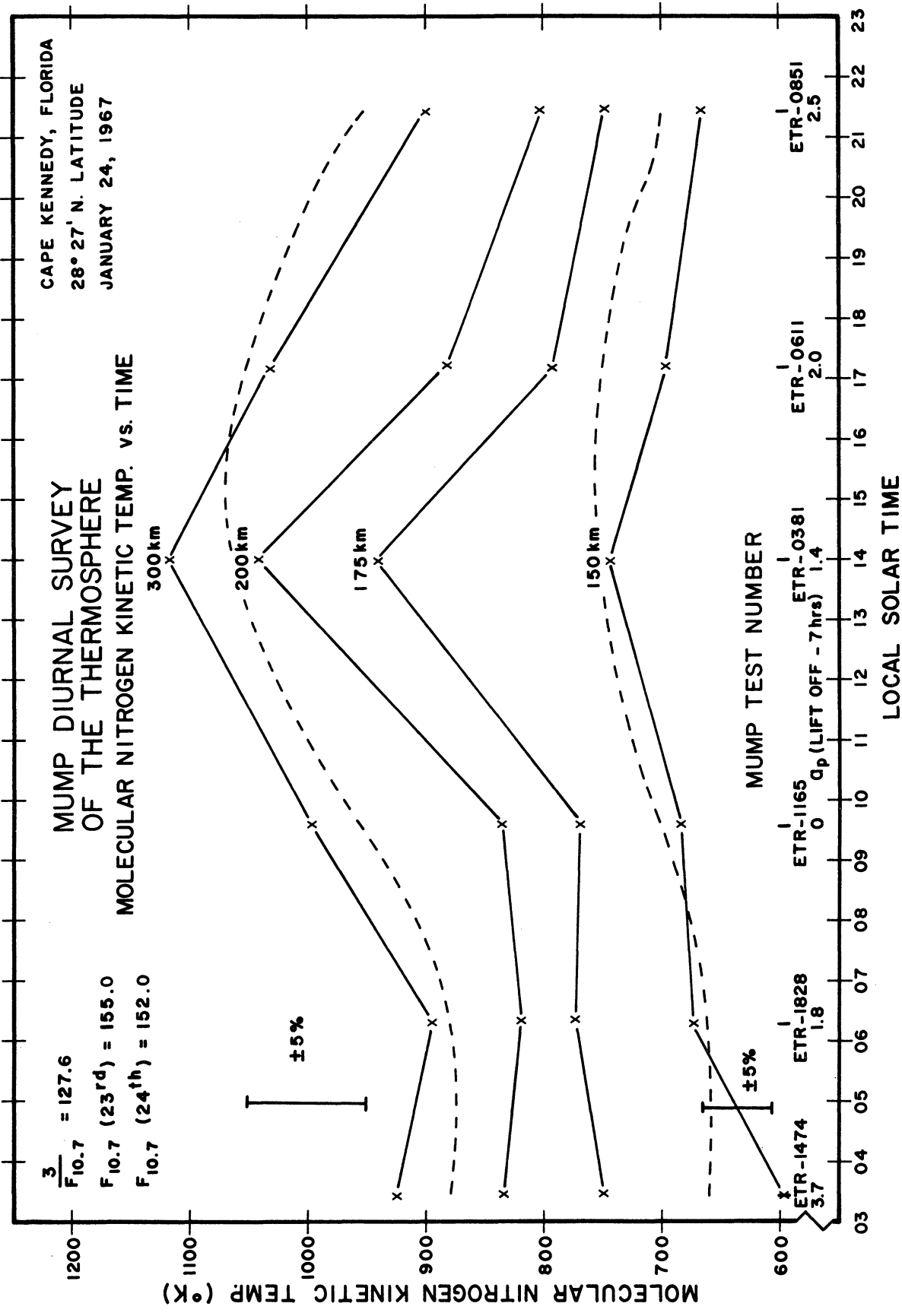
Figure 71. N_2 temperature vs. local solar time.

9.2 CHARGED PARTICLE TEMPERATURE AND DENSITY

The electron temperature and density results obtained from the Langmuir probe experiments were shown in Figures 57 through 64. The ion temperatures shown in these figures were calculated by using the following expression given by Dalgarno, et al., (1967), which is based on the assumption that only O^+ ions are present:

$$T_i = T_n + \frac{5 \times 10^{-7} (T_e - T_n)}{T_e^{3/2}} n_e^2$$

$$\left\{ \frac{5 \times 10^{-7} n_e^2}{T_e^{3/2}} + n_e [9 \times 10^{-14} n(O) + 6 \times 10^{-14} n(N_2) + 6 \times 10^{-15} n(He)] \right\}^{-1}. \tag{4}$$

All the quantities which appear in this equation were measured simultaneously except $n(O)$ and $n(He)$. The values used in the calculations for the oxygen density were obtained from Jacchia's (1965a,b) model and the effect of neglecting helium was found to be negligible at these altitudes. Figure 72 shows the diurnal variation of the electron temperature T_e at the various altitudes, as measured by the Langmuir probes on January 24, 1967. The pre-sunrise effect in T_e is clearly shown by these results. The average rate of pre-sunrise temperature rise at 300 km is about 4°K/min which is of the same order as the value given by Carlson (1966). A significant rise in the electron temperature was also present at sunset on this day, as may be seen from Figure 72. The rate at which energy is transferred from the electron gas to oxygen ions and which is approximately equal to the rate of energy input to the electrons, was calculated using equation (5) and plotted in Figure 73.

$$L_{ei} = \frac{5 \times 10^{-7} (T_e - T_i)}{T_e^{3/2}} n_e^2 \quad eV \ cm^{-3} \ sec^{-1}. \tag{5}$$

The calculations clearly indicate that the energy input varies smoothly; the sunset peak in T_e is apparently caused by a rate of decrease in the electron density which was somewhat larger than usually observed. The cooling rates calculated by Dalgarno, et al., (1967) for a similar flight in November, 1963, are also shown in Figure 73 for comparison. A similar sunset peak was recently observed at Arecibo and reported by Wand at the University of Illinois Thomson Scatter Conference.

The results of the sunrise flight (ETR 1828) were shown in Figure 62; the changing solar zenith angles during the flight were also indicated. It is interesting to note that, although the electron density changed considerably during the flight, no detectable change in T_e was observed. This behavior can be explained by a rate of increase in the electron density which is of the right order to offset the increase in the heat input, resulting in no significant change in the electron temperature.

Thomson scatter measurements of the electron and ion temperatures were also made on January 24 by the Millstone Hill Radar Facility and the Jicamarca Radar Observatory. Figure 74 shows both the rocket and Thomson scatter results. The ion temperature results obtained from Jicamarca are in good agreement with the results obtained from the rocket data; the ion temperature results from Millstone are, however, lower than would be expected. There is only a gross agreement between the Millstone and Cape Kennedy T_e results shown in Figure 74, but this is reasonable, since electron temperatures exhibit significant spatial variations.

The comparison between the results of the April daytime flight and the preliminary backscatter results from Jicamarca, Arecibo, and Millstone are shown in Figure 75. There is good agreement between the ion temperatures obtained from the rocket data and those measured by Jicamarca and Arecibo; however, the results from Millstone are again low.

The preliminary analysis of the data obtained from these eight rocket flights has already improved our understanding of the diurnal behavior of the upper atmosphere; these series of flights have also provided an excellent opportunity to compare the results of rocket-borne measurements with those obtained by Thomson scatter technique.
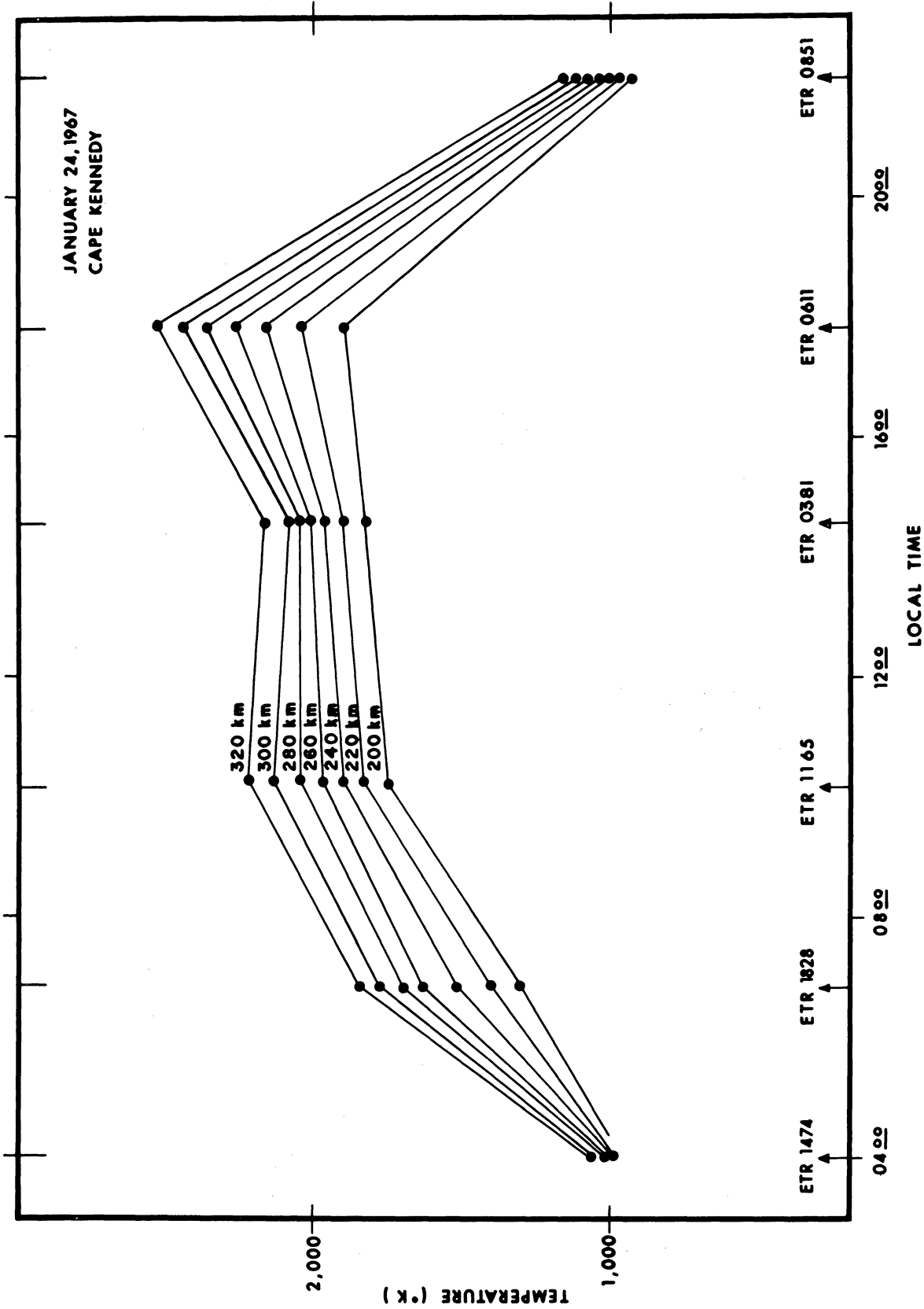
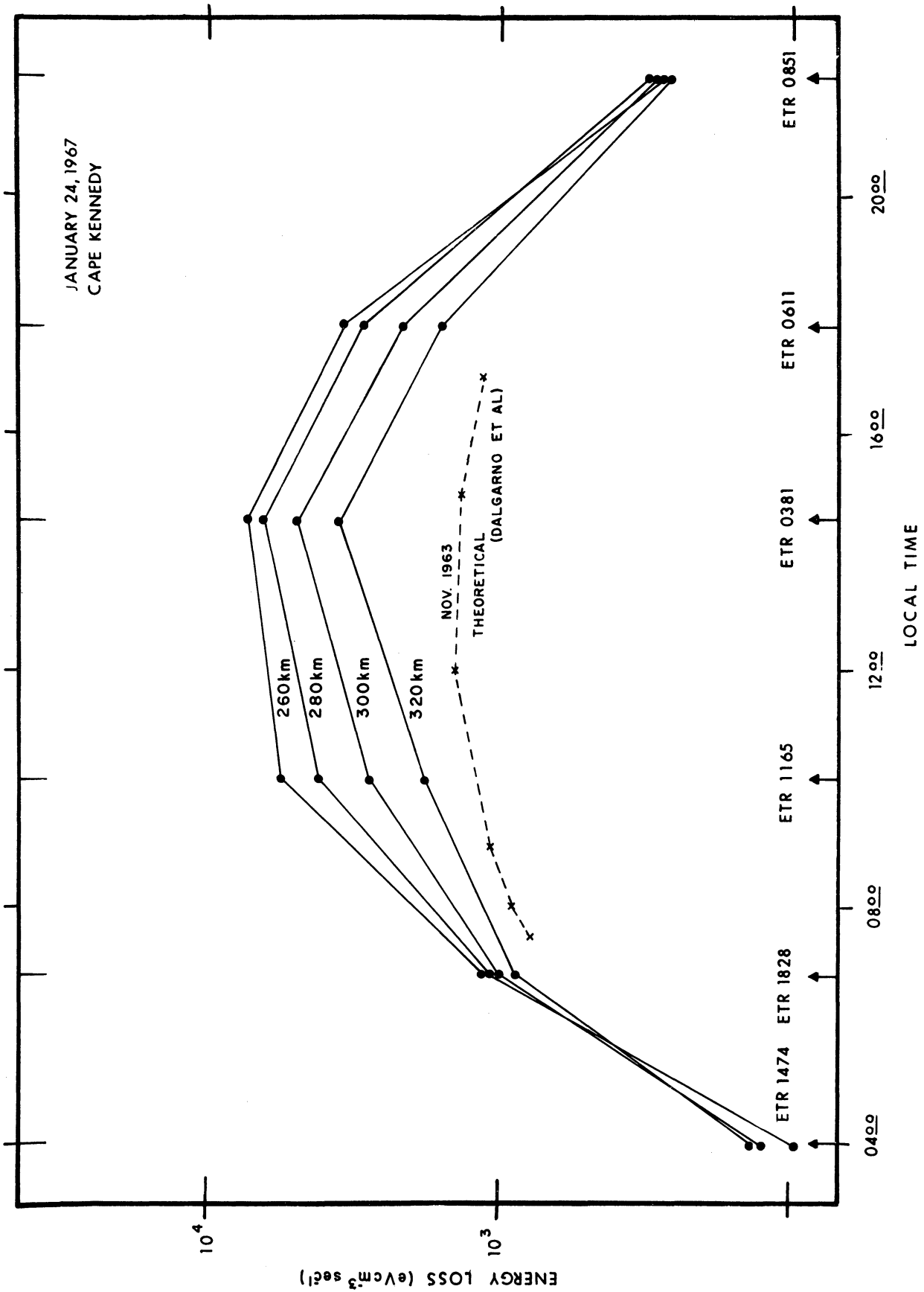Figure 72. Diurnal variation of the measured electron temperatures.

133

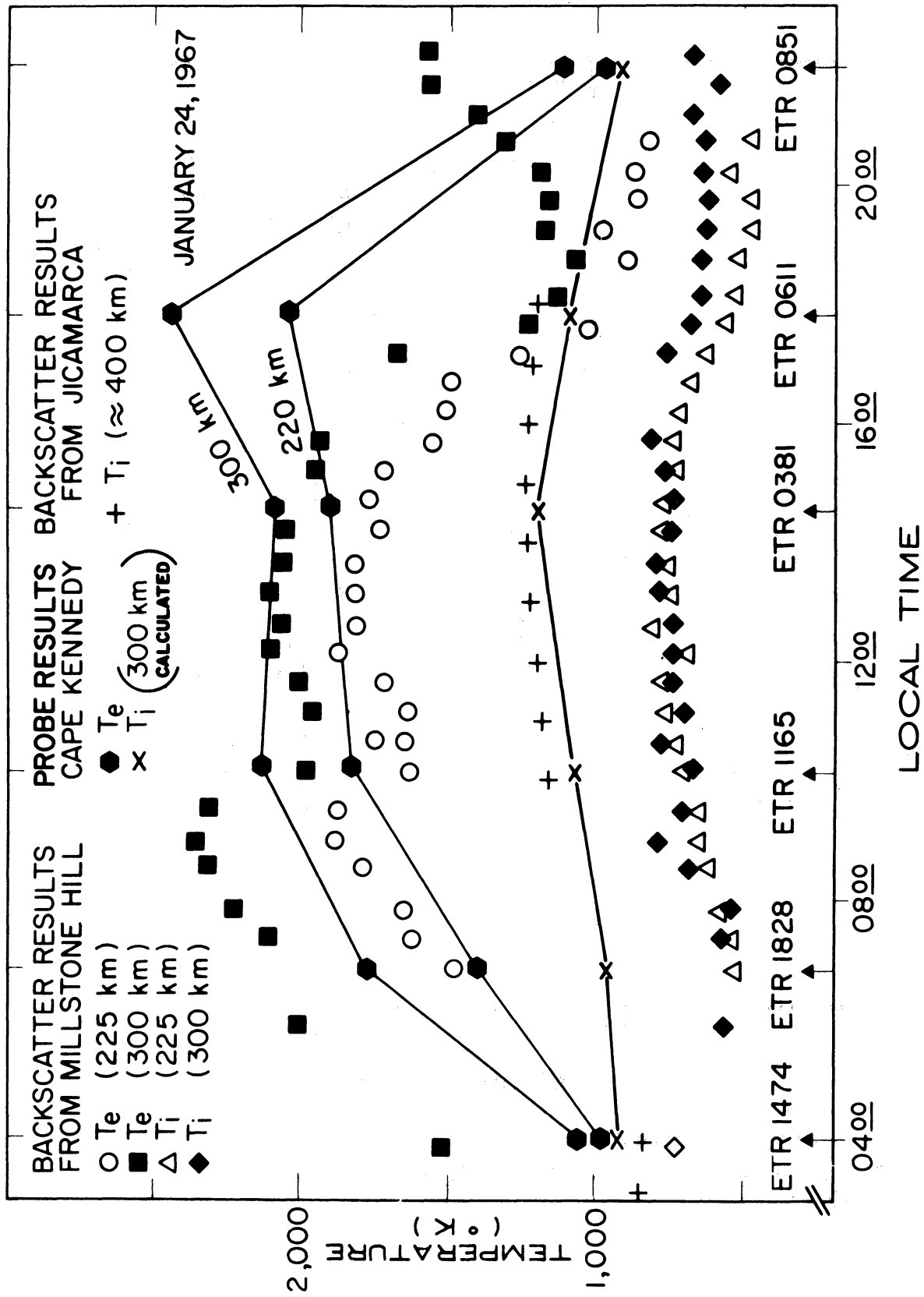Figure 73. Diurnal variation of the calculated electron energy loss rates.

Figure 74. Comparison between the charged particle temperatures measured by the Langmuir probe and the ones obtained by Thomson scatter measurements (January 24, 1967).
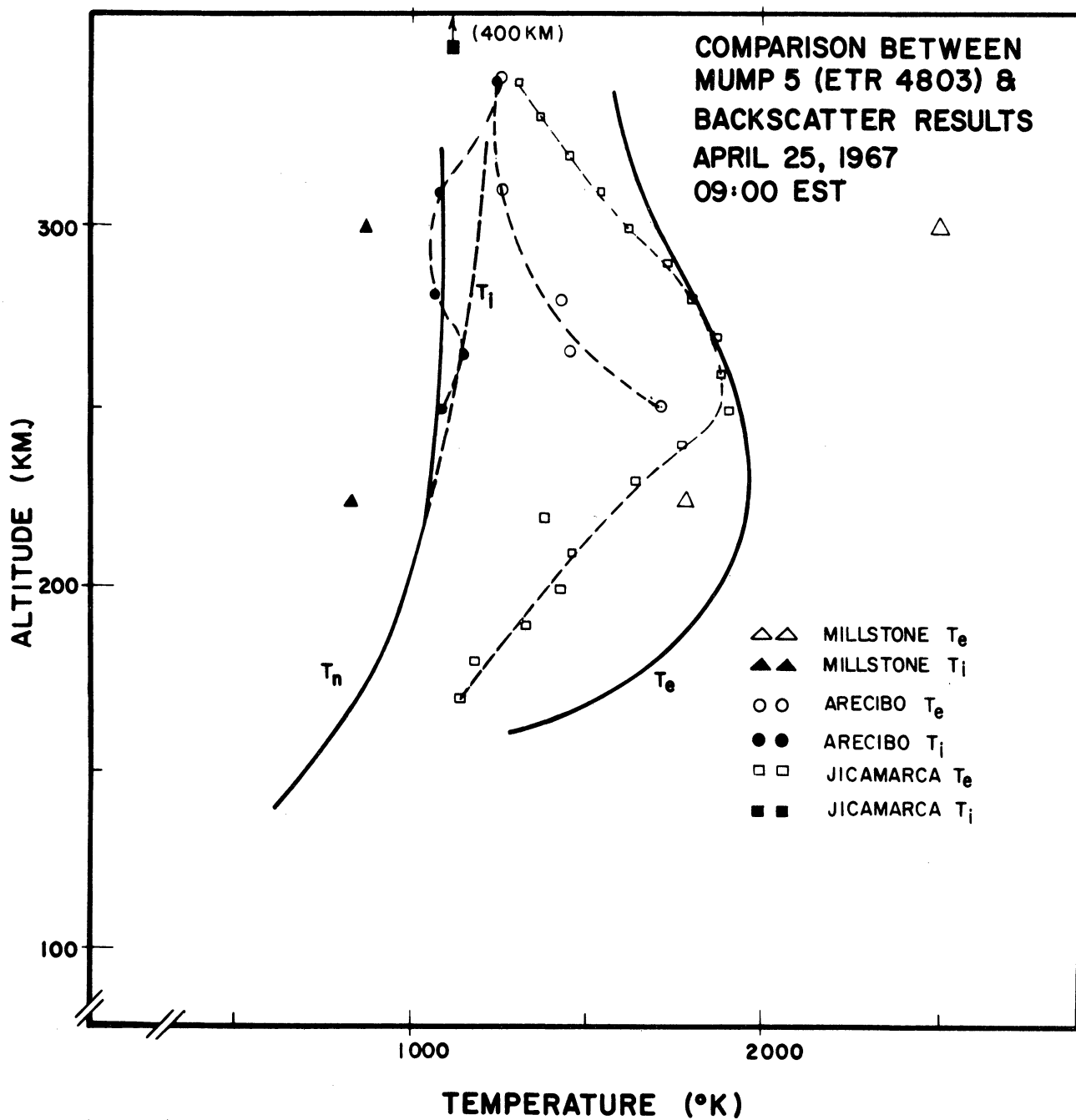
135

Figure 75. Comparison between the charged particle temperatures measured by the Langmuir probe and the ones obtained by Thomson scatter measurements (April 25, 1967).

136

10. REFERENCES

Ballance, James O., *An Analysis of the Molecular Kinetics of the Thermosphere Probe*, George C. Marshall Space Flight Center, NASA Technical Memorandum, NASA TM X-53641, July 31, 1967.

Boggess, R. L., Brace, L. H., and Spencer, N. W., "Langmuir Probe Measurements in the Ionosphere," J. Geophys. Res., 64, 1627-1630. 1959.

Bourdeau, R. E., Whipple, E. C., Jr., Donley, J. L., and Bauer, S. J., "Experimental Evidence for the Presence of Helium Ions Based on Explorer VIII Satellite Data," J. Geophys. Res., 67, 467-475, 1962.

Brace, L. H., Spencer, N. W., and Carignan, G. R., "Ionosphere Electron Temperature Measurements and Their Implications," J. Geophys. Res., 68, 5397-5412, 1963.

Carlson, H. C., Jr., "Ionospheric Heating by Magnetic Conjugate-Point Photoelectrons," J. Geophys. Res., 71, 195-199, 1966.

CIRA, 1965 (COSPAR Intern. Reference Atmosphere), compiled by H. K. Kallmann-Bijl, et al. (North-Holland Publishing Comp., Amsterdam, 1965).

Dalgarno, A., McElroy, M. B., and Walker, J. C. G., "The Diurnal Variation of Ionospheric Temperatures," Planet. Space Sci., 15, 331, 1967.

Evans, J. V., "An F-Region Eclipse," J. Geophys. Res., 70, 131-142, 1965a.

Evans, J. V., "Ionospheric Backscatter Observations at Millstone Hill," Planet. Sci., 13, 1031, 1074, 1965b.

Harris, I. and Priester, W., *The Upper Atmosphere in the Range from 120 to 800 Km*, Goddard Space Flight Center, NASA, Institute for Space Studies Report, 1964.

Jacchia, L. G., "A Variable Atmospheric Density Model from Satellite Accelerations," J. Geophys. Res., 65, 2775, 1960.

Jacchia, L. G., "A Working Model for the Upper Atmosphere," Nature, 192, 1147, 1961.

Jacchia, L. G., "Variations in the Earth's Upper Atmosphere as Revealed by Satellite Drag," Rev. Mod. Phys., 35, 973-991, 1963.

Jacchia, L. G., "The Temperature Above the Thermopause," Smithsonian Astrophys. Obs. Spec. Rep., No. 150, 32 pages, 1964.

Jacchia, L. G., "Density Variations in the Heterosphere," Smithsonian Astrophys. Spec. Rep., No. 184, 1965a.

Jacchia, L. G., "Static Diffusion Models of the Upper Atmosphere with Empirical Temperature Profiles," Smithsonian Astrophys. Obs. Spec. Rept. No. 170, 1964; also published in Smithsonian Contrib. Astrophys., 8, 215-257, 1965b.

Jacchia, L. G. and Slowey, J., "The Shape and Location of the Diurnal Bulge in the Upper Atmosphere," Smithsonian Astrophys. Obs. Spec. Rep., No. 207, April 1, 1966.

Johnson, F. S., "Circulation at Ionospheric Levels," Southwest Center for Advanced Studies," Report on Contract Cub10531, January 30, 1964

Kanal, M., "Theory of Current Collection of Moving Cylindrical Probes," J. Appl. Phys., 35, 1697-1703, 1964.

Krassovsky, V. I., "Exploration of the Upper Atmosphere with the Help of the Third Soviet Sputnik," Proc. IRE, 47, 289-296, 1959.

McElroy, M. B., Models for the Terrestrial Atmosphere Above the 120 Km Level, Kitt Peak National Observatory, Contribution No. 55, 1964.

Moe, Kenneth and M. M., The Effect of Adsorption on Densities Measured by Orbiting Pressure Gauges, Publication No. 576, Institute of Geophysics and Planetary Physics, University of California, Los Angeles, California.

Mott-Smith, H. M., and Langmuir, I., "The Theory of Collectors in Gaseous Discharges," Phys. Rev., 28, 727, 1926.

Nagy, A. F., Brace, L. H., Carignan, G. R., and Kanal, M., "Direct Measurements Bearing on the Extent of Thermal Nonequilibrium in the Ionosphere," J. Geophys. Res., 68, 6401-6412, 1963.

Nagy, A. F. and Faruqui, A. Z., "Ionospheric Electron Density and Body Potential Measurements by a Cylindrical Langmuir Probe," J. Geophys Res., 70, 4847-4858, 1965.

Niemann, H. B. and Kennedy, B. C., "Omegatron Mass Spectrometer for Partial Pressure Measurements in Upper Atmosphere," Rev. Sci. Instr., 37, 722-728, 1966.

Paetzold, H. K. and Zschorner, H., "Bearings of Sputnik III and the Variable Acceleration of Satellites," Space Research I Proc. First. Internat. Space Sci. Sump., Ed., H. Kallman-Bijl, North-Holland Publishing Co., Amsterdam, 1960.

Parker, L. T., Jr., "A Mass Point Trajectory Program for the DCD 1604 Computer," Tech. Doc. Report AFSW-TDR-62-49, Air Force Spec. Weapons Center, Kirtland AF Base, New Mexico, August, 1962.

Spencer, N. W., Brace, L. H., and Carignan, G. R., "Electron Temperature Evidence for Nonthermal Equilibrium in the Ionosphere," J. Geophys. Res., 67, 151-175, 1962.

Spencer, N. W., Brace, L. H., Carignan, G. R., Taeusch, D. R., and Niemann, H. B., "Electron and Molecular Nitrogen Temperature and Density in the Thermosphere," J. Geophys. Res., 70, 2665-2698, 1965a.

Spencer, N. W., Taeusch, D. R., and Carignan, G. R., "N_2 Temperature and Density Data for the 150 to 300 Km Region and Their Implications," NASA, Goddard Space Flight Center, Report x-620-66-5, December, 1965b.

Taeusch, D. R., Carignan, G. R., Niemann, H. B., and Nagy, A. F. The Thermosphere Probe Experiment, Space Physics Research Laboratory, The University of Michigan, Scientific Report 07065-1-S, March, 1965.

Taeusch, D. R. and Carignan, G. R., Sounding Rocket Flight Report, NASA 18.02 Thermosphere Probe Experiment, Space Physics Research Laboratory, The University of Michigan, Rocket Report 07065-3-R, September, 1966a.

Taeusch, D. R. and Carignan, G. R., Sounding Rocket Flight Report NASA 18.03 Thermosphere Probe Experiment, Space Physics Research Laboratory, The University of Michigan, Rocket Report 07065-4-R, November, 1966b.

APPENDIX

DETERMINATION OF THE TOTAL PAYLOAD MOMENTS OF INERTIA

THE Bendix CORPORATION

REPORT NO. TR- 1219   DATE 2 Feb 66

PERFORMED FOR: University of Michigan
2455 Hayward
Northwood Campus
Ann Arbor, Michigan

TEST: Moment of Inertia Determination

ITEM: Thermosphere Probe MUMP-1

TEST DATE: 17 Jan 66

PERFORMED AT: Space Laboratories

WORK ORDER NO: 85191-441-01-2403

AUTHORIZATION: PO R-64522

REQUESTED BY: Otto Kruse

REPORT SENT TO: John Maurer

PREPARED BY: _____
R. W. Hyde
Test Engineer
Systems Test Department

APPROVED BY: _____
R. H. Culpepper
Project Engineer
Systems Test Department

ed

TR 1219

INTRODUCTION

The mass moments of inertia of a Thermosphere Probe MUMP-1, manufactured by the University of Michigan, were determined experimentally on the trifilar test stand. The purpose of the tests was to determine the mass constants about the spin axis as the split halves were placed at various angles. The mass constants were also determined for the test item in the lateral axis and the instrument package alone.

SUMMARY OF RESULTS

The moments of inertia of the test items are shown below.

	$lb\ ft\ sec^2 = slug\ ft^2$
Payload about the spin axis	0.2135
Payload halves open 7.73 in. (spin axis)	0.4732
Payload halves open 18.67 in (spin axis)	1.3413
Payload halves open 42.25 in. (spin axis)	5.8871
Payload halves open 72.675 in. (spin axis)	13.7881
Payload halves horizontal	16.3455
Payload about the lateral axis	7.9402
Instrument package about spin axis	0.07035
Instrument package about lateral axis	1.0018

Payload total weight 120 lbs
Instrument package weight 48.75 lbs

METHODS AND DATA

The test items were mounted on the trifilar pendulum apparatus as shown in Figures 1 through 3 and the platform was allowed to oscillate through approximately 1 to 2 inches. The period of oscillation of the combined test item and platform was determined. At the conclusion of testing the period of oscillation of the platform alone was determined.

$$I_{test\ item} = I_{combined\ test\ item\ and\ platform} - I_{platform\ alone} \quad or$$

$$I = \frac{w_t a_t^2 p_t^2}{4\pi^2 L} - \frac{w_p a_p^2 p_p^2}{4\pi^2 L}$$

143

Where: W_t = Platform plus test item weight
a = 20 inches
L = Filament length, 108.22 inches
W_p = Platform weight, 22 lbs
P_t = Period in seconds, combined test item and platform
P_p = Platform period in seconds, 1.49925
I = Test item moment of inertia in lb in $\sec^2$

The tests were witnessed by J. Maurer, L. Degener, and R. Simmons of the University of Michigan. The test items were returned to the University of Michigan by the University of Michigan personnel.
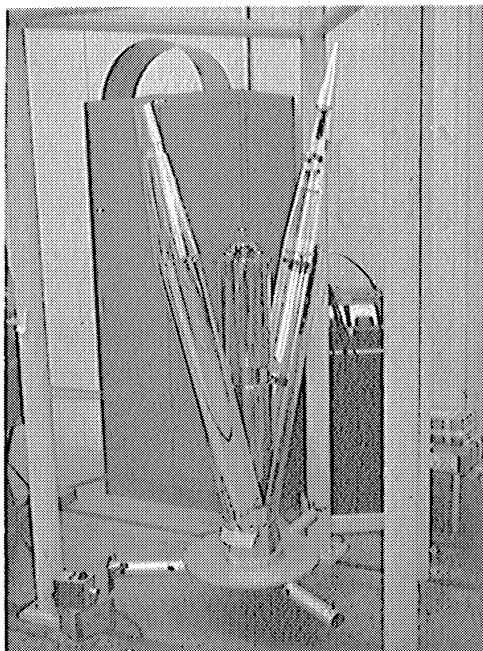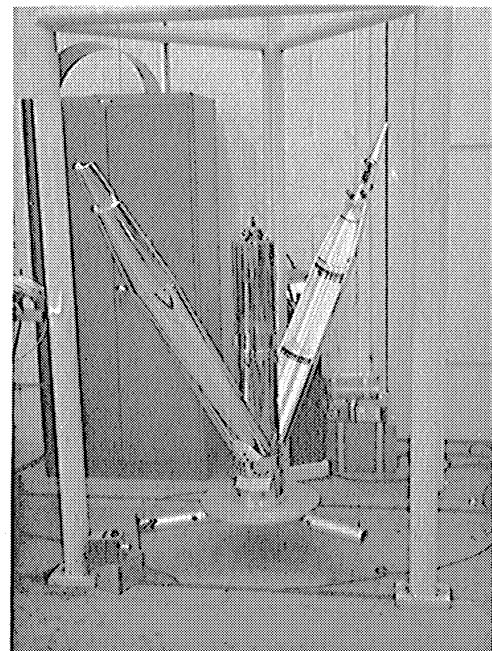
TEST SETUP
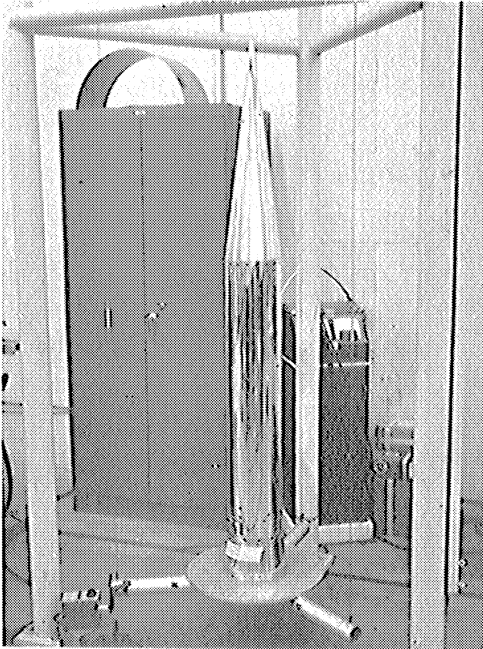
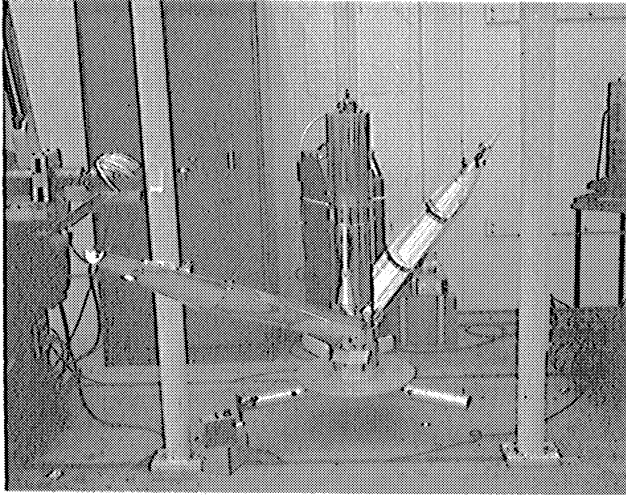Shell Closed
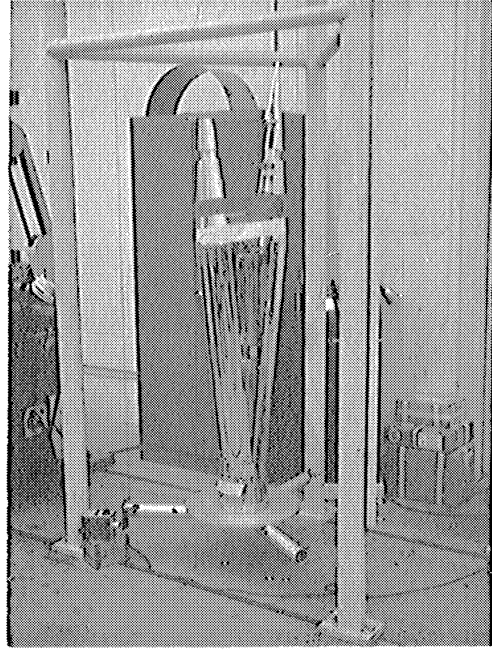
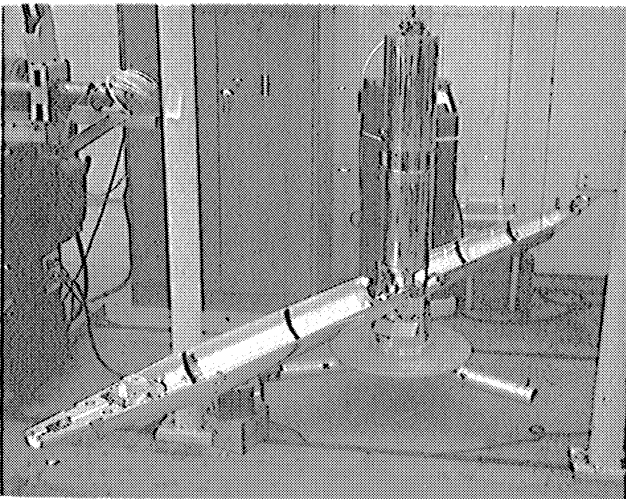Shell Open 7.73 inches

Shell Open 12.850 inches

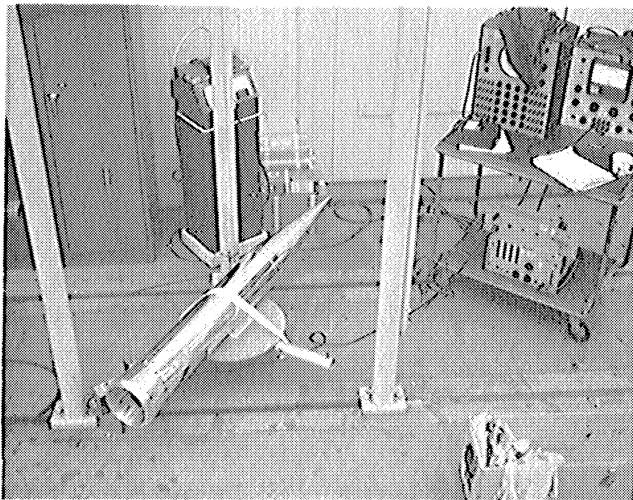Shell Open 18.67 inches

TEST SETUP

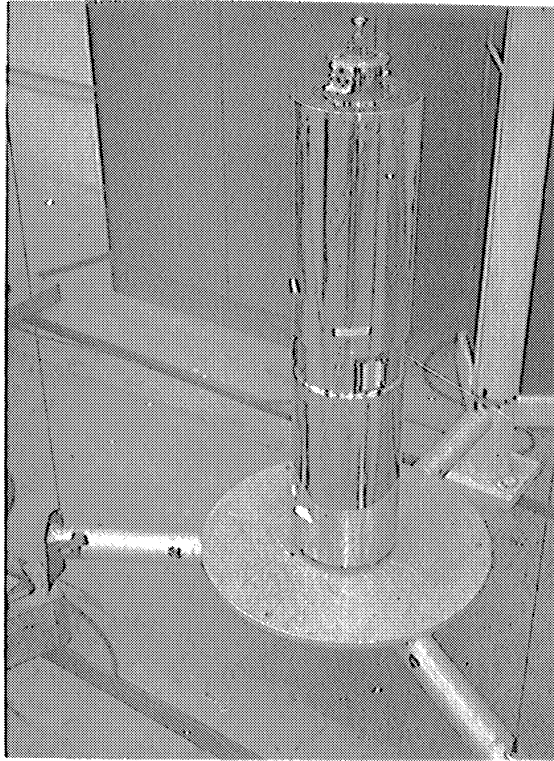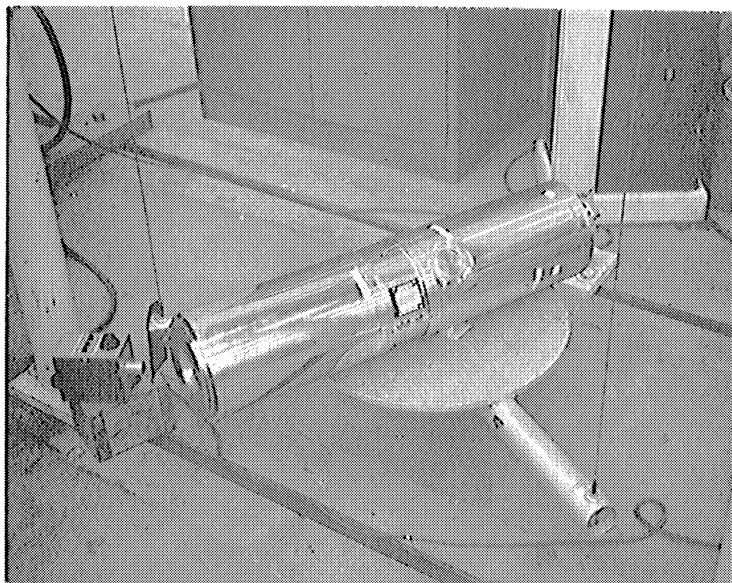
Shell open 72. 675 inches

Shell fully open

Lateral axis

146

INSTRUMENT PACKAGE TEST SETUP

Spin Axis

Lateral Axis

TEST EQUIPMENT

Test: Moment of Inertia

Date Used: 17 Jan 66

Test Item: Thermosphere Probe

Item	Model No.	BxS No.	Scale Range	Calibration Date	
Manufacturer	Serial No.	Accuracy	Quantity Measured	Last	Next
Electronic Counter	H 19-521 CR	IEC 50577		9-28	6-28
Hewlett-Packard			cps	65	66
Counter		50682		12-8	12-8
BSD			cycles	65	66